Aus dem

Department für Augenheilkunde Tübingen

Universitäts-Augenklinik

# Development of innovative electrodes for recording neuromuscular biopotentials of the ciliary muscle for adaptive control of artificial lenses in presbyopia

**Inaugural-Dissertation**
**zur Erlangung des Doktorgrades**
**der Humanwissenschaften**

**der Medizinischen Fakultät**
**der Eberhard Karls Universität**
**zu Tübingen**

**vorgelegt von**

**Schumayer, Sven**

**2026**

Dekanin: Professorin Dr. S. Y. Brucker

1. Berichterstatter: Dr. T. Straßer
2. Berichterstatter: Professor Dr. T. Schäffer

Tag der Disputation: 24.02.2026

# Table of Contents

## List of Figures

## List of Abbreviations

| | |
|---|---|
| ° | Degree (angle) |
| mm | Millimeter ($10^{-3}$ meters) |
| D | Diopter |
| m | Meter |
| ECG | Electrocardiogram |
| s | Seconds |
| Ca | Calcium |
| µl | Microliters ($10^{-6}$ liter) |
| min | Minutes (60 s) |
| FBN | Fibrillin |
| LTBP | Latent transforming growth factor beta-binding protein |
| µm | Micrometer ($10^{-6}$ meters) |
| nm | Nanometer ($10^{-9}$ meters) |
| AoA | Amplitude of Accommodation |
| e.g. | exempli gratia (Latin: “for example”) |
| cf. | confer |
| USD | US-Dollar |
| LASIK | Laser-assisted keratomileusis |
| IOL | Intraocular lens |
| cm | Centimeter ($10^{-2}$ meters) |

| | |
|---|---|
| FDA | U.S. Food and Drug Administration |
| MDR | Medical Device Regulation |
| MD | Medical device |
| AIMD | Active implantable medical device |
| ISO | International Organization for Standardization |
| d | Day |
| q.v. | quod vide (Latin: “which see”; cross-reference) |
| EO | Ethylene oxide |
| °C | Degree Celsius |
| g | Gram (outdated gm) |
| mil | 0.001 inches ($25.4^{-6}$ meters) |
| in | Inch (1 inch = 2.54 cm) |
| hr | Hour |
| RH | Relative humidity |
| V | Volt |
| USP | United States Pharmacopeia |
| CVD | Chemical vapor deposition |
| Pa | Pascal |
| ALD | Atomic layer deposition |
| PVD | Physical vapor deposition |
| ISCEV | International Society for Clinical Electrophysiology of Vision |

| | |
|---|---|
| VA | Visual acuity |
| IPA | Isopropyl Alcohol (known as isopropanol) |
| W | Watt |
| UV | Ultraviolet |
| DC | Direct current |
| Cu | Copper |
| MAR | Motorized accommodation ruler |
| ASIC | Application-specific integrated circuit |
| PET | Polyethylenterephthalat |
| PMMA | Polymethyl methacrylate |
| PFA | Perfluoroalkoxy |
| SLA | Stereolithography |
| PCB | Printed circuit board |
| $LiMnO_2$ | Lithium manganese oxide |
| $Al_2O_3$ | Aluminum oxide |
| $TiO_2$ | Titanium dioxide |

# 1. Introduction

Within the human eye, the sharpest vision is located 15° temporal and 1.5° inferior to the optic nerve in a circular area called the fovea (Atchison, 2023). At the center of this pit-like structure, with an approximate diameter of 1.5 mm, only cones are present. These cones are responsible for color vision and high visual acuity in daylight. Apart from the fovea, both rods and cones can be found (Kolb *et al.*, 2020; Atchison, 2023). The light must first be refracted to bring the incident light into focus on this area and thus enable the eye to perceive the surroundings sharply. This is mainly done (≈ 42 D) by the fixed refractive power of the cornea (Atchison, 2023) but also by the variable refractive power of the crystalline lens (16- 20 D) (Chen, Tan and Chen, 2016). The latter is required for focusing at a close range of less than 6 m (Levin *et al.*, 2011). The adjustment of the lens's refractive power by the ciliary muscle, known as accommodation, is inversely related to the viewing distance. Similar to an electrocardiogram (ECG), the muscle emits a bioelectric signal during contraction. These so-called "biopotentials" can be used as an input signal for an electronic control to adjust a tunable lens in an implant, a contact lens, or spectacles according to the wearer's subjective refractive needs.

Taken together, this work introduces a novel approach to quantifying the residual subjective amplitude of accommodation. In addition, it focuses on characterizing accommodation-related biopotentials using a contact lens electrode and an implant. Given the implant's exposure to the body's harsh internal environment, appropriate encapsulation techniques must be addressed in accordance with the medical device regulations. Overall, this research lays the foundation for a new class of visual aids that use bioelectrical signals to adjust a tunable lens.

## 1.1 Accommodation

Accommodation refers to the eye's ability to change its refractive power to focus on near objects (Atchison, 1995; Glasser, 2006). In primates, including humans, this change in dioptric power is primarily driven by contraction of the ciliary muscle, which reduces tension on the lens capsule (Glasser and Kaufman, 1999). Consequently, the lens's curvature increases (cf. Figure 1), leading to greater refractive power (Ciuffreda, 2006; Glasser, 2006). Since the mechanisms of accommodation, including its neural control and

structural components, are not yet fully understood (2025), ongoing research is conducted using animal models. These studies are based on the high anatomical similarity of the accommodative apparatus between humans and non-human primates, such as cynomolgus monkeys (Törnqvist, 1967; Glasser and Kaufman, 1999) or rhesus monkeys (Glasser and Kaufman, 1999; Qiao-Grider *et al.*, 2007; Croft *et al.*, 2013; Flügel-Koch *et al.*, 2016; Lin *et al.*, 2021).

### 1.1.1 Theoretical Accommodation Control Mechanism

Accommodation involves the coordinated action of the ciliary muscle, pupillary muscles, and extraocular muscles, a combination commonly referred to as the "near triad" (Myers and Stark, 1990; Charman, 2008; Levin *et al.*, 2011). Although the neurological processes are simulated in theoretical models, they are still the subject of scientific debate today (Read *et al.*, 2022). The difference between the perceived actual value and the required refraction (target value), referred to as defocus, is the neural trigger of accommodation and thus the control deviation in the negative feedback loop (Toates, 1972; Ciuffreda, 2006; Read *et al.*, 2022). From the perception of the defocus to the contraction of the ciliary muscle, approximately 0.3 - 0.4 seconds elapse (Campbell and Westheimer, 1960; Morgan, 1968; Myers and Stark, 1990; Heron, Charman and Schor, 2001), regardless of age (Heron, Charman and Schor, 2001). Defocus is detected using cues derived from the retinal image, particularly the blur induced by chromatic aberration (Fincham, 1951, 1953; Seidemann and Schaeffel, 2002; Stark *et al.*, 2002; Ciuffreda, 2006; Cholewiak, Love and Banks, 2018) and from depth perception (Ittelson and Ames, 1950; Heath, 1956). Chromatic aberration is caused by short-wave light (e.g., blue) being refracted more than longer-wave light (e.g., red), resulting in not being focused in the same plane. Depending on the strength of the stimulus in the form of defocus, the accommodation response varies. This circumstance is described by the sigmoidal signal-response curve, revealing how the response remains weak at low stimulus levels, increases linearly at intermediate levels, and reaches saturation at high stimulus levels (Morgan, 1944). The difference ($\Delta$) between the actual response and the stimulus is referred to as lag of accommodation ($\Delta < 0$) or lead of accommodation ($\Delta > 0$) depending on the sign indicator (Labhishetty *et al.*, 2021). In the absence of an accommodative stimulus, the eye goes into tonic accommodation and the ciliary muscle returns to its basal tone over time (Figure 1, left), resulting in a constant, subject-dependent refractive power of approximately 1 D

(Schor, Johnson and Post, 1984; McBrien and Millodot, 1987; Rosenfield *et al.*, 1993). Anatomically, there are different functional theories regarding the mechanism of accommodation. As early as 1801, Young proposed that a change of focus was achieved by altering the geometry of the crystalline lens (Young, 1801), a concept later confirmed by Helmholtz, 1855. Helmholtz stated that the contraction of the ciliary muscle reduces the tension of the zonular fibers attached to the lens (Helmholtz, 1855). In 1937, Fincham added that accommodation also occurs in the absence of the iris (Fincham, 1937). Furthermore, he demonstrated on an explanted lens that it changes into a spherical shape when removed from the lens capsule, concluding that the actual lens deformation is driven through the lens capsule. The associated tensile force is generated by the antero-inward movement of the ciliary muscle (Croft *et al.*, 2013). During the relaxation, it is assumed that the choroid also contributes to the posterior displacement of the ciliary body (Croft, Glasser and Kaufman, 2001; Ciuffreda, 2006; Read *et al.*, 2022). Today, Helmholtz's theory forms the basis for the current understanding of accommodation, with the enhancement provided by Fincham. However, alternative schools of thought shall be mentioned. According to Schachar, there is an increase in the equatorial but not the anterior and posterior zonular fiber tension during accommodation. This implies that the central part of the lens becomes rounder, while the peripheral lens flattens (Schachar *et al.*, 1996, 2024). There is also Coleman's theory, which builds on Helmholtz's theory and adds the hydraulic force of the vitreous on the posterior lens (Coleman, 1970).

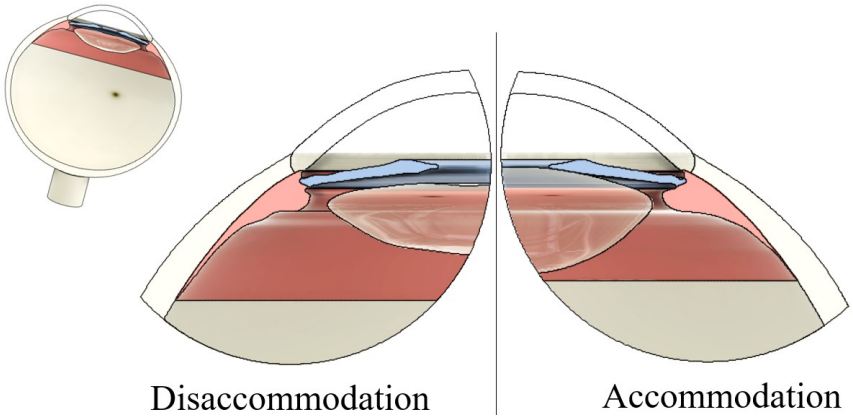


Figure 1 - Schematic accommodation: The depicted cross-section of an eye shown here illustrates the difference between accommodation and disaccommodation. During accommodation, the ciliary muscle contracts, moves further forward and toward the lens of the eye, thus reducing the distance between them. This decreases the tension of the zonular fibres between the lens and the muscle, and the lens moves into a more spherical shape. (Image edited using CAD)

### 1.1.2 Neurological Contribution

The autonomic nervous system, which includes parasympathetic and sympathetic branches, regulates involuntary processes such as heartbeat, blood pressure, and respiration, as well as physiological eye functions such as the regulation of intraocular pressure, pupil contraction, and accommodation (Ashwini and Raju, 2023). Although the ciliary muscle is innervated by sympathetic branches (Mallen, Gilmartin and Wolffsohn, 2005; McDougal and Gamlin, 2015), the parasympathetic component predominates (Gilmartin, 1986; Kandel *et al.*, 2000; Mallen, Gilmartin and Wolffsohn, 2005). Furthermore, the sympathetic branch does not seem to be active in everyone (Gilmartin, Mallen and Wolffsohn, 2002; Mallen, Gilmartin and Wolffsohn, 2005) and has, at most, a minor influence in rapid accommodation changes (Gilmartin, 1986). There are two prevailing concepts concerning the mode of action of sympathetic intervention. While some discuss that the sympathetic branch adapts the eye to distance vision and counteracts the adaptation of the parasympathetic system to near vision (Cogan, 1937; Gawron, 1983), others suggest that accommodation is a two-stage process in which a fast response driven by the parasympathetic system is modified by the slow (adaptation time: 30 - 40 s) sympathetic innervation (Rosenfield and Gilmartin, 1989). The origin of the sympathetic signals is the diencephalon, from which the signals travel via the lower cervical and upper thoracic spinal cord to the superior cervical ganglion (Ciuffreda, 2006). Through the trigeminal nerve, as well as via the long and short ciliary nerves, the signals reach the ciliary muscle (Ciuffreda, 2006), where mainly noradrenaline is released to the muscle receptors (Atchison, 1995). The control signal of the parasympathetic system, on the other hand, originates from the visual cortex, which detects defocus via afferent signals from the retina. An efferent signal is then, consequently, sent to the Edinger-Westphal nucleus in the oculomotor complex (Atchison, 1995). This parasympathetic nucleus complex, located in the midbrain, transmits the control signal via its preganglionic axons to the third cranial nerve, the oculomotor nerve, until it reaches the postganglionic cells in the ciliary ganglion (Warwick, 1954; Ruskell, 1990). Here, the control signal is transmitted via the chemical synapses of the short ciliary nerves to the ciliary muscle, where the nerve endings then attach to the muscle fibers. An incoming presynaptic action signal in the form of an ion flow leads to a change in the membrane charge distribution and the opening of voltage-gated calcium channels, causing calcium ions ($Ca^{2+}$) to flow into the cell (Kandel

*et al.*, 2000). This shift in charge leads to a presynaptic action potential and activation of the vesicles inside the cell (He *et al.*, 2018). These vesicles contain a certain amount of the neurotransmitter acetylcholine and fuse with the presynaptic membrane, a process called exocytosis, resulting in the release of acetylcholine into the synaptic cleft (Atchison, 1995; Kandel *et al.*, 2000). Since a single vesicle results in the release of several neurotransmitters, signaling amplification is achieved (Kandel *et al.*, 2000). The acetylcholine binds to the predominant muscarinic M3 receptors of the postsynaptic membrane (Poyer, B'Ann and Kaufman, 1994; Mitchelson, 2012). The resulting signaling cascade and the influx of $Ca^{2+}$ ions lead to contraction of the muscle fibers (Mitchelson, 2012).

### 1.1.3 Anatomical Structures of Accommodation

The operating principle of the anatomical structures described here is based on Helmholtz's accommodation theory, as outlined in the chapter *Theoretical Accommodation Control Mechanism,* with Fincham's additions. The ciliary muscle, located in the ciliary body, is the single active component in the accommodation process. The increase and reduction of tensile force on the zonular fibers lead to the corresponding deformation of the lens within the lens capsule. The anatomy (Figure 2) and functional mechanisms of each component involved in the process of accommodation is briefly described below.

#### 1.1.3.1 Ciliary body and ciliary muscle

The torus-shaped corpus ciliaris around the lens is enclosed anteriorly by the iris, posteriorly by the ora serrata, and laterally by the sclera and the corpus vitreum. Its cross-sectional wedge-shaped body is divided into a broader, anterior section and a posterior section (pars plana). The anterior section, called pars plicata, is characterized by its ciliary processes, a radially arranged, wave-shaped surface that produces the aqueous humor (1 - 2 µl/min) essential for maintaining the intraocular pressure (Delamere, 2005), as well as for the nutrition of the crystalline lens and the cornea (McDougal and Gamlin, 2015). The ciliary muscle located within the ciliary body is delimited anteriorly by the scleral spur and externally by the sclera (Levin *et al.*, 2011). The smooth muscle consists of three types of muscle fibers: longitudinal, radial, and circular muscle fibers, based on their orientation (Levin *et al.*, 2011). Schematically, the radial fibers are located along the vitreous

body, while the longitudinal fibers run along the sclera, with the radial fibers predominating in the anterior part (Tamm and Lütjen-Drecoll, 1996). Excitation leads to a synergetic contraction of the different fiber types, causing the circular fibers to increase their tone. Today, the assumption is that these fibers also have the greatest influence on reducing the tensile force and, therefore, on lens curvature, while longitudinal and radial fibers lead to a forward lens movement (Knaus, Hipsley and Blemker, 2021).

#### 1.1.3.2 Zonules

The zonular fibers represent a suspensory ligament capable of stretching up to four times its length and serve both to suspend and to transmit the tensile force of the ciliary body to the lens capsule (Canals *et al.*, 1996). The direction of the force application and the resulting lens deformation are still evaluated today (Schachar *et al.*, 2024). The zonula fibers, which consist mainly (≈ 65%) of fibrillin (FBN 1-3) and (≈ 11%) of LTBP (1-3) (De Maria *et al.*, 2017), terminate in bundles with diameters of 10 - 60 µm at the lens capsule, while individual fibers have an average diameter of 10 nm (Streeten, 1977). These bundles are radially orientated at varying angles and span the distance between the ciliary processes and the lens capsule of 1.07 mm in youth and decline to 0.65 mm with age, independent of the accommodation effort (Kasthurirangan *et al.*, 2011). The distinction between posterior, anterior, and vitreous zonules, based on their origin, remains a subject of ongoing research (Flügel-Koch *et al.*, 2016). For clarity, it should be noted that zonula fibres are resistant to conventional histological stains like haematoxylin and eosin (Bassnett, 2021) and are therefore not visible in Figure 2.

#### 1.1.3.3 Lens

The biconvex and transparent lens consists of the capsule, the lens epithelium, and the lens fibers. In adults, the lens measures approximately 9 mm in diameter with a thickness ranging from 3.31 to 4.66 mm, depending on age (Jones, Atchison and Pope, 2007; Kasthurirangan *et al.*, 2011). The lens thickness increases with age by 13 to 23 µm/year (Koretz *et al.*, 1989; Jones, Atchison and Pope, 2007; Kasthurirangan *et al.*, 2011) resulting in an average weight gain of 1.38 mg/year (Augusteyn, 2007). The refractive index of the lens cortex is 1.365, while the nucleus has a refractive power of 1.44, which reduces slightly (0.00034 D/year) over life (Moffat, Atchison and Pope, 2002).

The lens capsule thickness varies, measuring 21-23 µm at the equator and 2-3 µm posterior, containing two types of epithelial cells that compose the lens (Chen, Tan and Chen, 2016). While the lens epithelium, as a monolayer, covers the anterior surface facing the cornea (Figure 2, lower left), the lens fibers are arranged in concentric layers. By a cellular signaling pathway, lens epithelial cells near the posterior equator differentiate by elongation into lens fiber cells, without a nucleus, leading to the ingrowth of older layers (Menko, 2002). The absence of organelles and high concentration of cytoplasmic proteins contribute to the lens's transparency. Multiple factors can cause damage to the lens epithelium, particularly oxidative stress, leading to protein denaturation and thus opacification of the crystalline lens (Muranov and Ostrovsky, 2022). Untreated cataractogenesis, initially noticeable as blurred vision, progresses steadily and can eventually lead to blindness after full cataract formation. Cataracts remain one of the most common causes of visual impairment globally, affecting over 15 million people over the age of 50 (Bourne *et al.*, 2021). They can be effectively treated by replacing the opaque lens with an artificial intraocular lens (Liu *et al.*, 2017; Pesudovs *et al.*, 2024).

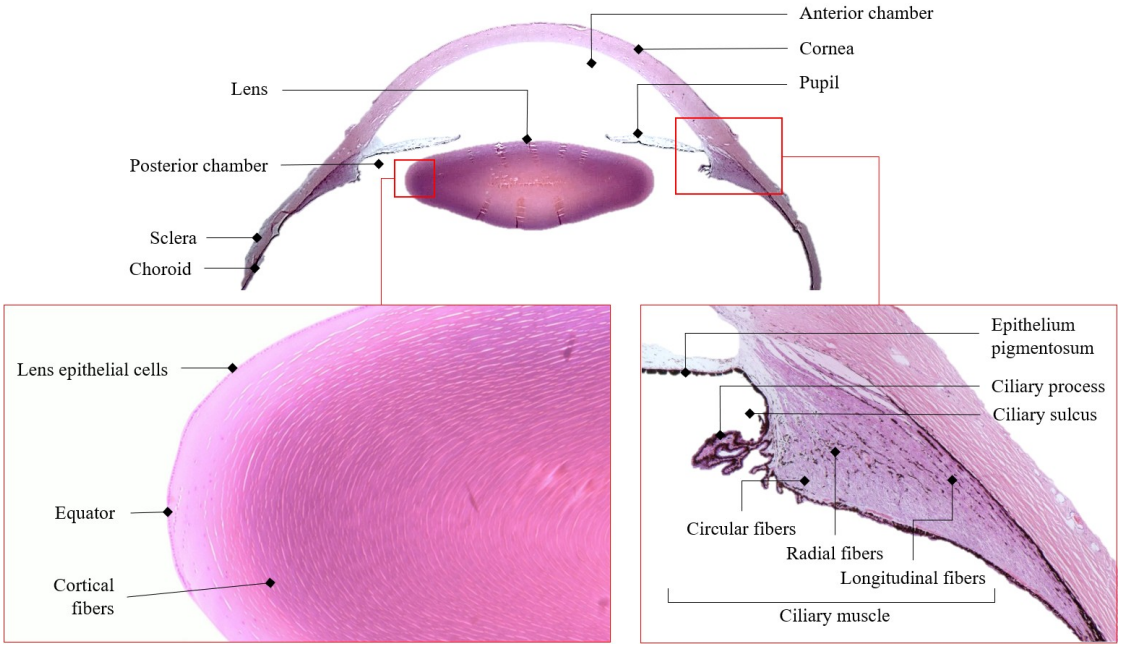


Figure 2 - The anatomy of the accommodation apparatus in a cynomolgus monkey eye: While the lower left represents a magnified illustration of the lens, the right shows the single muscle fibers of the ciliary muscle together with the ciliary sulcus and the processes from where zonules are guided and attached. (Hematoxylin and eosin staining by Sylvie Bolz, for highlighting single anatomical components; contrast was adjusted)

### 1.1.4 Measuring Accommodation

By measuring accommodation, both the focal distance and the near point of the eye can be determined, providing insights into accommodation insufficiency and the progression of presbyopia (Duane, 1912; Charman, 2017; Hussaindeen and Murali, 2020). An essential parameter hereby is the Amplitude of Accommodation (AoA), the minimum distance at which the focal plane can still be perceived sharply. This measurement is part of routine eye examinations in some countries (Burns *et al.*, 2020). The AoA parameter can be assessed either subjectively or objectively. While subjective methods provide information about the person's perception, the objective techniques quantify the actual change in lens refraction.

The latter methods tend to be more expensive and to require more space, time, and trained personnel. Furthermore, closed systems like aberrometers or autorefractors (e.g., Nikon NR7000) can induce instrument myopia (Miwa, 1992), the unconscious accommodation when looking through optical systems (Schober, Dehler and Kassel, 1970). On the contrary, aberrometers and autorefractometers are particularly recommended due to their proven high repeatability and reproducibility (Vargas *et al.*, 2019). In both measurement approaches, a beam of light is projected into the eye and the reflection from the retina is analyzed. While the autorefractor detects the distortions of the projected light beam, the aberrometer measures the non-planarity of the reflected wavefront.

Subjective defocus techniques assess accommodation by increasing the eye's refractive demand through the placement of negative lenses in front of the eye, thereby stimulating it to accommodate and bring a distant visual target into focus. However, they do not directly assess the eye's natural focusing ability on a real, approaching object, as they lack proximal cues (Atchison, Capper and McCabe, 1994). Other subjective measurement methods utilize standardized symbols or characters termed optotypes that are manually moved along a ruler, either towards the eye until the optotype becomes blurry (push-up) or away from the eye from blurred until clear perception (push-down) with best corrected distance vision (Levin *et al.*, 2011). The reciprocal of the distance in meters between the optotype and the participant's eye represents the AoA in diopters. Due to their simplicity, these methods are commonly executed in clinical practice (Rutstein, Fuhr and Swiatocha, 1993; Adler, Scally and Barrett, 2013; Momeni-Moghaddam, Kundart and Askarizadeh,

2014; Esmail and Arblaster, 2017). Criticism of these methods includes subjectivity of the participant's perception of clarity, the potential variability due to depth of focus caused by different pupil diameters, and the examiner's ability to handle these devices (Levin *et al.*, 2011; Burns *et al.*, 2014).

Another approach is to measure neuromuscular electrical potentials elicited by the ciliary muscle during contraction. These accommodation-dependent potential changes were first detected in emmetropes and in one presbyope by Schubert et al. (1955). This was confirmed by Alpern et al. (1958), Jacobson et al. (1958), Hagiwara and Ishikawa (1962) and Clouse (2017), the latter a recent researcher in Prof Zrenner's group at the Institute of Ophthalmic Research at the University of Tübingen. Alpern and Clouse described a saturation above a certain accommodation requirement and showed that the extraocular muscles and the pupil do not influence the detected signal (Alpern, Ellen and Goldsmith, 1958; Clouse M.M, 2017). Hagiwara has proven that an eye under cycloplegia and the associated suppression of parasympathetic muscle activation still generates an albeit reduced biosignal (Hagiwara and Ishikawa, 1962). These signals were recorded with needle electrodes (Jacobson *et al.*, 1958; Hagiwara and Ishikawa, 1962) and scleral contact lens electrodes (Schubert, 1955; Bornschein and Schubert, 1957; Jacobson *et al.*, 1958; Hagiwara and Ishikawa, 1962; Adel, 1966) as well as saline-impregnated cotton wools that were fixed to the sclera by a spring (Jacobson *et al.*, 1958).

Scleral contact lenses, with diameters up to 25 mm, are larger than regular contact lenses and used in clinical routine to protect the healing process of the ocular surface (Van Der Worp *et al.*, 2014). Scleral lenses are particularly useful for detecting the electrical biopotentials of the ciliary muscle, as they benefit from the self-centering nature and ensure a large distance between the two concentrically applied electrode surfaces (Schumayer *et al.*, 2022).

## 1.2 Presbyopia

Presbyopia combines the ancient Greek words "presbys" and "ops", meaning "old eye" (Atchison, 1995). The term can be defined as the age-related reduction in the eye's ability to see clearly at near distances, while far vision imperfections are corrected (Wolffsohn, Naroo, *et al.*, 2024). For individuals, an increased reading effort becomes noticeable from

around the mid-forties (Plainis, Charman and Pallikaris, 2014; Charman, 2017), with a remaining, subjectively measured AoA of three to four diopters (Charman, 2017). This is illustrated by Duane's curve, which shows the gradual decline of the subjectively measured amplitude of accommodation with age (Duane, 1922). From the age of 60, an object closer than one meter to the observer can only be perceived with blurred vision. However, as of 2024, there is still no standardized testing procedure to assess presbyopia (Markoulli *et al.*, 2024).

The reasons for the declining ability to focus near are still being researched, in particular, whether biomechanical or geometric lens changes dominate (Pu *et al.*, 2025). Interestingly, the ciliary muscle itself seems to retain its function in presbyopes (Sheppard and Davies, 2011; Tabernero *et al.*, 2016). Besides the discussion of the dominant declining factor, the inward growth of the lens towards the center (cf. Figure 2, lower left) results in mechanical and geometric changes in the lens properties throughout the lifetime (Koretz *et al.*, 1989; Augusteyn, 2007; Jones, Atchison and Pope, 2007; Kasthurirangan *et al.*, 2011). Consequently, presbyopia is not a disease but rather an age-related condition that everyone experiences from a certain age onwards. It is assumed that 2.1 billion people worldwide will have presbyopia by 2030 (Fricke *et al.*, 2018). Untreated presbyopia reduces quality of life (Berdahl *et al.*, 2020; Markoulli *et al.*, 2024), as over 80% of presbyopes report difficulties with near-vision tasks (Berdahl *et al.*, 2020). Estimates regarding the economic impact vary. Ma et al. (2022) estimate the global economic loss in 2019 at USD 53.41 billion, while Frick et al. (2015) assume economic losses of USD 11 billion at a working age of 50 and USD 25.4 billion at a working age of 65, respectively. Especially in developing countries, presbyopia treatment seems to offer significant economic potential, as in 2008, 94% of the world's uncorrected presbyopes lived in these regions (Holden *et al.*, 2008). For instance, a study where near vision correction was provided to workers in Bangladesh showed that the self-reported median monthly income increased by 33.4% compared to the control group (Sehrin *et al.*, 2024). Therefore, Bastawrous and and Suni (2020) estimate that, by 2050, low-cost presbyopia intervention could boost the economy by USD 1.05 trillion.

### 1.2.1 Treatments of Presbyopia

Presbyopia treatments can be divided by their operating principle into non-invasive, invasive, and pharmacological treatments. All of them have their merits and limitations. Non-invasive, such as reading, bifocal, and progressive glasses, influence the external appearance (Terry, 1990; Hasart and Hutchinson, 1993; AlRyalat *et al.*, 2022). Moreover, the correction of presbyopia with spectacles is accompanied by a reduction in quality of life (Luo *et al.*, 2008; Stokes *et al.*, 2022). Regardless of where a multifocal lens is placed, it has the drawback that the user must learn to concentrate on the correct focal plane (Grzybowski, Markeviciute and Zemaitiene, 2020; Orman and Benozzi, 2021). The duration of the learning phase of this neuroadaptive process depends on the individual (Grzybowski, Markeviciute and Zemaitiene, 2020). Visual impressions through multifocal contact lenses are influenced by pupil diameter, lens centering, and aberrations (Rio, Woog and Legras, 2016). While vision correction with contact lenses always involves certain compromises (Charman, 2014a), their insertion can pose an additional hurdle in people of advanced age. Therefore, invasive corrective measures also have their place, despite a comparably higher risk. These include corneal inlays, which act as a pinhole and therefore increase the depth of field, known as the pinhole effect, as well as corneal index of refraction modification (Moarefi, Bafna and Wiley, 2017). However, small apertures reduce the amount of light on the retina and consequently reduce contrast in low-light conditions (Manion and Stokkermans, 2024). Cornea shrinkage and the resulting abrasion of the corneal collagen due to an energy input represent another method of adjusting the refractive power, which is termed according to the energy source and treatment site (Charman, 2014b; Papadopoulos and Papadopoulos, 2014). LASIK (laser-assisted keratomileusis), for instance, requires a femtosecond laser (> 1000 nm) as an energy source and involves the temporary folding of the corneal flap (Callou *et al.*, 2016). After surgery, the healing of the cornea can influence the contour and therefore the result (Charman, 2014b). Intraocular lenses (IOLs) are another approach, implanted for treating refractive errors of the eye (Bellucci, 2013). They are commonly implanted into the capsular bag during a cataract correction surgery (Bellucci, 2013; Liu *et al.*, 2017), but they can also be inserted into the sulcus of the anterior chamber of the eye (Mehta and Aref, 2019). If stabilization is required, capsular tension rings can be implanted in the ciliary

sulcus (Chen *et al.*, 2020) and also in the lens capsule, preventing, for instance, the capsule from collapsing (Weber and Cionni, 2015). While monofocal IOLs restore near vision only for a certain distance, multifocal IOLs reduce contrast vision and can also lead to visual artifacts such as halos, glare, or starburst (Charman, 2014b; Khandelwal *et al.*, 2019; Schallhorn *et al.*, 2021). Accommodating IOLs are intended to deform in the same way as the human lens, depending on the required accommodation, and thus change the refractive power, but have not yet proven their effectiveness in practice (Beiko, 2013; Pepose, Burke and Qazi, 2017; Varssano, 2024). Accommodating spectacles that utilize gaze tracking and/or distance sensors (Padmanaban, Konrad and Wetzstein, 2019; Agarwala *et al.*, 2022; Karkhanis *et al.*, 2022) measure gaze, vergence, and distance. However, these systems seem to have problems correcting for the near working distance of 36 cm (Bababekova *et al.*, 2011), as well as focusing on small objects. Hosp et al. (2024) showed that participants prefer manual focus control rather than the vergence and gaze control algorithms. Remote-controlled contact lenses currently being researched, capable of switching the focus between distant and near, tend to be too bulky and neglect the oxygen supply to the cornea (Tremblay *et al.*, 2013; Bailey *et al.*, 2022). Pharmacological treatments, in the form of eye drops, could compensate for the drawbacks of the described methods (Stokes *et al.*, 2022). They aim to soften the lens, for example (Grzybowski and Ruamviboonsuk, 2022), while the U.S. Food and Drug Administration (FDA) approved pilocarpine is intended to increase the depth of field by contracting the pupil (Grzybowski, Kapitanovaite and Zemaitiene, 2024; Onyszkiewicz *et al.*, 2024). Although interest in the pharmacological treatment of presbyopia is growing, for both the lens-softening approach and the pin-hole approach, long-term follow-up results are lacking (Grzybowski and Ruamviboonsuk, 2022; Grzybowski, Kapitanovaite and Zemaitiene, 2024). Furthermore, the pilocarpine hydrochloride triggered pin-hole effect leads to public concern about the possible side effects, such as retinal detachment (Wakabayashi *et al.*, 2023). Electric stimulation therapies on the ciliary muscle to restore accommodation (Nesterov and Khadikova, 1997; Gualdi *et al.*, 2017) show a positive effect and increase the amplitude of accommodation by up to 54% (Nesterov and Khadikova, 1997). So far, such treatments were performed for a relatively short period of two (Gualdi *et al.*, 2017) and six months (Nesterov and Khadikova, 1997). In addition, the morphological change

in the ciliary muscle due to the electrical stimulation is still being investigated (Wagner *et al.*, 2023).

## 1.3 Medical Devices and Encapsulation

As part of this work, an intraocular implant and an electrode were developed, with the development of both oriented on the European Medical Device Regulation (MDR) and the relevant standards.

The MDR defines a medical device (MD) as "any instrument, apparatus, appliance, software, implant, reagent, material or other article intended by the manufacturer to be used, alone or in combination, for human beings for medical purposes" such as diagnosis, monitoring, and treatment (Regulation (EU) 2017/745) . As part of the MDR, the terms "active device" and "implant" are also defined. The latter is intended to remain in the body after surgery. Active device refers to the circumstances in which these devices need a source of energy to operate, other than generated by the human body or gravity (Regulation (EU) 2017/745). Devices such as pacemakers, cochlear implants, or, in terms of vision restoration, the subretinal implant, which can partially restore vision in blind retinitis pigmentosa patients (Zrenner *et al.*, 2017), are known as Active Implantable Medical Devices or AIMDs for short. For the approval of such devices, the MDR requires a classification of the device regarding its purpose and risks, clinical evaluation, risk management, and evidence of the biological safety of the device, which can be described in a standardized manner using the results and guidelines of the ISO 10993 series of standards. ISO 10993-1:2024-07 defines the term biocompatibility as follows: "The ability of a medical device or material to function in a given application with an appropriate host response". In this context, the standard describes the consideration of various effects such as toxicity, sensitization, and irritation to ensure that the materials and implant do not harm the body and functionality is guaranteed. The standard also references other standards in the ISO 10993 series to test the aforementioned effects. As the weight, geometry, and flexibility of the implant also influence the body's reaction (Hassler, Boretius and Stieglitz, 2011), compliance with biocompatibility is clarified via ISO 10993-6:2024-06. If sufficient documentation regarding physical, chemical properties, and place of action is similar to that of existing medical devices, biological equivalence can be assumed, thereby reducing the required biological evaluation (ISO 10993-1:2024-07). Considering AIMDs and their

electronic components, a hermetical encapsulation with an excellent diffusion barrier is necessary to prevent the electrical circuit from short-circuiting and corrosion, and the body from possibly toxic materials such as soldering tin. Besides metals and ceramics, polymers are also considered as packaging materials, depending on the implants' given circumstances such as place of implantation or operating time (Mariello *et al.*, 2022). According to ISO 10993-1:2024-07, implants are therefore divided into limited (< 1d), prolonged (1 – 30 d) and long-term (> 30 d) operating time.

Many metals offer exceptional mechanical and tribological properties as well as excellent impermeability, though, over time, leaching of ions can lead to body reactions (Ashish Daniel *et al.*, 2024). However, metals and ceramics lack the feasibility of microfabrication (Ahn, Jeong and Kim, 2019). Although the latter offers excellent corrosion resistance, mechanical hardness, and good impermeability, it is brittle and non-bendable (Shekhawat *et al.*, 2021). Polymers have an enormous variety of mechanical, physical, and chemical properties (Rahmati *et al.*, 2018), whilst their basic moisture absorption makes hermetic sealing difficult. A polymer with relatively low moisture absorption that is increasingly becoming the focus of encapsulation is Parylene C, of which context-relevant properties are briefly described in the section below (q.v. *1.3.1 Encapsulation with Parylene C*).

The choice of material further depends on other requirements such as the need for miniaturization, interaction with the target tissue, manufacturing process, or sterilization process. The latter is essential in ensuring that the device is free of viable microorganisms, termed sterile, according to the ISO 11139:2018 + Amd 1:2024. Commonly, heat, radiation, and chemicals serve as a sterilant with different merits and limitations, and shall be discussed elsewhere (Sundaram Muthuraman, 2015). The chemical ethylene oxide (EO) sterilization process is particularly preferable for temperature-sensitive devices (Mendes, Brandão and Silva, 2007; Sundaram Muthuraman, 2015; Shintani, 2017). Compared to heat sterilization, which exceeds temperatures above 100°C (Sundaram Muthuraman, 2015), or radiation sterilant that tends to cause material degradation (Mendes, Brandão and Silva, 2007; Shintani, 2017), the EO is mostly compatible with all materials and has a low and dry operational temperature between 35 to 60°C (Shintani, 2017).

### 1.3.1 Encapsulation with Parylene C

Parylene C, due to its relatively low water vapor transmission rate (0.12 gm/mil/100in²/24hr at 38°C, 90%RH), is moving into the focus of hermetic encapsulation of medical devices. Further, it has a high dielectric strength of 220 V/µm at a thickness of 25.4 µm, a melting point of 290°C, and a low coefficient of friction of 0.29, measured for both static and dynamic conditions (VSI Parylene, 2025). The material was declared as a highly biocompatible and bio-insulating polymer (Lin *et al.*, 2020), being able to withstand the standard EO sterilization, keeping mechanical and electrical stability (von Metzen and Stieglitz, 2013). It fulfils the strict requirements of USP (United States Pharmacopeia) Class VI, ensuring its suitability for medical applications. It is also FDA approved and fulfills the ISO 10993 standards for biocompatibility (VSI Parylene, 2025).

Before a medical device can be encapsulated by Parylene C, it has to be cleaned to increase adhesion strength. Utilizing the thin film coating technique (q.v. *1.3.2 Thin film coating*), chemical vapor deposition (CVD), the polymer polymerizes at room temperature in vacuum (2 Pa), on the substrate surface after the dimer (poly-para-xylylene) has previously been vaporized at >100°C and pyrolyzed at >500°C, known as the Gorrham process (Golda-Cepa *et al.*, 2020). The polymerization directly from the gas phase without changing to the liquid state reduces the influence of interfacial physical effects, enabling homogeneous layer growth on complex geometries and a deep penetrating ability.

### 1.3.2 Thin film coating

Surface functionalization can be achieved using thin-film techniques without significantly influencing the geometry of the surface, with layer thicknesses of up to around 5 µm (DIN EN 62047-1:2016-12). These techniques are particularly suitable for the miniaturization of components and devices. Functionalization can be used to create chemical, physical and biological properties on the substrates to make them electrically conductive or insulating, improve their tribological properties, give them a more attractive appearance or hermetically encapsulate the underlying material from external influences (Deflorian, 2020). By applying layer thicknesses in the atomic range as in atomic layer deposition (ALD), the properties of the coating can be precisely adjusted (George, 2010). Due to ALD's unique layer-by-layer growth, complex structures can be coated with high conformity and without pinholes, even at nanometer-scale thicknesses (Passlack *et al.*,

2023). Depending on the substrate composition, geometry and required functionalization, different coating processes are to be considered. The most common processes can be categorized in chemical vapor deposition (CVD) and physical vapor deposition (PVD) processes, or a combination of these (Griesser, 2016; Jilani, Abdel-wahab and Hammad, 2017). Both process technologies require preparation in which the substrate is cleaned or activated accordingly via plasma (Kaplan and Rose, 1991; Petasch *et al.*, 1995). For the coating to adhere, the substrate pre-treatment of the coating to be applied is decisive. Any contamination has a negative effect; hence, both CVD and PVD (Mattox, 2002) take place in a controlled vacuum environment. During the PVD process, material is transferred from the solid phase to the gas phase through physical processes such as vaporization or sputtering. This vaporized or ionized material then condenses on the substrate surface (Mattox, 2002). In the CVD process, on the other hand, a gaseous precursor reacts with the substrate surface due to an energetic imbalance. This chemical reaction leads to the deposition of a solid layer on the substrate surface, while excess reaction products are removed from the vacuum chamber by a continuous gas flow (Sun *et al.*, 2021). One modified form of the CVD process is ALD, in which reaction gases are cyclically introduced into the coating chamber in defined and temporally separated process steps, whereby they react in a self-limiting manner with the coating chamber and build up a thin, atomic layer by layer (George, 2010; Griesser, 2016). Figure 3 highlights the advantages and limitations of CVD, PVD, and ALD processes (Breitweiser, Varadarajan and Wafer, 1970; Mattox, 2002; Xu *et al.*, 2021; Yu *et al.*, 2024).


Figure 3 - Comparing coating techniques: The spiderweb-plot shows the essential properties of the different coating techniques atomic layer deposition (ALD), physical- (PVD), and chemical vapor deposition (CVD). (Data compiled from Breitweiser, Varadarajan, and Wafer, 1970; Mattox, 2002; Xu et al., 2021; Yu et al., 2024)

## 1.4 The Scientific Impact

A gradual decline in the ability to focus on close objects with age, called presbyopia, is becoming increasingly apparent in the ageing society. The progression of presbyopia is currently assessed using the residual subjective amplitude of accommodation (AoA), despite the well-known limitations in reproducibility, examiner dependence, and lack of methodological standardization. Reducing known limitations and improving the reliability of AoA is not only relevant for clinical diagnostics but also for its potential role in studies investigating the electrophysiological basis of accommodation. Early studies from the 1960s and 1970s reported the presence of accommodation-related biopotentials presumably emitted by the ciliary muscle. However, these investigations lacked sufficient methodology, and no substantial research activity followed in the decades since. As a result, these signals remain poorly characterized, and their potential functional relevance is largely unexplored.

Since the ciliary muscle remains active with age, even when lens elasticity declines, these neuromuscular signals are hypothesized to be suitable as control inputs for adaptive visual aids aimed at restoring the natural accommodation. Current treatments for presbyopia offer compensation, but not restoration of the dynamic focusing mechanism.

To advance beyond these constraints, this doctoral thesis presents the development of a motorized, examiner-independent system for measuring the subjective AoA, aimed at reducing known limitations and enabling consistent stimulus control. In parallel, ciliary muscle biopotentials were recorded non-invasively using contact lens electrodes during controlled accommodation, with subsequent analysis of signal characteristics and correlation with refractive changes measured via eccentric infrared photorefraction. To improve signal quality at the anatomical source and to avoid external artifacts, a bipolar intraocular ring electrode was designed and fabricated using microsystem technologies. In addition, the encapsulation process of the implant, consisting of electronics and battery, was optimized to allow the implant unit to be mechanically flexible for implantation on the eyeball. The implant was validated in a non-human primate model, including simulated long-term stability of the Parylene C encapsulation and impedance monitoring to assess functional integrity under physiological conditions. Beyond that, in an ongoing study in presbyopes, these signals, measured via a contact lens electrode, shall be utilized

as an input to restore the natural accommodation-reflex loop by a tunable lens. In conclusion, this doctoral thesis is structured around the following scientific inquiries:

- Does a newly developed measurement system for determining the amplitude of accommodation have higher reliability compared to conventional subjective measurement methods?
- Are neuromuscular biopotentials from the ciliary muscle, measured on the ocular surface during accommodation with a contact lens electrode, distinctly measurable and characterizable?
- Are these electrical neuromuscular signals also detectable *in vivo* in the form of an implant using a new type of bipolar ring electrode?
- Are neuromuscular signals from the ciliary muscle still present in individuals with presbyopia?
- Can the natural accommodation-reflex loop be reestablished through a tunable lens, provided that neuromuscular signals from the ciliary muscle can be detected and used as a control input?

# 2. Results

## 2.1 Publication – Motorized Push-Up Ruler

Schumayer, S., Laukhuf, J., & Straßer, T. (2025). Comparing a Novel Motorized Push-Up Ruler with Conventional Subjective Methods for Measuring the Amplitude of Accommodation. Current Eye Research, 1–9. doi:10.1080/02713683.2025.2531524

CURRENT EYE RESEARCH
https://doi.org/10.1080/02713683.2025.2531524

Taylor & Francis
Taylor & Francis Group

OPEN ACCESS Check for updates

# Comparing a Novel Motorized Push-Up Ruler with Conventional Subjective Methods for Measuring the Amplitude of Accommodation

Sven Schumayer[a,b,c], Jona Laukhuf[c] and Torsten Straßer[b,d]

[a]Faculty Mechanical and Medical Engineering (MME), Institute for Microsystems Technology (iMST), Furtwangen University, Furtwangen, Germany; [b]Institute for Ophthalmic Research, University of Tuebingen, Tuebingen, Germany; [c]Research Group Strasser, Institute for Ophthalmic Research, University Hospital of Tuebingen, Tuebingen, Germany; [d]University Eye Hospital Tuebingen, Tuebingen, Germany

**ABSTRACT**

**Purpose:** Determination of the amplitude of accommodation (AoA) is a clinical technique used in ophthalmology and optometry to assess the eye's ability to focus on near objects. This study compares the reliability of a novel motorized push-up variant with conventional manual push-up and push-down methods for the determination of AoA in 26 emmetropes.

**Methods:** The motorized push-up method reduces limitations of the manual methods, such as differences due to varying examiner abilities, ruler placement (forehead, zygomatic bone, spectacle plane), and inconsistent target movement speeds. This is achieved by providing a participant-controlled, constant target movement of 2 cm/s, with the medial zone of the zygomatic bone as the reference point for ruler placement. Additionally, digital image-based and traditional ruler-based AoA measurements were compared. The participants' impressions of the three methods were assessed based on ease of use, confidence in measurement reliability, and comfort of experience, using a questionnaire.

**Results:** The comparison of the AoA across the methods revealed no statistically significant differences. However, the concordance correlation coefficient was highest between the motorized and manual push-up method ($\rho_c$ = 0.72). All methods showed good test-retest reliability with the highest ICC found for the motorized push-up method (0.83), which also had the narrowest limits of agreement interval for accommodative demand (3.22 cm). Beyond digital and ruler-based measurements showed underestimation by both rulers, with a mean bias of 0.3 cm for the motorized ruler compared to about 2.0 cm for the conventional ruler. The questionnaire responses suggest that the motorized version outperforms the manual versions being 5 times more likely to score higher for ease of use and 6 times more likely for confidence in measurement reliability.

**Conclusion:** These findings demonstrate that the motorized push-up method effectively measures the AoA, reduces interfering factors, and provides higher reliability without compromising precision, making it a valuable alternative to conventional methods.

**ARTICLE HISTORY**
Received 23 December 2024
Accepted 3 July 2025

**KEYWORDS**
Amplitude of accommodation; push-up method; motorized accommodation ruler

## Introduction

Accommodation enables clear near vision by altering the shape of the crystalline lens.[1–3] This ability decreases throughout life, mainly due to physiological changes in the lens of the eye, which eventually leads to presbyopia.[3] Consequently, the near point, measured as the amplitude of accommodation (AoA), shifts into the distance. Other factors besides aging affecting the AoA are, amongst others, type 1 diabetes[4–6] or binocular accommodation insufficiency.[7,8] A 2021 Portuguese study investigating accommodative and binocular vision dysfunctions in a clinical population found that accommodative insufficiency was the most prevalent single dysfunction, present in 11.5% of non-presbyopic patients consulting an optometrist.[8] Accommodative insufficiency has also been reported as the most prevalent cause of asthenopia (50.7%).[9] Therefore, determining the AoA is part of the standard ophthalmic examination in many countries[10] for diagnosis and treatment.[11] Objective measurement methods provide more accurate values but require more complex and expensive equipment,[12,13] which is not available in every clinical setting, especially not in developing countries. Furthermore, they need a certain amount of space for installation and considerable time for staff training and measurement execution. Therefore, due to their simplicity, subjective measurement of AoA is generally used in routine clinical procedures[11,14–16] and research.[5,17–20] Subjective measurement methods consider individual perception to determine visual comfort by utilizing blur of an accommodative target (e.g. Duane's figure) created either by decreasing (push-up) or increasing (push-down) the target distance relative to the eye or by adding minus lenses until the target blurs. The former methods provide the clinically more important subject's point of clear vision[21] using

**CONTACT** Jona Laukhuf jona.laukhuf@student.uni-tuebingen.de Research Group Strasser, Institute for Ophthalmic Research, University Hospital of Tuebingen, Elfriede-Aulhorn-Street 7, 72076 Tuebingen, Germany

Supplemental data for this article can be accessed online at https://doi.org/10.1080/02713683.2025.2531524.

measuring instruments such as the Royal Air Force (RAF) ruler, where a slide with a target is moved along a ruler length.[22,23] Criticisms of the subjective method include the variable speed of slide movement resulting in latencies,[10,24] and possible mishandling of the device,[10] which may explain the reported low inter-examiner repeatability.[16,25] According to Burns et al. total latency consists of the time it takes the participant to detect the blur, the time it takes to notify the examiner, and the examiner's response time to stop the slide.[10] Even if the target is moved manually at an apparently constant speed, fluctuations occur, affecting the measurement precision. Other criticisms include the placement of the ruler and the end point of the measurement, such as the lens plane,[12] the forehead,[17] the cheek near the lower orbital rim,[20] or the zygomatic bone. Endpoint and placement are often not reported in the literature [13,15,26] limiting comparability between subjective measurements and between subjective and objective measurements. Kanclerz et al. (2022) showed a moderate agreement ($r = 0.5502$, $p < 0.001$) between AoA measured with a Nidek Autorefractormeter AR-1a and the subjective push-up method using an RAF near-point ruler.[12] To improve the precision and repeatability of the AoA measurements, we developed a novel push-up ruler with a motorized target slider that moves at a constant speed of 2 cm/s, controlled by the participant, eliminating the examiner's reaction time. The AoA obtained with the newly developed motorized ruler was compared with those measured with the conventional push-up and push-down methods in 26 young emmetropic volunteers and analyzed for reliability and repeatability. In addition, we defined the medial zone of the zygomatic bone as the reference point for ruler placement and compared the conventional distance measurement with a digital evaluation based on images. Further, the participants were asked to rate the ease of use, confidence in measurement reliability, and comfort of each instrument using a questionnaire.

## Material and methods

The Motorized Accommodation Ruler (MAR, Figure 1(a)) was designed using commercially available components to ensure that other research groups could easily and inexpensively rebuild the ruler to replicate the experiment. A detailed description of components is provided in the *Supplementary Materials*.

### Accommodative target

The figure to focus on was a 0.2 mm thick and 10 mm long line between two 5 mm thick and 10 mm long black rectangles on a white background, also known as the Duane's figure (Figure 1(b)). Duane tested different objects, such as parallel lines or geometrical figures, but concluded that a line 0.2 mm thick and 3 mm long was the most practicable object to focus on.[27] Additionally, due to the figure's simplicity, it is also suitable for children and illiterate people.

### Target movement speed

The target movement speed of the accommodative target (2 cm/s) is defined as the product of maximum resolution ($x$) and the considered reaction time of 300 ms, which reflects the delay between perceiving blur and releasing the trigger. The resolution ($x$) was calculated using Equation 1, with the minimum length ($f$) set at 7.4 cm, based on the maximum achievable AoA in 10-year-old children, which is on average 13–13.5 D,[28] and the constraint that the tolerance ($\Delta D$) should not exceed +1 diopter.

$$\Delta D = \frac{1}{f - x} - \frac{1}{f} \qquad \text{(Eq. 1)}$$

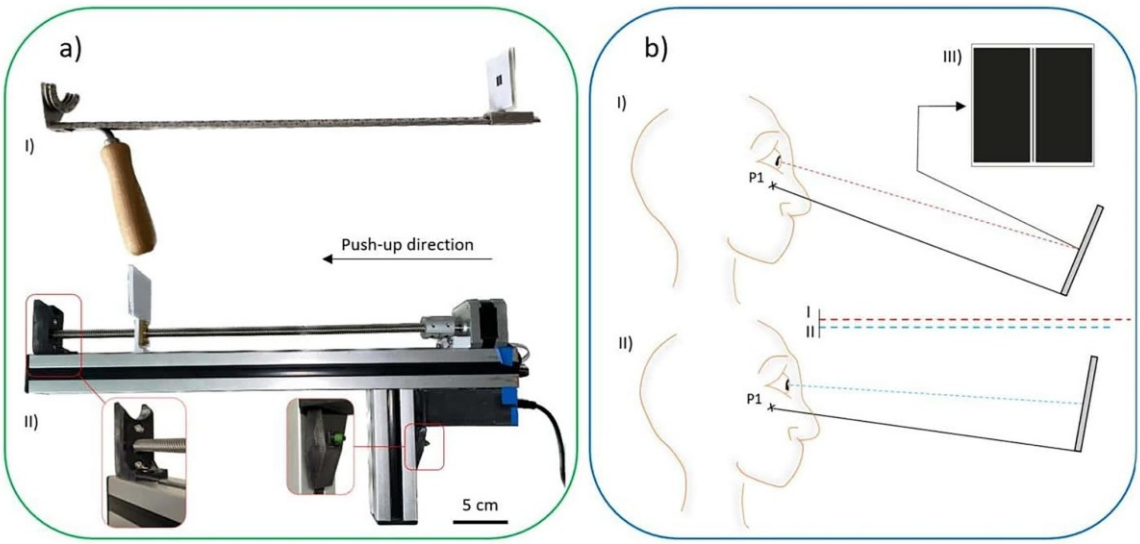


**Figure 1.** Accommodation rulers and the influence of angle.

### Participants and pre-examination

Young emmetropic participants were recruited from the student body of the University of Tübingen and included in the study based on the following inclusion criteria: age between 18 and 35 years with corrected spherical equivalent refractive error < ± 0.5 D and no more than < −4.0 to 0.5 D uncorrected, with best-corrected visual acuity ≥ 20/20 and astigmatism less than 2.0 D. Participants with previous or current eye injury, strabismus, amblyopia, pseudophakia, intake of drugs with a known complication for measuring the accommodation were excluded from the study. Objective refraction and visual acuity were measured using an autorefractometer (AR-330A/AR-360A, NIDEK CO., LTD., Gamagori, Japan). Additionally, the dominant eye was determined by placing both outstretched hands on top of each other to form a hole of approximately 3 cm in size for focusing a distant target, similar to the Dolman hole-in-card test.[29,30] The study followed the tenets of the Declaration of Helsinki and was approved by the Institutional Review Board of the Medical Faculty of the University in Tuebingen (618/2023BO2). All participants gave written informed consent for voluntary participation after receiving the participant's information.

### Measurement procedure

The randomized order of the different measurement methods was determined before testing. The ambient brightness was kept between 40 and 80 lx to reduce a possible pinhole effect, which could increase the depth of field due to a small pupil size.[31] Additionally, the accommodation amplitude was measured monocularly in the corrected dominant eye to prevent vergence and reduce pupillary constriction.[32,33] Before measurement, the different methods were explained to the participants. Care was taken to ensure that all received the same explanations about the measurement's blurred and sharp endpoints. In all three measurement methods, the volunteer held the respective accommodation ruler (Figure 1(a)) and rested against the medial zone of the zygomatic bone. Once a stable and correct alignment of the manual accommodation ruler was assured, the examiner tried to move (push-down: away from the participant; push-up: towards the participant) the slide with the target at a constant speed of 2 cm/s in the respective direction until the participant perceived the image as sharp or blurred. For the motorized push-up measurement, with the MAR, the participant was instructed to focus on Duane's figure after a stable and correct alignment and to press the button until the figure was perceived to be out of focus. The manual and motorized push-up method started at a distance of 36 cm. The distance between the figure and the cheek support was measured and the reciprocal was calculated. For the subsequent digital measurement, participants were instructed to hold the ruler with the target in its stopping position while side-view images were captured, by a 12-megapixel camera (Iphone 12, Apple Inc.; Cupertino, CA, USA), to document the distance between the center of the participant's cornea and the center of the target. The digital evaluation is expected to eliminate the influence of the inclination of the accommodation ruler (c.f. Figure 1(b)). Each measurement method was performed three times and repeated three more times after a 15-minute break, reducing potential training effects. After the measurements, the participants were asked to rate the measurement methods on a Likert scale from 1 to 10 in terms of ease of use, confidence in measurement reliability, and convenience of operation, with 10 being the best rating.

### Data processing & statistics

The agreement between the three measurement techniques – push-up, push-down, and motorized push-up – was assessed using Lin's concordance correlation coefficient (CCC).[34,35] The limits of agreement (LOA) were determined through Bland-Altman analysis.[36] In both analyses, three linear mixed-effects models (LMMs) were employed for each combination of measurement techniques (1: motorized push-up vs. push-up, 2: motorized push-up vs. push-down, 3: push-down vs. push-up,), with the measured distance as dependent variable (y) and the independent variables technique as fixed (a) and participant (β) as random effects as well as their interaction (Equation 2), to utilize all data from all repetitions ($t = 1.6$) while accounting for repeated measures.[37,38]

$$y_{ijt} = \mu + a_i + \beta_j + (a\beta)_{ij} + \varepsilon_{ijt} \quad \text{(Eq. 2)}$$

In a second analysis, the test–retest reliability of each measurement technique was assessed using the intra-class coefficients (ICC), type 3,1[39] calculated from the results of the first three trials with those of the subsequent three trials measured approximately 15 min later using random effects models with distance as the dependent variable and the random factors participant (α) and pass (β: first, second) nested in participant, using data from all repetitions ($t = 1.6$) (Equation 3). Subsequently, ICC confidence intervals were estimated by bootstrapping ($n = 5000$).

$$y_{ijt} = \mu + a_i + a\beta_{i|j} + \varepsilon_{ijt} \quad \text{(Eq. 3)}$$

The mean difference between the first and second pass and the LOA for Bland-Altman analyses were estimated using linear mixed-effects models for each measurement technique separately with distance as the dependent variable, the fixed effect pass (b: first, second), and the random effects participant (α) and pass nested in participant, including all repetitions again ($t = 1.6$) (Equation 4).[40]

$$y_{ijt} = \mu + \alpha_j + b_i + ab_{i|j} + \varepsilon_{ijt} \quad \text{(Eq. 4)}$$

All assumptions were checked and reported if violated before leveraging the results of the linear mixed-effects models.

The agreement between the measurements obtained manually and digitally was evaluated by differences and the LOA using Bland-Altman analysis. The digital measurement was obtained by counting pixels in the image. Using the known

thickness of the cheek rest (15 mm) as a reference, a scaling factor was determined in ImageJ (version 1.54h)[41] to calculate the distance between the center of the participant's cornea and the center of Duane's line figure. The mean of the three measurements from the first pass of each measurement method was used, after verifying normality, and reported in the case of violations.

Ordinal logistic regression analyses were conducted to examine the relationship between users' ratings regarding 1) ease of use, 2) confidence in measurement reliability, and 3) comfort of experience, all measured on an ordinal 1–10 Likert scale, and the type of measurement (manual vs. motorized) as the independent variable. Before the interpretation of the models' results, the assumptions of ordinal logistic regression, the goodness of fit, and the parallelism of the lines were evaluated and reported if violated.

Besides the SPSS 29.0.2.0 (IBM, Armonk, NY, USA) analyses to determine the ICC, all other statistical analyses were performed using JMP Pro 17.2 (JMP Statistical Discovery LLC, Cary, NC, USA) and R version 4.4.1[42] with the packages lme4 version 1.1–35.4,[43] emmeans version 1.10.4,[44] and boot version 1.3–30.[45] Alpha was set to 0.05 for all statistical analyses.

**Table 1.** Five-number summary statistics of the amplitude of accommodation for the 26 study participants, measured in two passes of three trials each, with a 15-minute break in between.

| | | | Distance (cm) | | | | |
|---|---|---|---|---|---|---|---|
| Pass | Trial | Method | Min. | Q1 | Median | Q3 | Max. |
| First | 1 | Motorized push-up | 9.7 | 11.4 | 13.4 | 15.9 | 19.5 |
| | | Push-down | 11.3 | 12.1 | 13.8 | 16.0 | 24.0 |
| | | Push-up | 10.0 | 11.1 | 13.0 | 15.8 | 19.4 |
| | 2 | Motorized push-up | 8.5 | 11.9 | 14.3 | 15.6 | 19.4 |
| | | Push-down | 10.0 | 12.5 | 13.5 | 15.7 | 18.2 |
| | | Push-up | 9.9 | 11.5 | 12.8 | 16.0 | 19.9 |
| | 3 | Motorized push-up | 10.5 | 11.7 | 14.0 | 15.6 | 19.4 |
| | | Push-down | 10.5 | 12.5 | 13.5 | 15.7 | 18.4 |
| | | Push-up | 10.0 | 11.3 | 13.2 | 16.2 | 20.2 |
| Second | 1 | Motorized push-up | 10.0 | 12.1 | 14.3 | 16.7 | 19.9 |
| | | Push-down | 9.4 | 12.3 | 13.5 | 15.4 | 20.1 |
| | | Push-up | 10.1 | 11.7 | 13.8 | 17.3 | 24.3 |
| | 2 | Motorized push-up | 10.0 | 11.6 | 14.0 | 16.4 | 20.1 |
| | | Push-down | 9.3 | 12.2 | 13.7 | 15.6 | 20.0 |
| | | Push-up | 10.4 | 11.5 | 13.3 | 17.0 | 21.4 |
| | 3 | Motorized push-up | 9.7 | 11.0 | 13.1 | 16.5 | 19.0 |
| | | Push-down | 10.0 | 12.0 | 13.5 | 15.4 | 19.5 |
| | | Push-up | 9.7 | 10.7 | 12.8 | 16.1 | 18.7 |

This was repeated for each measurement technique – push-up, push-down, and motorized push-up – in a randomized order.

## Results

A total of 26 emmetropic participants (19 males; age 19 – 32 years, median 26 years) were included in the study. Table 1 presents the five-number summary statistics of the amplitude of accommodation.

### *Comparison of the different measurement techniques*

The standard agreement model assumptions[37] were met except for the model's motorized push-up vs. push-down and push-down vs. push-up, which both exhibited heteroscedasticity. Table 2 lists the least-squares means of the distances depending on the measuring technique and the 95% confidence intervals predicted by the models, along with the converted values in diopters.

The models revealed no statistically significant differences between the paired comparisons of the least-squares means of the measurement techniques (c.f. Table 3). LOA intervals of accommodative demand were shortest between the motorized push-up and push-up method (8.65 cm), followed by

**Table 2.** Least-squares means of the amplitude of accommodation for each measuring technique, with 95% confidence intervals predicted by the models, including the corresponding values in diopters.

| | | AoA LS means ± SE (cm) | | 95% CI | |
|---|---|---|---|---|---|
| LMM | Method | (cm) | (D) | (cm) | (D) |
| 1 | Motorized push-up | 14.00 ± 0.54 | 7.1 | [12.90, 15.10] | [6.6, 7.8] |
| | Push-up | 13.92 ± 0.54 | 7.2 | [12.82, 15.02] | [6.7, 7.8] |
| 2 | Motorized push-up | 14.00 ± 0.48 | 7.1 | [13.03, 14.97] | [6.7, 7.7] |
| | Push-down | 14.04 ± 0.48 | 7.1 | [13.07, 15.01] | [6.7, 7.6] |
| 3 | Push-down | 14.04 ± 0.50 | 7.1 | [13.02, 15.07] | [6.6, 7.7] |
| | Push-up | 13.92 ± 0.50 | 7.2 | [12.89, 14.95] | [6.7, 7.8] |

**Table 3.** Comparison of the different measurement techniques: The table shows the differences, 95% confidence intervals of the differences, and limits of agreement (LOA) from the Bland-Altman analysis, with diopter values provided as reference.

| | Difference | | 95% CI | | LOA | |
|---|---|---|---|---|---|---|
| Comparison | (cm) | (D)[a] | (cm) | *p*-value | (cm) | (D)[a] |
| Push-up – motorized push-up | −0.08 | 0.04 | [−0.59, 0.43] | .3821 | [−4.40, 4.25] | [−3.2, 1.7] |
| Push-down – motorized push-up | 0.05 | −0.05 | [−0.53, 0.62] | .3940 | [−4.83, 4.92] | [−3.8, 1.8] |
| Push-up – push-down | −0.12 | 0.06 | [−0.64, 0.39] | .3582 | [−4.51, 4.26] | [−3.3, 1.7] |

[a]The diopters are calculated relative to the absolute values of the minuends.

the push-up vs. push-down method (8.77 cm), with the largest interval between the motorized push-up vs. push-down method (9.75 cm). These values correspond to diopter values relative to the reference minuend of 4.9 D, 5.0 D, and 5.6 D, respectively (Figure 2, Bland-Altman analyses).

The concordance correlation coefficients calculated using the variance components of the linear mixed-effects models were 0.72 between the push-up and the motorized push-up technique, 0.69 between the push-up and push-down technique, and 0.56 between the motorized push-up and the push-down technique.

### Test–retest reliability of the different measurement techniques

According to the guidelines of Koo and Li,[46] all three measurement methods demonstrate good test–retest reliability. The motorized push-up method had the highest ICC at 0.83 (95% CI: [0.77, 0.89]), followed by the manual push-up method with an ICC of 0.81 (95% CI: [0.71, 0.89]). The manual push-down method showed the lowest ICC, at 0.70 (95% CI: [0.57, 0.83]). Accordingly, none of the post hoc tests of the results of the linear mixed-effects models revealed a statistically significant difference between the least-squares means of the amplitude of accommodation of the first and the second run of the measurements (Table 4).

In line with the ICC values, the LOA of agreement of the accommodative demand is the shortest for the motorized push-up method (3.22 cm). However, the manual push-up method (4.44 cm) and the manual push-down method (3.90 cm) are longer.

### Comparison of the manual and digital evaluated distances

The Bland-Altman analyses (Figure 3) show a systematic mean difference (MD) between the digitally calculated (calc.) and manually measured (meas.) values. For the push-up method, the mean difference (MD) was 1.965 cm (95% CI: [1.49, 2.48], $p < 0.001$), and for the push-down method 1.859 cm (95% CI: [1.44, 2.28], $p < 0.001$), indicating that the measured values (meas.) were underestimated in both cases. However, no significant mean difference was found for the motorized push-up method based on the MAR (MD: 0.258 cm, 95% CI: [−0.26, 0.81], $p = 0.294$). There is a strong positive correlation between the two evaluations calc. and meas., which is mostly similar between the different AoA measurement methods ($ICC_{push\text{-}up}$: 0.8979, $ICC_{push\text{-}down}$: 0.8899, $ICC_{motorized\ push\text{-}up}$: 0.8808).

### Questionnaire

The model fits for model 1) ease of use and model 2) confidence in measurement were statistically significant, whereas the fit for model 3) comfort of experience was not, suggesting that the former two were effective in differentiating the volunteers' subjective impression of ease of use and confidence of measurement between the manual and motorized procedures (Table 5). However, the Pseudo-$R^2$ values (Nagelkerke) suggest only weak relationships between the type of measurement and the resulting scores. In both models, the factor type of measurement was statistically significant (model 1: $b = 1.64$, SE 0.53, Wald = 9.463, $p$ = .002;

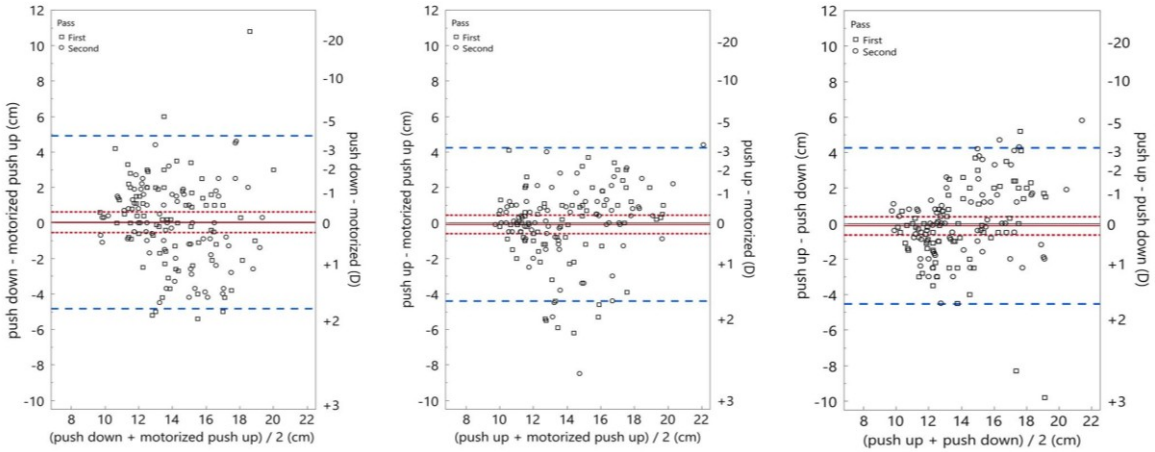


Figure 2. Bland-Altman analyses of the measurement techniques.

Table 4. Least-squares means of the amplitude of accommodation (AoA) for the three measurement techniques during the first and second passes, the differences (first – second pass) with bootstrapped 95% confidence intervals, as well as the limits of agreement (LOA).

| | AoA LS means ± SE (cm) | | | | | |
|---|---|---|---|---|---|---|
| Method | First | Second | Difference (cm) | 95% CI (cm) | *p*-Value | LOA (cm) |
| Motorized push-up | 13.89 ± 0.53 | 14.10 ± 0.53 | −0.21 | [−0.68, 0.26] | .3830 | [−1.82, 1.40] |
| Push-up | 13.72 ± 0.57 | 14.12 ± 0.57 | −0.39 | [−0.88, 0.09] | .1124 | [−2.61, 1.83] |
| Push-down | 14.08 ± 0.46 | 14.00 ± 0.46 | 0.08 | [−0.46, 0.62] | .7655 | [−1.87, 2.03] |

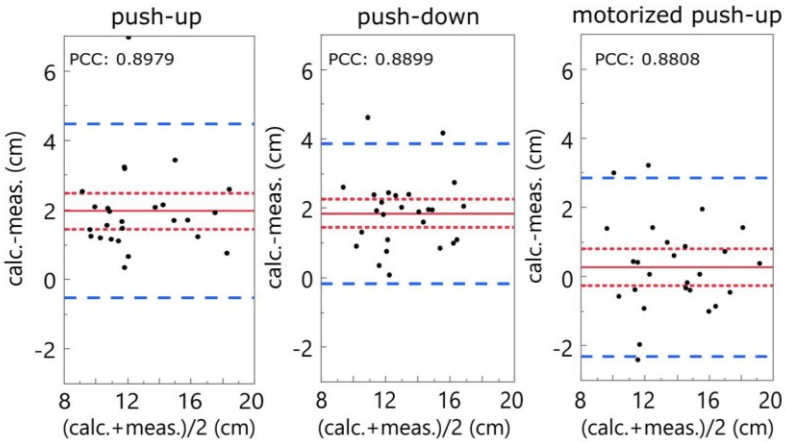


**Figure 3.** Evaluation of the manual and digital measurement.

**Table 5.** Fitting information and assumption checks for the ordinal logistic regression models.

| Model | Fitting information | Goodness-of-fit[a] | Pseudo-$R^{2b}$ | Test of parallel lines |
|---|---|---|---|---|
| 1) Ease of use | $\chi^2(1)=10.100, p=.001$ | $\chi^2(5)=2.365, p=.797 p=.797$ | .18 | $\chi^2(5)=2.604, p=.761 p=.761$ |
| 2) Confidence in measurement | $\chi^2(1)=11.897, p<.001 p<.001$ | $\chi^2(7)=8.461, p=.294 p=.294$ | .20 | $\chi^2(7)=13.800, p=.055 p=.055$ |
| 3) Comfort of experience | $\chi^2(1)=3.400, p=.065 p=.065$ | $\chi^2(7)=9.225, p=.237 p=.237$ | .06 | $\chi^2(7)=15.254, p=.033 p=.033$ |

[a]Pearson, [b]Nagelkerke Pseudo $R^2$.

model 2: $b=1.77$, SE = 0.53, Wald = 11.122, $p < .001$) with positive relationships suggesting a 5.13-fold odds ratio (95% CI: [1.85, 15.2]) for greater perceived ease of use and a 5.85-fold odds ratio (95% CI: [2.11, 17.3]) for greater confidence in measurement using the motorized in contrast to the manual procedure. However, the type of measurement does not seem to affect the comfort of the experience. The evaluation of the summarized ratings is shown in supplementary material (S1).

## Discussion

With the increasing focus on new solutions for presbyopia, such as accommodative aids[47] and pharmacological treatments,[48] the need for fast and reproducible methods to measure the amplitude of accommodation (AoA) is becoming more important. Beyond presbyopia, the motorized accommodation ruler could be used to determine the near point of convergence and thus help to assess convergence insufficiency, a condition that affects approximately 5% of individuals performing near work and reading tasks.[22] Also utilizing it as a screening tool, particularly to address the prevalence of refractive asthenopia, such as observed in computer science students.[9]

The commonly applied ruler-based methods to measure the AoA are known to have limitations,[10,16,24,28] in particular, high variability that can cause differences of up to 3 D. Some of the variability may be due to inter-examiner differences; others are most likely due to individual differences in the perception of blur. Additionally, the variable speed of movement of the accommodative target used in the studies, ranging from 4 mm/s[49] to 5 cm/s,[25,50] most likely also contributes to the reported variability.[16,24] Burns et al. (2014) identified five categories of error in clinical measurements of AoA using the push-up and -down methods,[51] which they later refined into eleven different sources.[10] In addition to depth of focus (DOF), they highlighted reaction time as the major source of error. They also noted that other errors associated with Duane-style methods – such as the reference point for measurement, instrumentation error, and operator bias – can be at least partially mitigated.[51] To address the limitations of the current methods and to increase the reliability of measurements, the motorized push-up accommodation ruler was developed, in which the accommodative target moves with constant speed until the participant starts to perceive blur and releases a trigger, thereby eliminating inter-examiner variability and reducing delays to the participant's reaction time only. The speed of movement of the accommodative target is rarely considered in studies, although it can significantly influence results. We used a constant linear target speed of 2 cm/s to ensure a practical balance between test duration and participant response time. This speed was chosen because it is fast enough to enable efficient testing, yet still allows participants sufficient time to detect blur onset. However, the accommodative demand increases nonlinearly as the target moves closer to the eye. Therefore, using a nonlinear speed profile, such as diopters per second, may provide a more physiologically meaningful stimulus and potentially improve measurement accuracy, particularly in the proximity of the near point. While the motorized ruler permits electronically controlled speed adjustments, including nonlinear trajectories, this aspect was not addressed in the present study. Instrumentation error is reduced by defining a fixed reference point for measurement and digitally assessing the exact distances between the visual target and the center of the cornea. To account for a possible effect of

depth of field, the room illumination should be kept between 40 and 80 lx to avoid a pinhole effect resulting from small pupil diameters. In a recent review, Charman (2019) found a linear dependence between total DOF and pupil diameter for diameters larger than approximately 2 mm, while for diameters smaller than 2 mm, the DOF increases exponentially.[52] However, with the defined illumination, neither young (20–29 years) nor old (≥ 70 years) participants are likely to have pupil diameters less than 2 mm,[53] limiting the resulting total DOF to about 0.7 D.[52] For the sake of completeness, it should also be mentioned, that while the objective measurement of the AoA is not affected by the DOF, it can be affected by instrument myopia.[54]

The comparison between the different measurement methods tested in the study (push-up, push-down, motorized push-up) showed no statistically significant differences between the mean AoA determined by the different methods. The test–retest reliability was good for both the motorized push-up (ICC: 0.83) and the push-up method (ICC: 0.81), while it was moderate for the push-down method (ICC: 0.70). The motorized push-up method demonstrated the narrowest limits of agreement for the repeated measurements (3.22 cm), outperforming the manual push-down (3.90 cm) and push-up method (4.44 cm). The results show that the motorized push-up method is the most consistent and reliable.

Manual measurement of the AoA showed an underestimation of approximately 2 cm for both the push-up and push-down methods compared to values determined from digital photographs. In contrast, the motorized push-up method exhibited a much smaller underestimation of approximately 0.3 cm. This discrepancy may be due to design differences between the measurement instruments. While conventional accommodative rulers are often designed to rest on the zygomatic bone, they may not always achieve this alignment, which can lead to tilting. In contrast, the motorized accommodation ruler is positioned directly in front of the eye with a notch-like indentation that prevents misalignment.

Whereas image-based measurements use the cornea's center as the reference point to ensure consistent and precise determination of the AoA, manual methods rely on less standardized reference points due to anatomical variability, as there is no universally defined "offset" distance between the eye and the ruler to adjust measurements. Burns et al. discuss the influence of ruler tilt relative to the head and the measurement reference point on AoA, further underscoring the limitations of manual techniques.[10] This variability is particularly significant in young emmetropic persons with high AoA where an accurate reference point is critical. Under these conditions, the MAR showed minimal variation compared to manual methods, indicating that it provides a more precise and practical assessment of AoA and is closely aligned with image-based measurements.

The results of the assessment of the subjective impressions of the application of the different methods for measuring the AoA show that the acceptance of the motorized version is superior to the manual version in terms of ease of use, with a 5-fold chance of a higher score, and in terms of confidence in the reliability of the measurement, with a 6-fold chance of a higher score. However, the comfort of experience score did not significantly differ between the motorized and manual measurements.

The simplicity and reproducibility of accommodation rulers will encourage scientists and clinicians to continue using them in the future. Certain limitations and potential improvements of this study should be acknowledged. The weight distribution and form factor of the motorized accommodation ruler require further optimization to improve its usability and convenience. Beyond that, the study population had a mean age of 26 years, which limits the generalizability of the results. Future studies should evaluate the handling and measurement accuracy of the device in a broader population, including older presbyopic individuals and younger emmetropic participants.

## Conclusion

The new motorized accommodation ruler reduces the influence of the examiner by moving the accommodative target at a constant speed of 2 cm/s while the participant holds the trigger until blur is noticed. The motorized accommodation ruler is on par with current clinical routine measurement methods but offers higher retest reliability with lower variability, improved user-friendliness, and higher confidence in the measurement system by the participants. Due to its design, the MAR shows a lower susceptibility to underestimation of the amplitude of accommodation. The next steps will be to test the device in daily clinical practice to determine its potential to replace existing methods.

## Disclosure statement

The authors declare that the research was conducted in the absence of any commercial or financial relationships that could be construed as a potential conflict of interest.

## Funding

Sven Schumayer and Torsten Straßer were funded by the Carl Zeiss Foundation "Breakthroughs at Universities 2020: Intelligent Solutions for an Aging Society," the University of Tuebingen, the Faculty of Medicine of the University of Tuebingen, and the Center for Ophthalmology at the University of Tuebingen. We acknowledge support by Open Access Publishing Fund of University of Tübingen.

## Data availability statement

The data that support the findings of this study are available from the corresponding author, JL, upon reasonable request.

## References

1. Atchison DA. Accommodation and presbyopia. Ophthalmic Physiol Opt. 1995;15(4):255–272. doi:10.1046/j.1475-1313.1995.9500020e.x.
2. Glasser A. Accommodation: mechanism and measurement. Ophthalmol Clin North Am. 2006;19(1):1–12, v. doi:10.1016/j.ohc.2005.09.004.

3. Charman WN. The eye in focus: accommodation and presbyopia. Clin Exp Optom. 2008;91(3):207–225. doi:10.1111/j.1444-0938.2008.00256.x.
4. Adnan E, Sirakaya E, Abokyi S, Hussaindeen JR, Franco S, Amalia H, Burns DH, Rutstein RP, Kanclerz P, Win-Hall DM, et al. Amplitude of accommodation in type 1 diabetes. Invest Ophthalmol Vis Sci 2014;55(10):7014–7018. doi:10.1167/iovs.14-15376.
5. Sirakaya E, Arici C, Ozbas M, Karahan E, Yilmaz E. The influence of type 1 diabetes mellitus on amplitude of accommodation. Curr Eye Res. 2020;45(7):873–878. doi:10.1080/02713683.2020.1726406.
6. Abokyi S, Ilechie A, Asaam KA, Ntodie M. Fasting plasma sugar: a predictor of accommodative function in diabetes. Curr Eye Res. 2016;41(6):791–797. doi:10.3109/02713683.2015.1056803.
7. Hussaindeen JR, Murali A. Accommodative insufficiency: prevalence, impact and treatment options. Clin Optom (Auckl). 2020;12:135–149. doi:10.2147/OPTO.S224216.
8. Franco S, Neves H, Queiros A, Lopes-Ferreira D, Jorge J, Gonzalez-Meijome JM. Accommodative and binocular vision dysfunctions in a Portuguese clinical population. J Optom. 2022;15(4):271–277. doi:10.1016/j.optom.2021.10.002.
9. Amalia H, Jusuf K, Prihartono N. Accommodative insufficiency as cause of asthenopia in computer-using students. Universa Med. 2010;29(2):78–83. doi:10.18051/UnivMed.2010.v29.78-83.
10. Burns DH, Allen PM, Edgar DF, Evans BJW. Sources of error in clinical measurement of the amplitude of accommodation. J Optom. 2020;13(1):3–14. doi:10.1016/J.OPTOM.2019.05.002.
11. Rutstein RP, Fuhr PD, Swiatocha J. Comparing the amplitude of accommodation determined objectively and subjectively. Optom Vis Sci. 1993;70(6):496–500. doi:10.1097/00006324-199306000-00008.
12. Kanclerz P, Pluta K, Momeni-Moghaddam H, Khoramnia R. Comparison of the amplitude of accommodation measured using a new-generation closed-field autorefractor with conventional subjective methods. Diagnostics (Basel). 2022;12(3):568. doi:10.3390/diagnostics12030568.
13. Win-Hall DM, Ostrin LA, Kasthurirangan S, Glasser A. Objective accommodation measurement with the Grand Seiko and Hartinger coincidence refractometer. Optom Vis Sci. 2007;84(9):879–887. doi:10.1097/OPX.0b013e3181559ace.
14. Esmail H, Arblaster G. A comparison of conventional and modified push-up methods of measuring the near point of accommodation. Br Ir Orthopt J. 2016;13:35–39. doi:10.22599/bioj.100.
15. Momeni-Moghaddam H, Goss DA, Taheri H, Sobhani M, Lotfi H. Comparing measurement techniques of accommodative amplitudes. Indian J Ophthalmol. 2014;62(6):683–687. doi:10.4103/0301-4738.126990.
16. Adler P, Castaño VD, Esteve-Taboada JJ, Montés-Micó R. Test–retest reproducibility of accommodation measurements gathered in an unselected sample of UK primary school children. Br J Ophthalmol. 2013;97(5):592–597. doi:10.1136/bjophthalmol-2012-302348.
17. Castagno VD, Vilela MAP, Meucci RD, Resende DPM, Schneid FH, Getelina R, Nasiloski MR, Fassa AG. Amplitude of accommodation in schoolchildren. Curr Eye Res. 2017;42(4):604–610. doi:10.1080/02713683.2016.1220586.
18. Evans BJW, Drasdo N, Richards IL. Investigation of accommodative and binocular function in dyslexia. Ophthalmic Physiol Opt. 1994;14(1):5–19. doi:10.1111/j.1475-1313.1994.tb00550.x.
19. Wagner S, Altay L, Nguyen NX, Weindler J, Reinhard T, Wilhelm H, et al. Monocular transcorneal electrical stimulation induces ciliary muscle thickening in contralateral eye. Exp Eye Res. 2023;231:109475. doi:10.1016/j.exer.2023.109475.
20. Parkinson J, Khurana RN, Griepentrog GJ, Diehl NN, Mohney BG. Subjective measurement of the near point of accommodation in pre/early literates. Am Orthopt J. 2001;51(1):75–83. doi:10.3368/aoj.51.1.75.
21. Atchison DA, Capper EJ, McCabe KL. Critical subjective measurement of amplitude of accommodation. Optom Vis Sci. 1994;71(11):699–706. doi:10.1097/00006324-199411000-00005.
22. Sharma IP. RAF near point rule for near point of convergence – a short review. Ann Eye Sci. 2017;2(3):16–16. doi:10.21037/aes.2017.02.05.
23. Neely JC. The RAF near-point rule. Br J Ophthalmol. 1956;40(10):636. doi:10.1136/bjo.40.10.636.
24. Salvador-Roger R, Bueno-Gimeno I, García-Lázaro S, Luque-Cobija J, Vera J, et al. Subjective and objective measurements of the amplitude of accommodation: revisiting the existing methods and clinical evaluation of newer techniques. Ophthalmic Physiol Opt. 2025;45(3):761–768. doi:10.1111/opo.13482.
25. Antona B, Barrio A, Barra F, Gonzalez E, Sanchez I. Repeatability intraexaminer and agreement in amplitude of accommodation measurements. Graefes Arch Clin Exp Ophthalmol. 2009;247(1):121–127. doi:10.1007/s00417-008-0938-9.
26. Win-Hall DM, Glasser A. Objective accommodation measurements in pseudophakic subjects using an autorefractor and an aberrometer. J Cataract Refract Surg. 2009;35(2):282–290. doi:10.1016/j.jcrs.2008.10.033.
27. Duane A. An attempt to determine the normal range of accommodation at various ages, being a revision of Donder's experiments. Trans Am Ophthalmol Soc. 1908;11(Pt 3):634–641.
28. Wold RM. The spectacle amplitude of accommodation of children aged six to ten. Am J Optom Arch Am Acad Optom. 1967;44(10):642–664. doi:10.1097/00006324-196710000-00004.
29. Pointer JS. Sighting dominance, handedness, and visual acuity preference: three mutually exclusive modalities? Ophthalmic Physiol Opt. 2001;21(2):117–126. doi:10.1046/j.1475-1313.2001.00549.x.
30. Dolmen P. Tests for determining the sighting eye. Am J Ophthalmol. 1919;2:867. doi:10.1016/S0002-9394(19)90258-3.
31. Morgan MW. Accommodation and vergence. Am J Optom Arch Am Acad Optom. 1968;45(7):417–454. doi:10.1097/00006324-196807000-00002.
32. Bharadwaj SR, Wang B, Candy TR. Pupil responses to near visual demand during human visual development. J Vis. 2011;11(4):6–6. doi:10.1167/11.4.6.
33. Chirre E, Prieto PM, Schwarz C, Artal P. Dynamics of the near response under natural viewing conditions with an open-view sensor. Biomed Opt Express. 2015;6(10):4200–4211. doi:10.1364/BOE.6.004200.
34. Lin LI. A concordance correlation coefficient to evaluate reproducibility. Biometrics. 1989;45(1):255. doi:10.2307/2532051.
35. Chen CC, Barnhart HX. Comparison of ICC and CCC for assessing agreement for data without and with replications. Comput Stat Data Anal. 2008;53(2):554–564. doi:10.1016/j.csda.2008.09.026.
36. Bland JM, Altman DG. Statistical methods for assessing agreement between two methods of clinical measurement. Lancet. 1986;1(8476):307–310.
37. Parker RA, Scott C, Inácio V, Stevens NT. Using multiple agreement methods for continuous repeated measures data: a tutorial doi:10.1186/s12874-020-01022-x.
38. Parker RA, Weir CJ, Rubio N, Rabinovich R, Pinnock H, Hanley J, McCloughan L, Drost EM, Mantoani LC, MacNee W, et al. Application of mixed effects limits of agreement in the presence of multiple sources of variability: exemplar from the comparison of several devices to measure respiratory rate in COPD patients. PLoS One. 2016;11(12):e0168321. doi:10.1371/journal.pone.0168321.
39. Shrout PE, Fleiss JL. Intraclass correlations: uses in assessing rater reliability. Psychol Bull. 1979;86(2):420–428. doi:10.1037/0033-2909.86.2.420.
40. Bland JM, Altman DG. Measuring agreement in method comparison studies. Stat Methods Med Res. 1999;8(2):135–160. doi:10.1191/096228099673819272.
41. Schneider CA, Rasband WS, Eliceiri KW. NIH Image to ImageJ: 25 years of image analysis. Nat Methods. 2012;9(7):671–675. doi:10.1038/nmeth.2089.
42. Team RC. R: a language and environment for statistical computing. 2024.
43. Bates D, Mächler M, Bolker B, Walker S. Fitting linear mixed-effects models using lme4. J Stat Softw. 2015;67(1):1–48. doi:10.18637/jss.v067.i01.
44. Lenth VR. emmeans: estimated marginal means, aka least-squares means. 2024.
45. Davison AC, Hinkley DV. Bootstrap methods and their application. Cambridge: Cambridge University Press; 1997.

46. Koo TK, Li MY. A guideline of selecting and reporting intraclass correlation coefficients for reliability research. J Chiropr Med. 2016;15(2):155–163. doi:10.1016/j.jcm.2016.02.012.
47. Charman WN. Developments in the correction of presbyopia II: surgical approaches. Ophthalmic Physiol Opt. 2014;34(4):397–426. doi:10.1111/opo.12129.
48. Grzybowski A, Markeviciute A, Zemaitiene R. A review of pharmacological presbyopia treatment. Asia Pac J Ophthalmol (Phila). 2020;9(3):226–233. doi:10.1097/APO.0000000000000297.
49. Somers WW, Ford CA. Effect of relative distance magnification on the monocular amplitude of accommodation. Optom Vis Sci. 1983;60(11):920–924.
50. Majumder C, Afnan H. Amplitude of accommodation among students of a Malaysian private university as assessed using subjective and objective techniques. Korean J Ophthalmol. 2020;34(3):219–226. doi:10.3341/kjo.2019.0138.
51. Burns D, Allen PM, O'Leary DJ. Clinical measurement of amplitude of accommodation: a review. Optom Pract. 2014;15:75–86.
52. Charman WN. Pinholes and presbyopia: solution or sideshow? Ophthalmic Physiol Opt. 2019;39(1):1–10. doi:10.1111/opo.12594.
53. Koch DD, Samuelson SW, Haft EA, Merin LM. Pupillary responsiveness: implications for selection of a bifocal intraocular lens. Ophthalmology. 1991;98(7):1030–1035. doi:10.1016/S0161-6420(91)32181-X.
54. Miwa T. Instrument myopia and the resting state of accommodation. Optom Vis Sci. 1992;69(1):55–59. doi:10.1097/00006324-199201000-00009.

## 2.2 Publication – Contact Lens Electrode

Schumayer, S., Sigdel, B., Jarboui, M. A., Zrenner, E., Bucher, V., Straßer, T., & Wagner, S. (2025). Non-invasive measuring of biopotentials of the ciliary muscle during accommodation in emmetropes. Scientific Reports, 15(1), 19389. doi:10.1038/s41598-025-04165-3

www.nature.com/scientificreports

scientific reports

Check for updates

OPEN

# Non-invasive measuring of biopotentials of the ciliary muscle during accommodation in emmetropes

Sven Schumayer[1,2], Bishesh Sigdel[2], Mohamed Ali Jarboui[3], Eberhart Zrenner[2], Volker Bucher[1], Torsten Straßer[2,4]✉ & Sandra Wagner[2]

**To see near objects clearly, the ciliary muscle shapes the human eye's crystalline lens to adjust its refractive power, a process known as accommodation. This contraction of the ciliary muscle also results in an electrical potential change. Previous work from the 1950s and 1960s reported electrical voltages in the microvolt range that were attributed to the accommodating ciliary muscle, however without clarifying the interaction between lens and muscle. Here, we present data of 12 emmetropic participants using a custom-developed scleral contact lens electrode which enables to record accommodation-dependent biopotentials of the ciliary muscle with an accuracy up to the millivolt range. Therefore, participants alternately shifted their focus from far to various near targets while the biopotentials of the ciliary muscle and the actual refractive change of the crystalline lens were recorded by a contact lens electrode and an eccentric infrared Photorefractor. In addition, the impact of confounding biopotentials such as squinting and eye movements was investigated. Our research points to a potentially new objective method of measuring accommodative change. Understanding these biopotentials could lead to the development of self-focusing visual aids as an alternative way of vision correction in presbyopes.**

**Keywords** Contact lens electrode, Biopotential, Ciliary muscle, Accommodation

To shift the focal point from a far to a near target, the ciliary muscle in the human eye increases the dioptric power of the crystalline lens, a process known as accommodation[1]. Today's understanding of accommodation is based on Helmholtz's theory of 1855[2] with Fincham's amendments[3] and remains a topic of ongoing debate[4]. The dominant stimuli triggering the change of the refractive power are blur and vergence[5–7] resulting in what is commonly referred to as a "near triad" of accommodation, convergence and pupil constriction[6,7]. Helmholtz postulated that the contraction of the triangular ciliary muscle, which is concentrically arranged around the lens, and in particular its differently arranged muscle fibers, causes the lens to become more spherical and translate the anterior lens surface forward[8,9]. This is obtained by zonular fibers, a suspensory ligament, that reduces the tension between the ciliary body and the elastic lens capsule[8,10]. However, the ability to accommodate diminishes with age, typically becoming noticeable between the age of 40 to 45 years[11]. This loss of function, known as presbyopia, is assumed to be due to physiological changes of the crystalline lens in terms of geometry and material properties, which are still the subject of current research[12,13]. Several vision correction methods are currently available, including spectacles[14,15] contact lenses[15] ophthalmic surgeries[14,16] and pharmaceutical treatments[14,17,18]. Each of these approaches has its own advantages and limitations, with some still requiring further research[19]. All of these options have in common that they only treat the symptoms of presbyopia and do not restore natural accommodation. In particular, they are unable to close the interrupted feedback loop of the accommodative system. This is due to the age-related non-functioning crystalline lens[20] resulting in an inability to close the feedback loop in presbyopes even with the intact ciliary muscle[21]. The ability to measure these signals from the human ciliary muscle using, for example, contact lens electrodes, was demonstrated by various researchers nearly a century ago[22–26]. Schubert et al., 1955 were the first to record bioelectric signals (0.3 mV) in

[1]Faculty Mechanical and Medical Engineering (MME), Institute for Microsystems Technology (iMST), Furtwangen University, Furtwangen, Germany. [2]Institute for Ophthalmic Research, University of Tuebingen, Tuebingen, Germany. [3]Core Facility for Medical Bioanalytics, Institute for Ophthalmic Research, University of Tuebingen, Tuebingen, Germany. [4]University Eye Hospital Tuebingen, Tuebingen, Germany. ✉email: torsten.strasser@uni-tuebingen.de

eight emmetropes and one presbyope, which they attributed to the ciliary muscle using exclusion proceedings[23]. In 1958, Alpern recorded voltage changes of up to 0.2 mV during a focus change from far to near, which were positively correlated with the accommodation effort. Alpern excluded electrical muscle artifacts based on the experimental setup and demonstrated that the contributions of the pupil response were negligible[26]. Hagiwara and Ishikawa (1962) measured potential changes of up to 0.15 mV in the accommodated state using a contact lens electrode, with these changes decreasing during cycloplegia[25].

The aim of the present study was to investigate the electrical potentials of the ciliary muscle during the controlled presentation of accommodative stimuli at various distances, using a previously described novel bipolar scleral contact lens electrode[27]. Biopotentials were recorded in a group of young healthy emmetropes while simultaneously measuring changes in the refractive state of the crystalline lens. Potential confounding sources of the recorded biopotentials other than the ciliary muscle were analyzed by eliciting pupillary responses, gaze changes, eye squinting, and by paralyzing the ciliary muscle using cycloplegia. Additionally, a proteomic analysis was performed to investigate if the contact lens wear triggers any major inflammatory response. The ability to reliably record the electrical potentials provides a new tool for advancing the research on the ciliary muscle, extending beyond just presbyopia. Ultimately, these biopotentials could be used to close the interrupted feedback loop of the accommodative system in presbyopia[20] by controlling an artificial lens to restore dynamic accommodation.

## Results

The refractive error in the spherical equivalent was $-0.06 \pm 0.33$ D (mean ± s.d.) and the amplitude of accommodation in the left eye was $8.2 \pm 1.39$ D. All participants presented with monocular visual acuity of 20/20 or better. The right eye was the dominant in 8 out of 12 participants.

### Biopotentials for different viewing distances

An overview of the measured biopotentials at the different distances is shown in Fig. 1a. The LMM ($R^2$= 0.4) reveals a highly significant influence of the fixed effect accommodation demand ($F(4, 97.01) = 9{,}3966$, $p < 0.0001$) while the fixed effect *session* ($F(1, 97.67) = 0.1247$, $p = 0.7248$) and the resulting interaction effect ($F(4, 97.26) = 0.148$, $p = 0.9635$) between *accommodation demand* and *session* showed no significant influence. The estimated least-squares means show that the accommodation demand of 4.0 D led to the highest biopotentials (-0.325 mV, 95% CI: [-0.45, -0.199]), while 2.0 D (-0.157 mV, 95% CI: [-0.282, -0.032]), 2.5 D (-0.219 mV, 95% CI: [-0.344, -0.093]) and 3.0 D (-0.187 mV, 95% CI: [-0.313, -0.062]) showed values that were similar in range. Compared to the far target at a distance of 0.2 D (0.186 mV, 95% CI: [0.06, 0.311]), a post hoc Tukey-HSD test shows a high significance (cf. Figure 1b) between the far and every near target. Similar results are seen in the LMM ($R^2$= 0.86) of the measured refractive changes of the participants (cf. Supplementary Figure S1). This model indicates a highly significant influence of the fixed effect *accommodation demand* ($F(4, 97.01) = 10.3704$, $p < 0.0001$), while neither *session* ($F(1, 97.03) = 0.1520$, $p = 0.6975$), nor their interaction ($F(4, 97.01) = 1.0234$, $p = 0.3992$) showed any significant influence. However, discrepancy was seen by the random effect *subject*. While 82.57% of the total variance of the mean refraction change could be explained by the random effect subject, it was 0.887% for the mean biopotential. A comparison between the normalized mean biopotential values and the change in refraction shows a weak positive correlation within the first session ($r = 0.208$; $p = 0.1108$).

Modeling the normalized biopotentials with logistic sigmoid functions revealed differences in the dynamic properties between accommodation and disaccommodation (Fig. 2): While both are not correlated with accommodative effort (2.0, 2.5, 3.0, 4.0 D), disaccommodation shows a higher growth rate compared to accommodation, indicating a faster response when focusing from near to far. Accordingly, the time of maximum change is slightly shorter for the disaccommodation, while the maximum and minimum response remain constant for all far-near and near-far responses.

### Measurement of confounding biopotentials

The course of the biopotential during the entire measurement of experimentally-induced confounding factors shows a signal characteristic which is distinguishable from the accommodation-related signals, noticeable in signal shape, amplitude level, and rate of change. Figure 3a shows the negative response at a rate of -167.6 µV/s reaching an average of $-0.211 \pm 0.313$ mV after changing accommodation from far (0.2 D) to near (3.0 D), and a positive response at 271.4 µV/s reaching $0.162 \pm 0.372$ mV after disaccommodation. In contrast, the rate of change of the signals resulting from horizontal gaze change (left to right: 37.5 µV/s; right to left: -36.3 µV/s), pupil constriction (-27 µV/s), and squinting (41 µV/s) is much lower. The entire measurement of the horizontal gaze change combined with the biopotential can be found in the Supplementary Figure S2. Furthermore, the signals exhibit greater variability between repetitions compared to those resulting from accommodation or disaccommodation, as indicated by the 95% confidence intervals (Fig. 3b).

### Cycloplegia

During cycloplegia, all 5 volunteers were unable to accommodate with their treated right eye, shown by an amplitude of accommodation far below 2 diopters. Contrary to expectations, however, the biosignals were only extinguished in 2 of the 5 participants (Fig. 4 left). A Bland-Altman analysis reveals no statistically significant differences between the mean amplitudes of the second and those of the third appointment under cycloplegia ($t(14) = -1.051$, $p = 0.3112$, two-tailed, cf. Figure 4 right). The mean biopotential velocity for the three volunteers, during disaccommodation from 4.0 D to 0.2 D, is 283.5 µV/s and for accommodation −315 µV/s after cyclopentolate application. Refractive change in the untreated left eye is unaffected and comparable to results before cycloplegia, also showing no significant difference between the second and third appointment ($t(14) = -0.176$, $p = 0.8629$, two-tailed).

a)

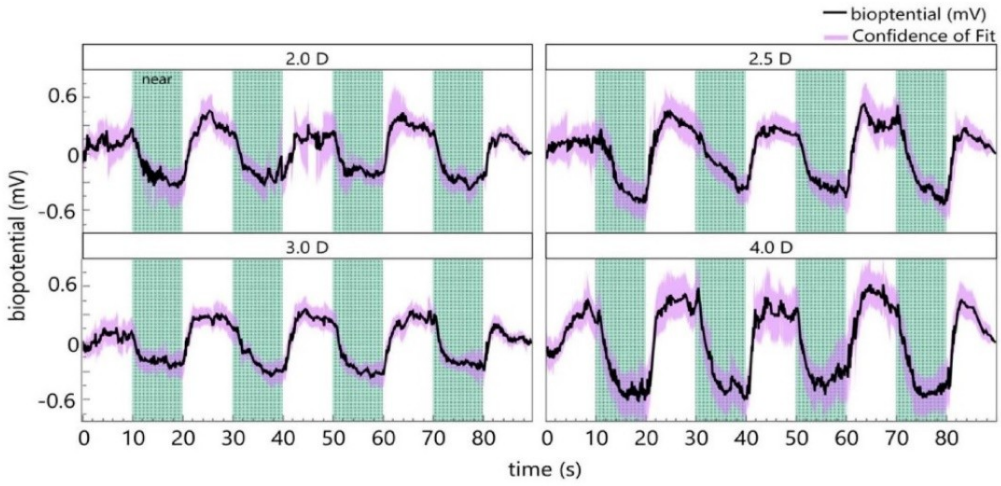


b)

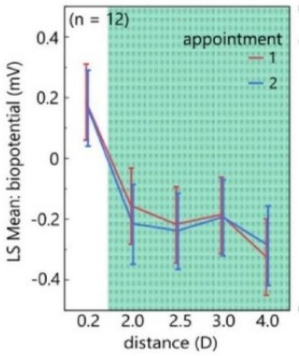


| Comparison | Difference (mV) | 95% CL | p-value |
|---|---|---|---|
| 0.2 D vs. 4.0 D | 0.5103 | [0.2629, 0.7577] | <.0001*** |
| 0.2 D vs. 2.5 D | 0.4042 | [0.1568, 0.6516] | .0002*** |
| 0.2 D vs. 3.0 D | 0.3730 | [0.1257, 0.6204] | .0006*** |
| 0.2 D vs. 2.0 D | 0.3426 | [0.0953, 0.5900] | 0.0019** |
| 2.0 D vs. 4.0 D | 0.1676 | [-0.0797, 0.4150] | 0.3330 |
| 3.0 D vs. 4.0 D | 0.1372 | [-0.1101, 0.3846] | 0.5380 |
| 2.5 D vs. 4.0 D | 0.1061 | [-0.1413, 0.3535] | 0.7558 |
| 2.0 D vs. 2.5 D | 0.0615 | [-0.1858, 0.3089] | 0.9579 |
| 3.0 D vs. 2.5 D | 0.0311 | [-0.2162, 0.2785] | 0.9967 |

α = .05, p < .001***, p < .01**, p < .05*

**Fig. 1**. Biopotentials for different viewing distances: (**a**) The biopotential was filtered (bandpass, 2nd order, 0.025–0.575 Hz) and arranged between 0 to 1. Moving average of the biopotentials (width:10) of the two measurement appointments for all participants[x] with the purple shaded area as the 95%-confidence of fit. Green bars represent the 10 s period of near vision at the different distances (2.0, 2.5, 3.0, 4.0 D). (**b**) (left) The LS mean plot of the electrical potential amplitude over the different accommodative demands for the first and second appointment. (Right) Results of the post hoc Tukey-HSD test, comparing the mean amplitude between different accommodative demands. [x]Measurements (ID:02 2.0D & ID:02 4.0D) were excluded.

## Proteomics analysis

Using DIA proteomics analysis, a total of 3738 proteins from 22 samples were identified and quantified. Principal component analysis (PCA) showed no clear clustering between the samples before or after lens wear. Furthermore, a paired two-sample t-test did not identify any proteins differentially changing in abundance between the 2 groups (before and after). These results suggest that the contact lens electrode wear did not trigger any major response that could lead to an increased abundance of specific proteins as a response mechanism to the wear of the scleral contact lens electrode (Fig. 5).

## Discussion

Using a newly developed bipolar scleral contact lens electrode[27] we were able to record electrical potentials from the ciliary muscle during accommodation in 12 emmetropic volunteers, which are consistent with results from previous literature[22–26,28]. In contrast to those, we measured the signal during an altering far-near-far stimulus together with the actual refractive change, using an eccentric infrared photorefraction. We did find a significant difference between the far and every near stimulus ($p < 0.0001$), however, the amplitude between different near targets did not differ significantly. This signal progression was already described in previous work[26] and this kind of behavior was seen for the ciliary muscle thickness changes during accommodation[29]. However, we believe that the amplitude of the biosignal may not be the key parameter for detecting finer accommodative changes. We hypothesize that the accommodative apparatus (including the crystalline lens, the ciliary muscle, and the retina as a blur detector), is a closed-loop system in which the ciliary muscle continuously adjusts the curvature of the

a)

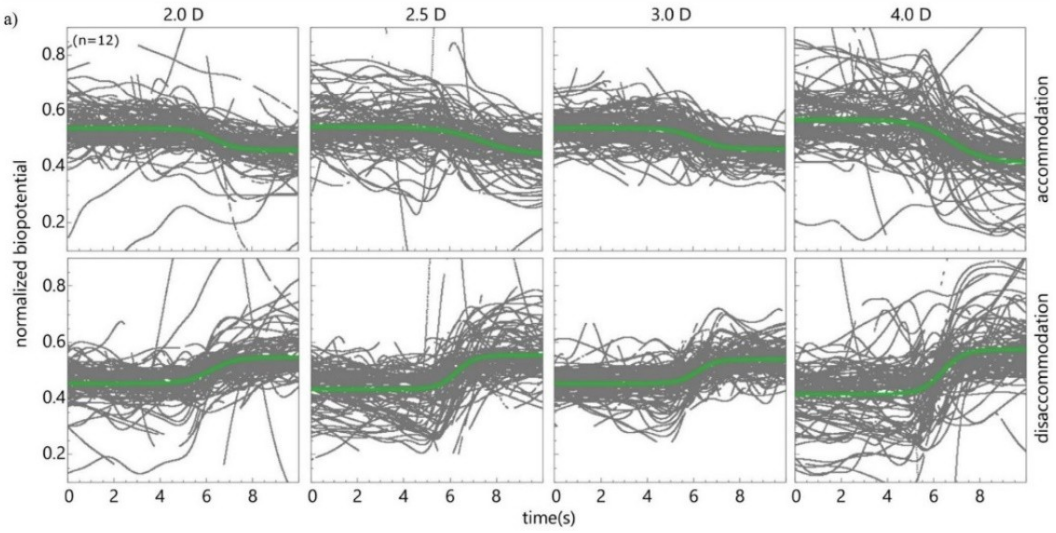


b)

| | 2.0 D | | 2.5 D | | 3.0 D | | 4.0 D | |
|---|---|---|---|---|---|---|---|---|
| **Estimated Parameter** | acc. | dis. | acc. | dis. | acc. | dis. | acc. | dis. |
| **a = Growth Rate** | -2.0229 | 1.9300 | -1.1301 | 2.4677 | -1.7951 | 2.4679 | -1.3225 | 2.1768 |
| **b = Inflection Point** | 6.3466 | 6.1959 | 7.3472 | 6.2742 | 6.1924 | 6.1751 | 6.7605 | 6.3725 |
| **c = Lower Asymptote** | 0.4609 | 0.4533 | 0.4441 | 0.4324 | 0.4635 | 0.4523 | 0.4158 | 0.4150 |
| **d = Upper Asymptote** | 0.5389 | 0.5460 | 0.5444 | 0.5541 | 0.5395 | 0.5391 | 0.5694 | 0.5745 |

acc. = accommodation
dis. = disaccommodation

**Fig. 2**. Curve fitting: (**a**) Logistic sigmoid curve fitting of normalized biopotential responses during accommodation (top row) and disaccommodation (bottom row) at different stimuli (2.0, 2.5, 3.0, 4.0 D). Each plot presents the individual responses to each sequence (grey lines, $n = 12$) with the fitted sigmoid curve (solid green line) over time (seconds). The time interval covers 5 s before and after the respective stimulus. (**b**) The table contains the estimated parameters from the sigmoid fitting showing the dynamic properties of the biopotential responses, with notable differences in rate of change (b.a) between dis- and accommodation, whereas lower (b.c) and upper (b.d) asymptote, stays mostly similar. The inflection point (b.b) seems to be slightly faster during disaccommodation.

lens as long as blur is present on the retina. Once the blur is minimized, the muscle will likely stop contracting and consequently, the biopotential change will stop. For a biomimetic visual aid with a tunable lens, the presence of this biopotential change is of significance.

Interestingly, the sigmoidal fitting indicates that the rate of change in biopotentials from near to far was higher compared to far to near, for near vision target greater than 2.0 D, which is consistent with findings reported in the literature for changes in refractive power[30,31]. The determined inflection point - the time of the strongest change - is slightly earlier in disaccommodation compared to accommodation. A non-significant ($p = 0.8064$) difference was seen between the two measurement appointments, revealing the repeatability of the biopotential measurement. The inter variability, known from measurements of the refractive changes, could also be observed for the biopotentials. One possible explanation is that differences in crystalline lens curvatures of individuals[9] result in different accommodative efforts. It is also known that the lag of accommodation varies among individuals[30] as does the tonic accommodation[32,33] and the individuum's ability to sympathetically control the accommodation[34]. In terms of electrophysiology, the fit of the lens on the eye surface of the participants is also an essential factor, as this defines the electrical contact area. Studies[35,36] have already established a concentric asymmetry and inter variability of the sclera. The polarity of the biopotential, becoming more negative during accommodation, can be explained by the connection of the electrode to the detection unit. While Schubert et al. (1955) and Hagiwara Ishikawa (1962), described an increasing positive polarity with a far-to-near stimulus, Alpern et al. (1958) described the opposite. Nonetheless, all three described an accommodation-related voltage change between 0.15 and 0.3 mV. This is consistent with this study, in which the 4.0 D accommodation demand resulted in the highest amplitudes of -0.32 ± 0.629 mV (mean ± s.d.). However, in some participants (e.g., ID: 08), amplitudes as high as -1.9 mV were measured.

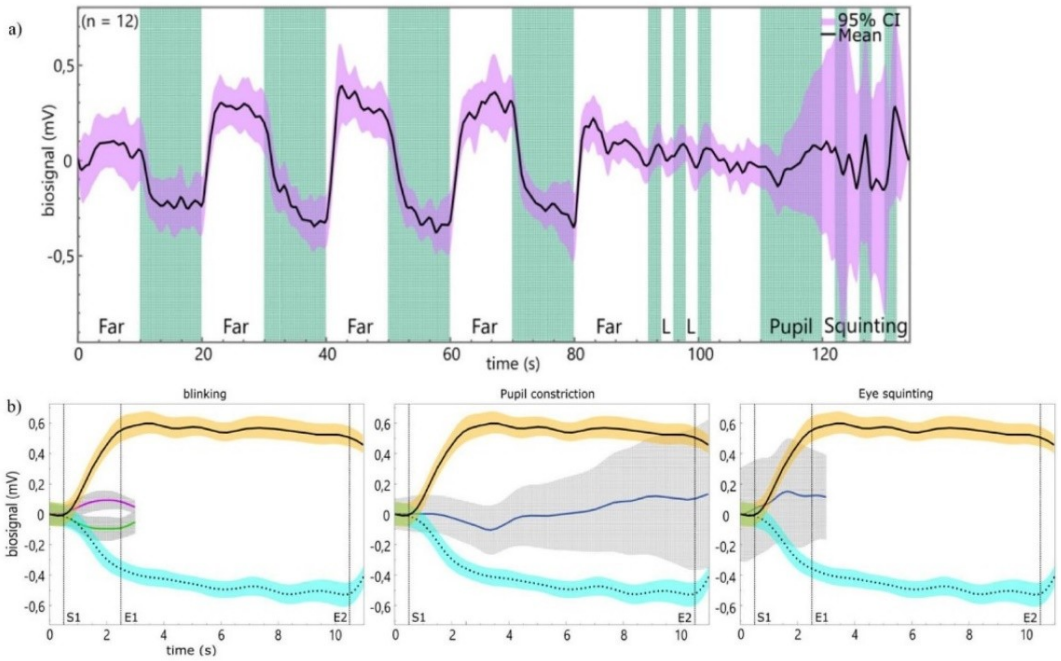


**Fig. 3**. Confounding biopotentials: (**a**) An overview of the entire confounding signal measurement, in which the 2° horizontal eye deflection to the right and left (L), the forced pupil constriction, and the eye squinting were measured after an iterative change between far and near. The y-axis represents the biopotentials in millivolt and the black line the mean for the two measurement appointments for all participants, while the 95% confidence interval is shown as the purple shaded area. Individual sequences are marked in green. The plots in (**b**) show different confounding signal means compared to the accommodation-related biopotentials together with the 95% confidence interval. Accommodation is shown by the black dotted line, while disaccommodation is represented by the black line and orange confidence intervals. The start (S1 at 0.5 s) and endings of the sequence (E1 at 2.5 s; E2 at 10.5 s) are marked by the vertical dashed lines. The signal progression during horizontal eye movement to the left is shown as a green (-) and to the right as a purple (+) line.

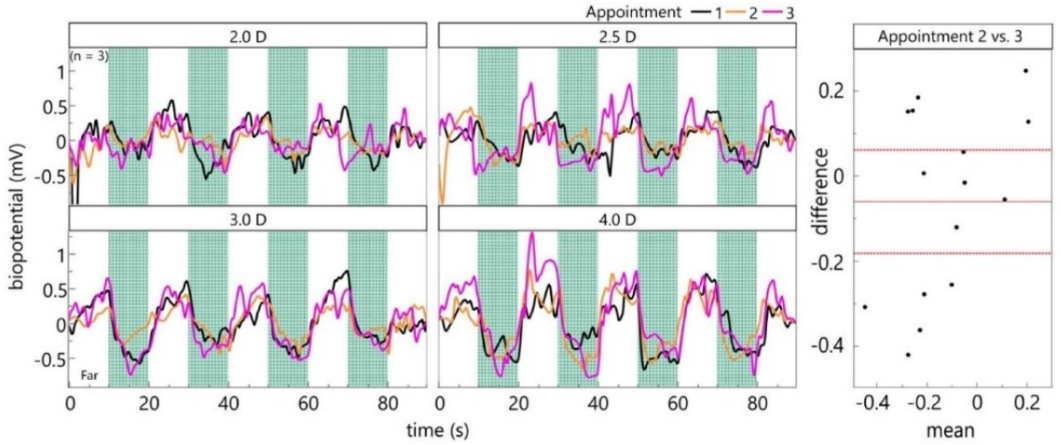


**Fig. 4**. Cycloplegia: Left: Averaged biopotentials of three participants for each appointment and accommodation demand. Right: Bland-Altman plot for the biopotentials shows no significant difference between the second and the third appointment (under cycloplegia) for the three participants.

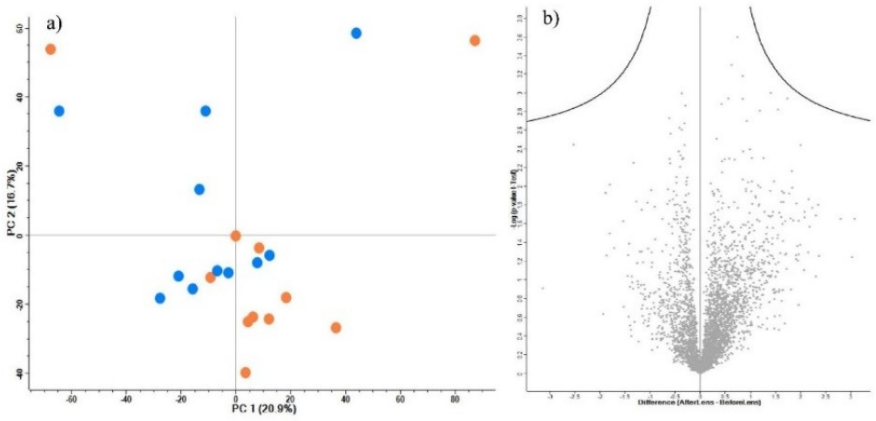


**Fig. 5**. Proteomics analysis: (**a**) The PCA plot shows no clear segregation between the proteome before (blue dots) or after (orange dots) contact lens electrode wear. (**b**) Volcano plot of differential proteins abundance analysis using two samples t-test shows no significant changes (two-sided student t-test using permutation-based truncation FDR < 0.05).

Presenting the participants different visual stimuli, we could show that those biopotentials caused by eye movements, squinting or pupil constriction differ noticeably in signal characteristics compared to accommodation driven ones, which was also mentioned, however not shown, in the work of Hagiwara and Ishikawa[25]. The calculated rate of change shows very similar behavior to the observations made when measuring different near distances. Interestingly, the horizontal eye movement between right and left differed in polarity and showed a waveform already described by Jacobson et al. (1958). Considering this shape, amplitude height, and the calibration of the setup before the measurement to minimize possible eye movements, the extraocular muscles can be neglected as the origin of the accommodation-related biosignals. Eye squinting caused the contact lens electrode to move, leading to a shift in the ion concentration and thus to a change in polarity. Taking the short ion-change into account, a spiking signal is expected. Additionally, the biosignals recorded during pupil constriction differ from those caused by accommodation, which excludes the sphincter pupillae muscle as the origin of the signal. By eliminating these muscles as the signal source, we assume to have measured the origin of the accommodation related biopotentials to the ciliary muscle. This consideration raises the question of whether the measured signal is a neuro- or muscular-electrical signal. To answer this question, the ciliary muscle was paralyzed temporarily in five participants. If the measured signal is of muscular origin, it should no longer be possible to record a signal due to paralysis. By applying the cycloplegia Cyclopentolate 1%, the receptors of the ciliary muscle are blocked against the parasympathetically released neurotransmitter acetylcholine. Comparison of the biopotentials with the previous measurements nevertheless shows no difference in 3 out of 5 participants. We also exclude the sympathetic nervous system as the source, as the ciliary muscle is mainly intervened by parasympathetic nerve endings[37] and the sympathetic part is characterized as relatively slow (30 to 40 s) and with low accommodation changes (≤ 2.0 D)[38] having no significant involvement in rapid focusing[39].

Beside probably the most common cycloplegic agent, cyclopentolate 1%[40], other commonly used agents such as tropicamide and atropine were also considered to clarify the origin of the signal. The ideal cycloplegic agent and its application are continuously discussed in the literature[40–43]. Atropine is regarded as the gold standard for achieving complete cycloplegia[41,42,44] especially when administered over a period of 3 days[42]. However, it effects persist for 8–14 days[42] and the risk of side effects is seven times higher than with cyclopentolate[45]. The latter reaches the maximum effect within 30[42] to 45[43] minutes, remains stable for 90 minutes[43]and lasts only for several hours[42]. According to previous studies, the difference in cycloplegic effect between atropine and cyclopentolate is not clinically relevant[46] or significantly different[42,47]. Tropicamide the second considered cycloplegia, reaches the maximum effect within 30 min, with an effective duration of 75 minutes[43]. However, the effectiveness of tropicamide compared to cyclopentolate is debated. Some studies[40,48] report a higher residual amount of accommodation with tropicamide than with cyclopentolate, while others describe little to no difference[43,44,49,50]. In order to avoid prolonged cycloplegia and to conservatively ensure a high level of cycloplegia, we decided in favor of cyclopentolate.

This study also has some limitations that should be considered. Firstly, the use of a one-size-fits-all scleral contact lens electrode represents a compromise between stable fit and signal quality due to individual variations in scleral curvature. Some participants reported an increased foreign body sensation when wearing the contact lens electrode, resulting in frequent blinking and movement artifacts, which had a negative impact on signal quality. Also, the empirically determined bandpass blink filter could slightly influence the shape of the recorded signals, although this effect is considered negligible. Secondly, the amplitude measurements between different near targets showed no significant differences, possibly due to lack of accommodation and non-linear changes in refractive power. The standardized measurement procedure with a constant sequence of trigger intervals

and the measurement of the refractive change instead of the actual refractive power limits the possibility of assessing training effects and fatigue. It should also be emphasized at this point that our assumption regarding the neurological origin of the signal needs to be further investigated with a larger sample. In our study, the paralyzing cyclopentolate was administered to only 5 participants. In addition, the measurement unit allows data acquisition at 125 samples per second, which may not be sufficient to capture the high-frequency components of the neuroelectric signals, limiting the ability to completely characterize these signals.

## Conclusion

Previous studies have demonstrated the feasibility of recording ciliary muscle electrical potentials during accommodation using various types of electrodes, ranging from invasive needle electrodes inserted into the ciliary muscle to less invasive approaches using contact lens electrodes. Inspired by the findings of these studies, we aimed not only to replicate them using a previously newly developed bipolar scleral lens electrode, but also to quantify and compare the recorded signals with the actual refractive change of the crystalline lens in response to varying accommodative demands. Furthermore, we analyzed the recorded signals for potential confounding sources. Using the exclusion procedure, we postulate that the signal origin is at least to a certain extent of neurological origin. In upcoming studies, we will focus on characterizing accommodation-related signals in presbyopes. In addition, we will test whether these measured signals can be used to control a visual aid with variable refractive power to realize a biomimetic system.

## Methods

### Study participants

12 emmetropic volunteers (5 males, age 24.6 (21–29 years)) were recruited from the student body of the University of Tuebingen after fulfilling all inclusion (age: 18–30 years; spherical equivalent refractive error: $< \pm$ 0.5 D; Snellen visual acuity: $\geqq$ 20/20; astigmatism: < 2.0 D; accommodation amplitude: > 4 D) and no exclusion (pregnant, hereditary eye disease, previous or current eye injury, strabismus, amblyopia, pseudophakia) criteria. Power estimation ($a = 0.05$, power = 0.80, two-tailed matched-pairs t-test) based on the amplitudes recorded during a preliminary study (accommodative effort: 0.5 to 2.0 D)[28] yielded an effect size of Cohen's $d = 1.3$, corresponding to a minimum of 7 participants. To balance robustness and account for potential dropouts while maintaining the feasibility of a pilot study, the sample size was set at 12, also in accordance with Julious (2005)[51]. In participants receiving cycloplegia, intraocular pressure was confirmed to be less than 20.5 mmHg. All participants were shown the contact lens electrode (Fig. 6a) and its dimensions before they received the informed consent form and gave their written consent for voluntary participation. The study was approved by the Ethics Committee of the Medical Faculty of the University of Tuebingen (690/2017BO2) and followed the tenets of the Declaration of Helsinki. Written consent to publish the photo in an open access publication was also obtained from the participant shown in Fig. 6b.

### Preliminary examination

In all participants, objective refraction was measured with an autorefractometer (AR-330 A/AR-360 A, NIDEK CO., LTD., Gamagori, Japan), and uncorrected monocular visual acuity was assessed with a Landolt C chart. Subsequently, the dominant eye was determined by the Dolman hole-in-card test[52,53]. The amplitude of accommodation of the left eye was measured by a motorized push-up method ($v = 2$ cm/s), focusing on a Duane's figure as the image target and repeated three times. Finally, a slit-lamp examination of the anterior eye segment and fundus was performed. A Schirmer test II (Schirmer Tear Test - Mark Blue, Optitech Eye Care, Prayagraj, India) was done in the right eye for later analysis by mass spectroscopy[54] to determine inflammatory markers before scleral contact lens insertion (as baseline) and after its removal. Participants were asked to close their eyes to reduce discomfort. To ensure a sufficient wetting, the paper strip was collected when reaching more than 15 mm of wetting or else after a five-minute waiting period. Attendees participating in the cyclopentolate measurement additionally underwent intraocular pressure measurements (AT 900, Haag-Streit AG, Koeniz, Switzerland) before and after the actual experiment.

### Experimental setup and stimulus paradigm

The setup, located in a dimly lit room (about 25 lx), has been described before[29]. In brief: It consists of a combined chin and head rest, a high-resolution near-fixation display (2048 × 1536, Adafruit Qualia 9.7" DisplayPort monitor, Adafruit, New York, USA) with adjustable distance (25, 33, 40, and 50 cm), and a far monitor (1360 × 768, NOLK-FD32HB-PNAZ, Richardson Electronics) located at 4.84 m. The axis of the near and the far display are perpendicular to each other and a 45-degree semitransparent mirror allows the stimuli to be superimposed on the visual axis of the fixating eye (Fig. 6c). The non-fixating right eye with the scleral contact lens electrode is covered by an optical long-pass filter (780 nm, RG780, Schott AG, Mainz, Germany). To induce accommodation, five-letter words are randomly drawn from a predefined list and presented at a frequency of 2 Hz in white-on-black Sloan font, with the middle letter highlighted in orange as a fixation aid, alternately for 10 s on the near or the far display at a constant viewing angle. The control of the monitors and the stimulus were implemented in PsychoPy 2022.2.4[55,56]. A high-resolution camera allows to record gaze, pupil diameter, and the refractive change of the crystalline lens during the test using eccentric infrared photorefraction at a sampling rate of 40 Hz[30,57].

### Participant Preparation

Two drops of local anesthetic (0.4% Novesine®, OmniVision GmbH, Puchheim, Germany) were administered to the participant's right eye. Approximately 2 $cm^2$ of the forehead was cleaned with an abrasive paste (Everi Abrasive

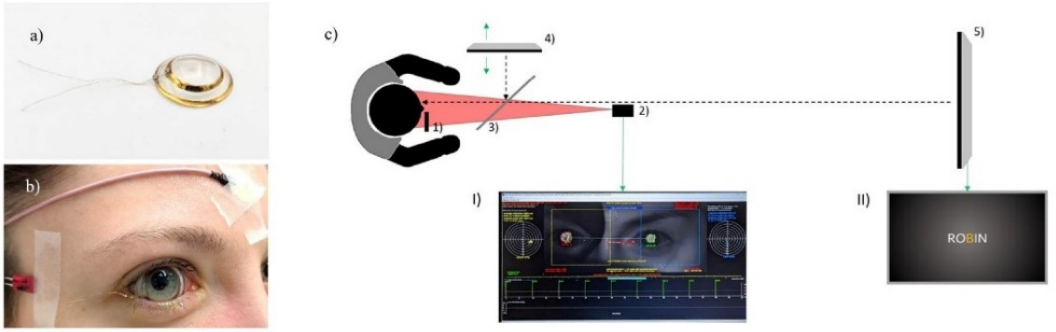


d)

| Step | Characteristic | Condition | Testing distance (D) | Duration (s) | Repetition |
|---|---|---|---|---|---|
| 1. | Accommodation | Far/Near | 0.2 – 4.0 – 0.2 | 10 – 10 – 10 | 4 |
| 2. | | Far/Near | 0.2 – 2.5 – 0.2 | 10 – 10 – 10 | 4 |
| 3. | | Far/Near | 0.2 – 2.0 – 0.2 | 10 – 10 – 10 | 4 |
| 4. | | Far/Near | 0.2 – 3.0 – 0.2 | 10 – 10 – 10 | 4 |
| 5. | Confounding Signals | Gaze change 4° | 0.2 | 2 | 5 |
| 6. | | Pupil constriction | 0.2 | 10 | 1 |
| 7. | | Pinching eyes | 0.2 | 10 | 3 |

**Fig. 6**. Measurement setup: (**a**) A scleral lens electrode without a connector for the measurement unit (**b**) A participant with a contact lens electrode and a reference electrode on the temple. The gold cables are guided out via the angulus oculi lateralis of the right eye and fixed with a tap. (**c**) Bird's eye view of the measurement setup. The infrared filter (1) enabling monocular vision but a binocular measurement for the eccentric infrared photorefraction (2). The semi-transparent mirror (3) is light-transmissive when illuminated from the far target. The near target (4) can be adjusted in distance (green arrow), while the far target (5) has a fixed distance of 4.84 m. (**c.a**) Graphical user interface of the custom-made eccentric infrared photorefraction. (**c.b**) Exemplary, a five-digit word presented to the participant. (**d**) Single measurement steps at the testing protocol. Besides examining the accommodation behavior, possible confounding signals were also measured.

Conductive Paste, Spes Medica s.r.l., Genoa, Italy) before a gold cup electrode filled with conductive paste (Elefix Z-401CE, Nihon Kohden Corporation, Tokyo, Japan) was placed on the forehead. The bipolar scleral contact lens electrode was filled with a tear substitute (Vidisic, Bausch & Lomb, Laval, Canada) by the ophthalmologist prior to insertion into the right eye to protect the cornea and improve electrical conductivity. During this procedure, the ophthalmologist ensured that the gold wires were guided out of the lateral canthus before firmly taping them onto the participant's temple. Participants undergoing temporary ciliary muscle paralysis underwent the same procedure except that two drops, as recommended by the manufacturer for diagnostic procedures, of a cycloplegic agent (Cyclopentolate Alcon® 1%, Alcon, Geneva, Switzerland) were instilled 5 minutes apart instead of the topical anesthetic. For maximum cycloplegia, cyclopentolate 1% was administered[58] and an instillation time of 20 minutes was given after the second drop. Once the inability to accommodate at near was established by the motorized accommodation ruler, topical anesthetic was administered immediately before the lens electrode insertion.

### Experimental procedure

The experiment included the following measurements, being subsequently performed in each participant. Firstly, to characterize the accommodation signals, an alternating far-near-far stimuli between the far target 0.2 D to different near targets (4.0, 2.5, 2.0, 3.0 D) was shown four times (cf. Figure 6d, Step: 1–4). Subsequently, after the testing distance of 3.0 D, to asses potential confounding signals, horizontal gaze change, pupil constriction and voluntary eye squinting were recorded (cf. Figure 6d, Step: 5–7), before an ophthalmologist removed the contact lens electrode. The experimental procedure ended with the examination of the cornea for abnormalities using the slit lamp and a second Schirmer test II to detect possible inflammatory markers caused by the scleral contact lens. A waiting period of at least three days was specified for the repeat measurement.

### Sample preparation of tear fluid

Punches of Ø 4 mm were taken from the Schirmer strips and transferred into 2.0 mL microcentrifuge tubes. Proteins were extracted as described previously[59]. The protein pellet was resuspended in 30 µL of 50 mM ammonium bicarbonate (ABC), 4 µL of RapiGest SF Surfactant, and 1 µL of 0.1 M dithiothreitol (DTT), and incubated at 60°C for 10 min. After cooling to room temperature, 1 µL of 0.3 M iodoacetamide (IAA) was added, and the mixture was incubated in the dark for 30 min. For enzymatic digestion, 1 µL of 0.5 µg/µL Trypsin/LysC

mix was added and incubated overnight at 37°C. The reaction was stopped by adding 3.2 µL of trifluoroacetic acid (TFA) to achieve a final concentration of 5%, followed by centrifugation at 9,000 g for 1 min. The mixture was transferred to a polypropylene insert in a 1.5 mL tube, incubated for 10 min at room temperature, and centrifuged at 16,000 g for 15 min. The clear solution was carefully transferred into new 0.5 mL tubes, avoiding the bottom pellet and upper oily phase. Peptides were cleaned and desalted using StageTips. These Tips were equilibrated with 20 µL of 80/5 solution (80% acetonitrile/5% TFA) and rinsed with 20 µL of 0/5 solution (5% TFA in water). The sample was applied to the StageTip, washed with 20 µL of 0/5 solution, and eluted with 20 µL of 50/5 solution (50% acetonitrile/5% TFA) followed by 20 µL of 80/5 solution. The eluates were pooled and concentrated to 1–5 µL using a SpeedVac concentrator, then stored at -80°C until LC-MS/MS analysis.

### Mass spectrometry

Mass Spectrometry analysis was performed on an Ultimate3000 RSLC system coupled to an Orbitrap Tribrid Fusion mass spectrometer. Tryptic peptides were loaded onto a µPAC Trapping Column (COL -TRPNANO16G1B2, Thermo Fisher Science Inc., Waltham MA, United States). Peptides were eluted and separated on a nano-LC column (µPAC.C18 COLNANOØ50GIB, Thermo Fisher Science Inc., Waltham MA, United States). The remaining peptides were eluted by a short gradient from 30 to 95% buffer B; the total gradient run was 120 min.

Spectra were acquired in DIA (Data Independent Acquisition) mode using 50 variable-width windows over the mass range 350–1500 m/z. The Orbitrap was used for MS1 (precursors) and MS2 (fragments) detection, with an AGC target for MS1 set to 20 × 104 and a maximum injection time to 100 ms. MS2 scan range was set between 200 and 2000 m/z, with a minimum of 6 points across the peak. Orbitrap resolution for MS2 was set to 30 K, isolation window set to 1.6, AGC target to 50 × 104 and maximum injection time to 54 ms. MS1 and MS2 data were acquired in centroid mode.

To reduce the possibility of carryover and cross-contamination between the samples, one TRAP and two BSA washes were used between samples.

### Data processing

Time series data of pupil diameter, gaze, and lens refractive changes recorded with the eccentric infrared photorefraction were upsampled to 250 Hz to match the sampling frequency of the biopotential amplifier. The biopotential data were band-pass filtered between the empirically determined range of 0.025 and 0.575 Hz with a second-order Butterworth filter to remove blink artifacts and correct biodrifting. Utilizing the average biopotential amplitude from the first 10 s of each measurement, baseline-correction was performed. Thereafter, the biopotential and the eccentric infrared photorefraction data were merged using the trigger signal. A self-developed Python script was created for this step of pre-processing. Two measurements (2.0 D, 4.0 D) of one participant (ID: 02) were excluded due to artifacts with biopotential data exceeding the average value by a factor of twenty.

Data from the far-near-far measurements (Fig. 6d, Step:1–4) were filtered based on pupil diameter and refractive changes, removing values more than two standard deviations from the mean. Additionally, data points where the horizontal or vertical gaze was outside the 95% confidence interval of the mean were also excluded. If the cables were accidentally swapped at the connections, the polarity of the signal was reversed accordingly.

### Filtering and statistics

All biopotential analyzes were done in JMP 16.0.0 (SAS Institute GmbH, Heidelberg, Germany) and 0.05 was defined as the critical alpha value for statistical assessments.

The mean of each 10 s sequence from the data of the far-near-far measurements (Fig. 6d, Step: 1–4) for biopotential and refractive change was calculated. Effects of these dependent variables were analyzed by linear mixed-effects models using restricted maximum likelihood (REML). As independent variables, accommodation demand (4.0 D, 2.5 D, 2.0 D, and 3.0 D), session as well as their interaction were set. To account for inter individual variability and repeated measurements participant was declared as a random effect. Knowing the robustness of linear mixed-effects models towards deviations from normality[60,61] the model's conditional residuals were verified (pq-plot, skewness, kurtosis) for at most moderate deviations from normal distribution. Homogeneity of the variances was ensured using the Brown–Forsythe test and reported in case of violations. Post hoc comparisons of the least squares mean were conducted using two-tailed Tukey HSD.

Due to the characteristic S-shape consisting of the three sections gradual onset, rapid change and stabilization, the logistic sigmoid function $sig_{(t)}$ was used for mathematical description of the accommodation-related signals over time ($t$). This involved initial normalization of the filtered signals (0 to 1) for better visualization. In order to obtain a complete picture of the accommodation and disaccommodation process, the time interval was set to 5 s before and after the respective stimulus.

$$sig_{(t)} = c + \frac{d - c}{1 + e^{-a(t-b)}} \tag{1}$$

.

To describe the range of speed in the confounding signals measurement, the delta of the y-value (in mV) was determined at time point 0 and 2 s and divided by the elapsed time of 2 s.

Before determining the repeatability between the measurements with and without cyclopentolate utilizing a Bland-Altman plot and a two tailed t-test the sequence means were checked for normal distribution (pq-plot, skewness, kurtosis).

The DIA MS RAW data were analyzed using DIA-NN 1.8.1 (PMID: 31768060) in library-free mode against the human database (UniProt release November 2023, 20405 proteins). First, a precursor ion library was generated using FASTA digest for library-free search in combination with deep learning-based spectra prediction. An experimental library generated from the DIA-NN search was used for cross-run normalization and Mass accuracy correction. Only high-accuracy spectra with a minimum precursor FDR of 0.01, and only tryptic peptides (2 missed Tryptic cleavages) were used for protein quantification. The match between runs option was activated and no shared spectra were used for protein identification. Data was analyzed and processed using the Perseus platform[62].

## Data availability

The datasets generated during the current study are available from the corresponding author on reasonable request.

Received: 16 January 2025; Accepted: 26 May 2025
Published online: 03 June 2025

## References

1. Young, T. The Bakerian lecture. On the mechanism of the eye. *Philos Trans. R Soc. Lond* **23–88** (1801).
2. von Helmholtz, H. Ueber die accommodation des Auges. *Archiv Für Ophthalmologie*. **1**, 1–74 (1855).
3. Fincham, E. F. *The Mechanism of Accommodation* vol. 8 (G. Pulman & sons, 1937).
4. Schachar, R. A. et al. Model of zonular forces on the lens capsule during accommodation. *Sci. Rep.* **14**, 5896 (2024).
5. Rosenfield, M., Ciuffreda, K. J., Hung, G. K. & Gilmartin, B. Tonic accommodation: a review. II. Accommodative adaptation and clinical aspects. *Ophthalmic Physiol. Opt.* **14**, 265–277 (1994).
6. Glasser, A. Accommodation: mechanism and measurement. *Ophthalmol. Clin. North. Am.* **19**, 1–12 (2006).
7. McDougal, D. H. & Gamlin, P. D. Autonomic control of the eye. *Compr. Physiol.* **5**, 439–473 (2015).
8. Knaus, K. R., Hipsley, A. M. & Blemker, S. S. The action of ciliary muscle contraction on accommodation of the lens explored with a 3D model. *Biomech. Model. Mechanobiol.* **20**, 879–894 (2021).
9. Dubbelman, M., Van Der Heijde, G. L. & Weeber, H. A. Change in shape of the aging human crystalline lens with accommodation. *Vis. Res.* **45**, 117–132 (2005).
10. Croft, M. A., Heatley, G., McDonald, J. P., Katz, A. & Kaufman, P. L. Accommodative movements of the lens/capsule and the strand that extends between the posterior vitreous zonule insertion zone & the lens equator, in relation to the vitreous face and aging. *Ophthalmic Physiol. Opt.* **36**, 21–32 (2016).
11. Plainis, S., Charman, W. N. & Pallikaris, I. G. The physiologic mechanism of accommodation. *Cataract Refractive Surg. Today Europe*. **4**, 23–29 (2014).
12. Glasser, A., Croft, M. A. & Kaufman, P. L. Aging of the human crystalline Lens and presbyopia. *Int Ophthalmol. Clin* **41** (2001).
13. Rich, W. & Reilly, M. A. A review of lens biomechanical contributions to presbyopia. *Curr. Eye Res.* **48**, 182–194. https://doi.org/10.1080/02713683.2022.2088797 (2023).
14. Katz, J. A. et al. Presbyopia – A review of current treatment options and emerging therapies. *Clinical Ophthalmology* vol. 15 2167–2178 Preprint at (2021). https://doi.org/10.2147/OPTH.S259011
15. Charman, W. N. Developments in the correction of presbyopia I: Spectacle and contact lenses. *Ophthalmic and Physiological Optics* **34**, 8–29. https://doi.org/10.1111/opo.12091 (2014).
16. Charman, W. N. Developments in the correction of presbyopia II: surgical approaches. *Ophthalmic Physiol. Opt.* **34**, 397–426 (2014).
17. Renna, A., Alió, J. L. & Vejarano, L. F. Pharmacological treatments of presbyopia: a review of modern perspectives. *Eye Vision* **4** (2017).
18. Grzybowski, A., Markeviciute, A. & Zemaitiene, R. A review of pharmacological presbyopia treatment. *Asia-Pac. J. Ophthalmol.* **9**, 226–233. https://doi.org/10.1097/APO.0000000000000297 (2020).
19. Onyszkiewicz, M., Hilmers, J., Rejdak, R., Zrenner, E. & Straßer, T. Effects of miosis on the visual acuity space under varying conditions of contrast and ambient luminance in presbyopia. *J Clin. Med* **13** (2024).
20. Toates, F. M. Accommodation function of the human eye. *Physiol. Rev.* **52**, 828–863 (1972).
21. Tabernero, J., Chirre, E., Hervella, L., Prieto, P. & Artal, P. The accommodative ciliary muscle function is preserved in older humans. *Sci Rep* **6**, (2016).
22. Adel, N. L. Electromyographic and entopic studies suggesting a theory of action of the ciliary muscle in accommodation for near and its influence on the development of myopia**. *Optom. Vis. Sci.* **43** (1966).
23. Schubert, G. Aktionspotentiale des M. ciliaris beim menschen. *Albrecht Von Graefes Archiv Für Ophthalmologie Vereinigt Mit Archiv Für Augenheilkunde*. **157**, 116–121 (1955).
24. Jacobson, J. H., Romaine, H. H., Halberg, G. P. & Stephens, G. The electric activity of the eye during accommodation. *Am. J. Ophthalmol.* **46**, 231–238 (1958).
25. Hagiwara, H. & Ishikawa, S. The action potential of the ciliary muscle. *Ophthalmologica* **144**, 323–340 (1962).
26. Alpern, M., Ellen, P. & Goldsmith, R. The electrical response of the human eye in Far-to-Near accommodation. *AMA Arch. Ophthalmol.* **60**, 592–602 (1958).
27. Schumayer, S. et al. Novel three-dimensional and biocompatible lift-off method for selective metallization of a scleral contact lens electrode for biopotential detection. *Fronti. Med. Technol.* **1**, 920384 (2022).
28. Margaret Clouse, M. Recording and processing of Tissue-Specific ocular electrical biosignals for applications in biomedical devices. *Tübingen* https://doi.org/10.15496/publikation-19708 (2017).
29. Wagner, S., Zrenner, E. & Strasser, T. Emmetropes and myopes differ little in their accommodation dynamics but strongly in their ciliary muscle morphology. *Vis. Res.* **163**, 42–51 (2019).
30. Schaeffel, F., Wilhelm, H. & Zrenner, E. Inter-individual variability in the dynamics of natural accommodation in humans: relation to age and refractive errors. *J. Physiol.* **461**, 301–320 (1993).
31. Kasthurirangan, S., Vilupuru, A. S. & Glasser, A. Amplitude dependent accommodative dynamics in humans. *Vis. Res.* **43**, 2945–2956 (2003).
32. Mcbrien, N. A. & Millodot, M. Differences in adaptation of tonic accommodation with refractive state. *Investig. Ophthalmol. Vis. Sci.* **29** (1988).
33. Gilmartin, B. & Hogan, R. E. The relationship between tonic accommodation and ciliary muscle innervation. *Invest. Ophthalmol. Vis. Sci.* **26**, 1024–1028 (1985).
34. Gilmartin, B., Mallen, E. A. H. & Wolffsohn, J. S. Sympathetic control of accommodation: evidence for inter-subject variation. *Ophthalmic Physiol. Opt.* **22**, 366–371 (2002).
35. Choi, J. Measurement of anterior scleral curvature using anterior segment OCT. *Optom. Vis. Sci.* **91**, 793–802 (2014).

36. Van der Worp, E., Graf, T. & Caroline, P. Exploring beyond the corneal borders. *Contact Lens Spectr.* **6**, 26–32 (2010).
37. Levin, L. A. & Adler, F. H. *Adler's Physiology of the Eye* (Saunders/Elsevier, 2011).
38. Rosenfield, M. & Gilmartin, B. Temporal aspects of accommodative adaptation. *Optom. Vis. Sci.* **66**, 229–234 (1989).
39. Gilmartin, B. A review of the role of sympathetic innervation of the ciliary muscle in ocular accommodation. *Ophlhal Physiol. Opt* **6** (1986).
40. Mutti, D. O. et al. The effect of cycloplegia on measurement of the ocular components. *Invest. Ophthalmol. Vis. Sci.* **35**, 515–527 (1994).
41. Arici, C., Turk, A., Ceylan, O. M., Kola, M. & Hurmeric, V. Effects of 1% cyclopentolate hydrochloride on anterior segment parameters obtained with Pentacam in young adults. *Arq. Bras. Oftalmol.* **77**, 228–232 (2014).
42. Farhood, Q. K. Cycloplegic refraction in children with cyclopentolate versus Atropine. *J. Clin. Exp. Ophthalmol.* **3**, 1–6 (2012).
43. LIN, L. L. K. et al. The cycloplegic effects of cyclopentolate and tropicamide on myopic children. *J. Ocul. Pharmacol. Ther.* **14**, 331–335 (1998).
44. Yazdani, N., Sadeghi, R., Momeni-Moghaddam, H., Zarifmahmoudi, L. & Ehsaei, A. Comparison of cyclopentolate versus tropicamide cycloplegia: A systematic review and meta-analysis. *J. Optom.* **11**, 135–143. https://doi.org/10.1016/j.optom.2017.09.001 (2018).
45. Wakayama, A. et al. Incidence of side effects of topical Atropine sulfate and cyclopentolate hydrochloride for cycloplegia in Japanese children: a multicenter study. *Jpn J. Ophthalmol.* **62**, 531–536 (2018).
46. Singh, R. P. et al. Comparison of cycloplegia with Atropine 1% versus cyclopentolate 1%. *Indian J. Ophthalmol.* **71**, 3633–3636 (2023).
47. Çelebi, S. & Aykan, U. The comparison of cyclopentolate and Atropine in patients with refractive accommodative Esotropia by means of retinoscopy, autorefractometry and biometric lens thickness. *Acta Ophthalmol. Scand.* **77**, 426–429 (1999).
48. BARTLETT, J. D. Administration of and adverse reactions to cycloplegic agents. *Optom. Vis. Sci.* **55**, 227–233 (1978).
49. Pei, R. et al. A randomized clinical trial using cyclopentolate and tropicamide to compare cycloplegic refraction in Chinese young adults with dark irises. *BMC Ophthalmol* **21** (2021).
50. Al-Thawabieh, W. et al. Tropicamide versus cyclopentolate for cycloplegic refraction in pediatric patients with brown irides: a randomized clinical trial. *Am. J. Ophthalmol.* **257**, 218–226 (2024).
51. Julious, S. A. Sample size of 12 per group rule of thumb for a pilot study. *Pharm. Stat.* **4**, 287–291 (2005).
52. Dolman, C. Perc. Tests for determining the sighting eye. *Am. J. Ophthalmol.* **2**, 867 (1919).
53. Pointer, J. S. Sighting dominance, handedness, and visual acuity preference: three mutually exclusive modalities? *Ophthalmic Physiol. Opt.* **21**, 117–126 (2001).
54. Yao, Y. N., Di, D., Yuan, Z. C., Wu, L. & Hu, B. Schirmer paper noninvasive microsampling for direct mass spectrometry analysis of human tears. *Anal. Chem.* **92**, 6207–6212 (2020).
55. Peirce, J. W. Generating stimuli for neuroscience using psychopy. *Front. Neuroinform.* **2**, 343 (2009).
56. Peirce, J. et al. PsychoPy2: experiments in behavior made easy. *Behav. Res. Methods.* **51**, 195–203 (2019).
57. Schaeffel, F., Farkas, L. & Howland, H. C. Infrared photoretinoscope. *Appl. Opt.* **26**, 1505–1509 (1987).
58. Morgan, I. G., Iribarren, R., Fotouhi, A. & Grzybowski, A. Cycloplegic refraction is the gold standard for epidemiological studies. *Acta Ophthalmologica* **93**, 581–585. https://doi.org/10.1111/aos.12642 (2015).
59. Dammeier, S. et al. Combined targeted analysis of metabolites and proteins in tear fluid with regard to clinical applications. *Transl Vis. Sci. Technol.* **7**, 22 (2018).
60. Knief, U. & Forstmeier, W. Violating the normality assumption May be the lesser of two evils. *Behav. Res. Methods.* **53**, 2576–2590 (2021).
61. Schielzeth, H. et al. Robustness of linear mixed-effects models to violations of distributional assumptions. *Methods Ecol. Evol.* **11**, 1141–1152 (2020).
62. Tyanova, S. et al. The perseus computational platform for comprehensive analysis of (prote) omics data. *Nat. Methods.* **13**, 731–740 (2016).



## Acknowledgements
The project is funded by the Carl Zeiss Foundation "Breakthroughs at Universities 2020: Intelligent Solutions for an Aging Society", the University of Tuebingen, the Faculty of Medicine of the University of Tuebingen, and the Center for Ophthalmology at the University of Tuebingen. We want to thank all ophthalmologists who supported us in this project. Furthermore, we would like to thank Margaret M. Deibel, on whose preliminary work formed the basis for this study.


## Author contributions
The initial study idea originated from E.Z. The study protocol was designed by S.W. and S.S., while the setup was developed by S.W. and T.S. The technical aspects of the contact lens electrodes and their subsequent use in the trial design were developed by E.Z, V.B and S.S. While the measurements were carried out by S.S. and B.S., the data analysis was performed by S.S., T.S. and M.J. S.S wrote the manuscript with input from S.W. and T.S. Results and the final version of the manuscript were discussed by all authors.


## Funding
Open Access funding enabled and organized by Projekt DEAL.


## Declarations

## Competing interests
The authors declare no competing interests.

## Additional information
**Supplementary Information** The online version contains supplementary material available at https://doi.org/10.1038/s41598-025-04165-3.

**Correspondence** and requests for materials should be addressed to T.S.

## 2.3 Publication – Ring Electrode

Schumayer, S., Zahrani, E. G., Azarhoushang, B., Bucher, V., & Straßer, T. (2025). Design and In Vivo Evaluation of an Intraocular Electrode for Ciliary Muscle Biopotential Measurement in a Non-Human Primate Model of Human Accommodation. Biosensors, 15(4), 247. doi: 10.3390/bios15040247

biosensors

MDPI

*Article*

# Design and In Vivo Evaluation of an Intraocular Electrode for Ciliary Muscle Biopotential Measurement in a Non-Human Primate Model of Human Accommodation

**Sven Schumayer [1,2,*], Esmaeil Ghadiri Zahrani [3,4], Bahman Azarhoushang [3], Volker Bucher [1] and Torsten Straßer [2,5]**

[1] Faculty Mechanical and Medical Engineering (MME), Institute for Microsystems Technology (iMST), Furtwangen University, 78120 Furtwangen, Germany
[2] Institute for Ophthalmic Research, University of Tuebingen, 72076 Tuebingen, Germany; torsten.strasser@uni-tuebingen.de
[3] Institute for Advanced Manufacturing (KSF), Furtwangen University, 78532 Tuttlingen, Germany
[4] Department of Microsystems Engineering (IMTEK), University of Freiburg, 79110 Freiburg, Germany
[5] University Eye Hospital Tuebingen, 72076 Tuebingen, Germany
* Correspondence: sven.schumayer@hs-furtwangen.de

**Abstract:** The measurement of electrical potentials in the human body is becoming increasingly important in healthcare as a valuable diagnostic parameter. In ophthalmology, while these signals are primarily used to assess retinal function, other applications, such as recording accommodation-related biopotentials from the ciliary muscle, remain poorly understood. Here, we present the development and evaluation of a novel implantable ring electrode for recording biopotentials from the ciliary muscle. Inspired by capsular tension rings, the electrode was fabricated using laser cutting, wiring, and physical vapor deposition coating. The constant impedance and weight over a simulated aging period of 391 days, demonstrated the electrode's stability. In vivo testing in non-human primates further validated the electrode's surgical handling and long-term stability, with no delamination or tissue ingrowth after 100 days of implantation. Recorded biopotentials from the ciliary muscle (up to 700 µV) exceeded amplitudes reported in the literature. While the results are promising, further research is needed to investigate the signal quality and origin as well as the correlation between these signals and ciliary muscle activity. Ultimately, this electrode will be used in an implanted device to record ciliary muscle biopotentials to control an artificial lens designed to restore accommodation in individuals with presbyopia.

**Keywords:** intraocular electrode; biopotential; electrode conception; accelerated aging; laser cutting



Received: 25 February 2025
Revised: 6 April 2025
Accepted: 8 April 2025
Published: 13 April 2025

**Citation:** Schumayer, S.; Zahrani, E.G.; Azarhoushang, B.; Bucher, V.; Straßer, T. Design and In Vivo Evaluation of an Intraocular Electrode for Ciliary Muscle Biopotential Measurement in a Non-Human Primate Model of Human Accommodation. *Biosensors* **2025**, *15*, 247. https://doi.org/10.3390/bios15040247



## 1. Introduction

Since Galvani's discovery of electrical activity in dissected skeletal muscle in 1786, followed by Matteucci's demonstration in 1842 that frog heartbeats generate an electrical current, significant advances have been made in the field of bioelectrical recording. This culminated in Waller's development of the electrocardiogram (ECG) in 1877, later refined by Einthoven, who was awarded the Nobel Prize in 1924 [1]. These milestones stimulated ongoing efforts to record electrical biopotentials from various tissues and organs throughout the body. The discovery of visually evoked potentials (VEP)—electroencephalographic (EEG) responses correlated with flashes of light—in the 1930s [2], triggered a growing interest in the study of biopotentials associated with vision and ocular function. Other

methods, such as the electroretinogram (ERG) or the electrooculogram (EOG), to measure electrical activity in the eye were invented and soon used for research and diagnostics [3]. From the mid-1950s on, several research groups began recording electrical activity from the ciliary muscle [4–11]. This circular muscle surrounding the crystalline lens plays a key role in controlling accommodation [12], the process by which the eye focuses images on the retina. Despite these findings, interest in the ciliary muscle biopotentials waned, leaving a limited understanding. In other areas, biopotentials are now used not only for research and diagnosis, but also to control prostheses. This is achieved by recording the electrical activity of muscles using electromyography (EMG) [13–15] or neuronal signals for brain–computer interfaces using EEG or electrocorticography (ECoG) [16] in order to restore lost physical abilities. In recent years, interest in the ciliary muscle was revived by evidence of its involvement in the most common forms of ametropia, myopia, and presbyopia. Studies revealed differences in ciliary muscle morphology between myopes and emmetropes [17,18] and researchers demonstrated that ciliary muscle function remains intact in older adults despite the presence of presbyopia [19–22]. It could be said that age-related farsightedness is the most common form of a lost physical ability, affecting everyone beyond a certain age [23]. In order to develop a prosthesis for the future treatment of age-related farsightedness that is capable of restoring the accommodative feedback loop which is disrupted by the stiffening of the crystalline lens [12], it was necessary to develop an implantable intraocular electrode. Another approach would be to realize the visual aid in the form of a smart contact lens, but current concepts struggle to ensure sufficient energy density to power themselves due to space limitations [24,25]. Instead of implanting a battery as is currently performed, the power supply could be realized similar to retina [26] or cochlear implants [27,28]. While a contact lens-based approach would provide a non-invasive method of recording the ciliary muscle biosignals [5–7,9,11], it remains susceptible to recording artifacts caused by factors such as blinking and varies in signal amplitude due to imperfect positioning of the electrode in relation to the ciliary muscle. Needle electrodes, as used in early studies [7,9], on the other hand are invasive, damaging the ciliary muscle. In addition, they record spike trains of muscle activity rather than the summed potentials measured with the contact lens electrode. To overcome these merits, an intraocular bipolar ring electrode was developed that is designed to be placed in the *ciliary sulcus*, behind the iris, in front of the ciliary body. The design of the ring electrode was inspired by capsular tension rings that are routinely used to stabilize the capsular bag in the case of weakened or damaged zonula fibers [29] and in special cases, are also implanted in the *ciliary sulcus* [30]. This allows a minimally invasive implantation, a relatively large contact surface to the surrounding tissue, and eliminates the influence of artifacts such as blinking.

## 2. Materials and Methods

### *2.1. Electrode Design*

Given the similarities in accommodative apparatus, eye anatomy, and functionality between cynomolgus monkeys and humans [31,32], cynomolgus monkeys were selected as the preclinical model. The *sulcus* diameter in these non-human primates was determined theoretically and compared with measurements from explants. In this calculation, the equation provided by Mehdi et al. [33] for estimating the *sulcus* diameter in the human eye was used with values for the horizontal corneal diameter [34] and the corneal curvature [35], specific to cynomolgus monkeys, resulting in an outer diameter of 10 mm for the ring electrode. The bipolar electrode, made of polyethylenterephthalat (PET; Tekra, LLC; New Berlin; WI; USA), consists of two concentric rings connected by 1 mm-spaced spokes, allowing it to measure potential differences generated by the ciliary muscle during accommodation. The developed ring electrode leverages the concepts of the commercially

available capsular tension rings (CTRs) and is implanted in the *sulcus ciliaris* behind the iris and in front of the ciliary body to keep the distance to the presumed target tissue as small as possible (Figure 1a). The geometry (Figure 1b) is a compromise between positioning, in terms of centering, contacting as well as implantability. In terms of biological safety (ISO 10993), only declared biocompatible materials were used, researched in the literature, and assured to withstand the selected overpressure ethylene oxide sterilization process.

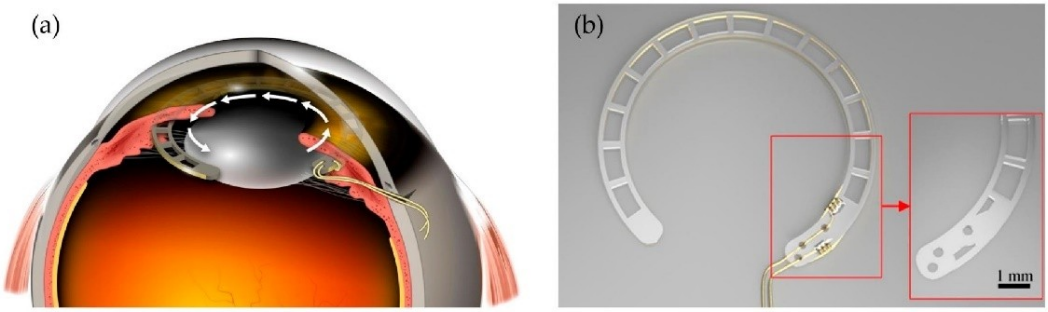


**Figure 1.** Ring-shaped bipolar electrode (**a**) Schematic drawing of a cross-section of the eye, where the ring electrode is inserted by an incision at the limbus and placed, by rotating (white arrow) it into the ciliary sulcus. (**b**) Rendering of the electrode. The inner and outer faces of the electrode are mainly connected by spokes. The magnification (red) highlights the geometry of the conducting area, where the gold wires are manually attached, before coating.

### 2.2. *Manufacturing—Laser Cutting*

The layout was cut from a 200 µm thick PET film using a Carbide-Model laser (CB3-40-0200-10-HB; Light Conversion Company; Vilnius; Lithuania) with an initial emission wavelength of 1064 nm and a capability of second harmonic generation. The laser source was integrated into a 5-axis machine (LP400U; GF Machining Solutions; Geneva; Switzerland), as shown in Figure 2a. The intensity profile at the laser output was near-Gaussian ($M^2 < 1.2$) and the beam spot size (2 $w_0$) was at 12 µm. The laser provided a femtosecond pulse with a duration of 260 fs, at a wavelength of 515 nm and an average laser power of 5 W (cf. Figure 2b), assuring minimal thermal damage. The laser was guided six times along the designed contour on the film with a nominal constant focus distance of 100 mm. Subsequently, the blanks were examined using optical (VHX-700F; Keyence; Osaka; Japan) and scanning electron microscopy (XL30 ESEM; Phillips; Eindhoven; The Netherlands).

#### 2.2.1. Manufacturing—Electrode Surface Wiring Integration

Two 140 µm diameter perfluoroalkoxy (PFA)-coated gold wires (A-M Systems, Inc.; Carlsborg; WA; USA) were cut to a length of 45 mm and the ends (5 mm) were stripped. Using a digital microscope (VHX-700F; Keyence; Osaka; Japan), the ends were threaded through the holes used as strain reliefs until the insulated part of the wires reached the respective wedge-shaped cutouts. The stripped wire ends were manually wrapped three times around the wedge-shaped recesses to increase the bonding area with electrically conductive adhesive (EPO-TEK MED H20S; Epoxy Technology Inc; Billerica; MA; USA). The adhesive was selectively applied with a hand-held dispenser (THE-200; TAEHA Corporation, Namyangju-Si, Republic of Korea) at a pressure of 300 kPa for 0.3 s and manually distributed. Curing was performed in a climatic chamber (MKF115 E1.3; Binder GmbH; Tuttlingen; Germany) at 80 °C for at least 10 h to ensure that the adhesive was fully cross-linked. The ring electrode blank was then cleaned with a 40% IPA solution in an ultrasonic tank at 35 °C for 3 min. To avoid a continuous coating and thus, short-circuiting

of the two electrode surfaces of the electrode, the biocompatible and masking material gelling sugar (2 plus 1; Suedzucker AG; Mannheim; Germany) was applied manually to the curves of the tips (cf. Figure 2f) and lifted off with an ultrasonic cleaner (RK 100H; Bandelin; Berlin; Germany) at 35 °C for 3 min after the coating process. Due to the upside-down position of the sample holder in the evaporation and sputtering unit (AUTO 306; HHV Ltd.; Crawley; UK), in which the conductive layers were to be applied, the 3D printed masking fixture was additionally equipped with two channels (Figure 2c). The wired blank was carefully placed on the upper part of the mask, which was then plugged together with the lower part and secured with gelling sugar injected into the channels (Figure 2c, red arrows). The entire mount was placed in a climate chamber at 60 °C and 5% humidity for 30 min to further reduce the moisture content of the gelling sugar.

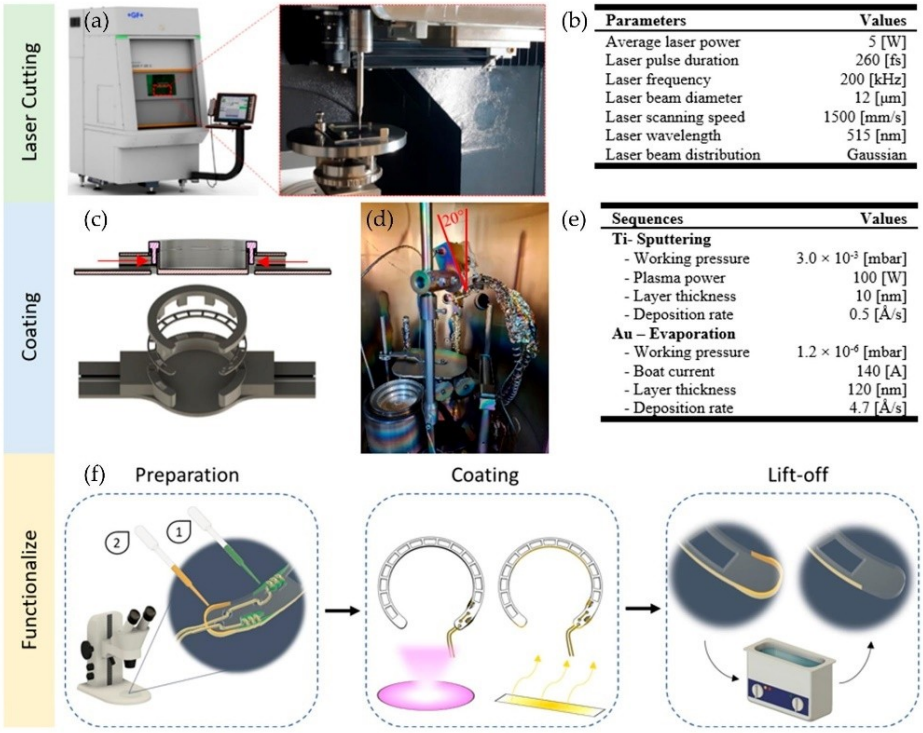


| Parameters | Values |
|---|---|
| Average laser power | 5 [W] |
| Laser pulse duration | 260 [fs] |
| Laser frequency | 200 [kHz] |
| Laser beam diameter | 12 [µm] |
| Laser scanning speed | 1500 [mm/s] |
| Laser wavelength | 515 [nm] |
| Laser beam distribution | Gaussian |

| Sequences | Values |
|---|---|
| **Ti- Sputtering** | |
| - Working pressure | $3.0 \times 10^{-3}$ [mbar] |
| - Plasma power | 100 [W] |
| - Layer thickness | 10 [nm] |
| - Deposition rate | 0.5 [Å/s] |
| **Au – Evaporation** | |
| - Working pressure | $1.2 \times 10^{-6}$ [mbar] |
| - Boat current | 140 [A] |
| - Layer thickness | 120 [nm] |
| - Deposition rate | 4.7 [Å/s] |

**Figure 2.** Manufacturing process of the ring electrode. (**a**) The 5-axis laser cutting machine with the magnified experimental setup within the machine, and the utilized laser parameters (**b**). (**c**) The "sandwich-like" masking, with the ring blank between. The cross-section shows the two channels (red arrows) where the gelling sugar is applied. (**d**) Setup in the physical vapor deposition (PVD) machine with the skewed (20°) sample holder and rotation unit above the shutter, which covers the gold boat. The silver round deepening at the lower left-hand side is the Ti-target. (**e**) The coating parameters of the ring electrodes for Ti as a bonding agent and Au as the electrode surface. (**f**) The schematic functionalization process, where first (1) the electrically conductive glue (green) is applied on the winded gold wires and cured at 80 °C for at least 10 h. Secondly (2), gelling sugar shown in orange, as a temporary masking agent, is applied on both tips of the ring electrode. Before evaporating 120 nm electrode material (Au), 10 nm Ti is sputtered as an adhesion promotor. The masking agent is dissolved within an ultrasonic cleaner for 3 min at 35 °C.

2.2.2. Manufacturing—Electrode Surface Coating

The blank was coated in an evaporation and sputtering system (AUTO 306; HHV Ltd.; Crawley; UK) with titanium (Ti) as an adhesion promoter, followed by gold (Au) as a conductive surface. Before deposition, a prepared sample plate and the connected rotation unit first had to be tilted 20° from the vertical position (cf. Figure 2d), to avoid shadowing effects. The gold wires were guided backward through a 3 mm drilling hole at the sample plate and covered with polyimide tape (3M; Saint Paul; MN; USA). Before sputtering, Ar-plasma cleaning for seven minutes was carried out with a glow discharge (3 kV; 50 mA; $8 \times 10^{-2}$ mbar). The deposition parameters are shown in Figure 2e. During the entire process, the sample holder rotated to improve the homogeneity of the coating.

*2.3. Testing—Estimated Post-Implantation Stability Through Accelerated Aging*

Electrodes are exposed to a harsh environment due to body temperature, increased humidity, and the physiologically expected sodium concentration [36,37]. Therefore, the long-term stability of the ring electrodes (n = 4) was tested in a biosimilar environment using an accelerated aging test based on the ISO 10993-13 [38] standard and the protocol for accelerated aging [39]. The norm recommends choosing a test solution as similar as possible to the in vivo environment. As in previous studies [36,40,41], phosphate-buffered saline (PBS; 0.14 M NaCl, 2.7 mM KCl, 10 mM phosphate) with a pH-value of 7.4 was used (ROTI®Fair PBS 7.4; Carl Roth GmbH + Co.KG; Karlsruhe; Germany). The selected PBS solution matches the pH value of the aqueous humor (6.5–7.5 pH) in the anterior part of the eye [42]. The accelerated aging temperature is based on the maximum temperature ($T_{max}$) of 60 °C recommended for testing polymers, at which it is guaranteed that the degeneration is primarily chemically driven according to the Arrhenius principle [39]. As specified in the standard ISO 10993-13, polypropylene tubes (50 mL tubes Cellstar® 30/115 mm; Greiner Bio-One GmbH; Frickenhausen; Germany) with a volume ratio of at least 1 g sample to 10 mL test solution were selected. The minimum duration to be tested in days ($R_{test}$) was determined by using the following equation:

$$R_{Imp} = R_{test} \cdot Q_{10}^{(T_{max} - T_{Imp})/10°C} \quad (1)$$

The ambient temperature of the implant in vivo ($T_{Imp}$) was determined to be 31.7 °C as a conservative estimate based on the temperature of the anterior chamber of the human eye of 29.9 ± 1.8 °C published in the literature [43]. The temperature coefficient ($Q_{10}$) relative to 10 °C is based on empirical observations and is defined as $Q_{10}$ = 2 for polymers used for medical applications [39]. The implantation period ($R_{Imp}$) in the preclinical model was set at one year, resulting in a test period of 52 days. The samples were kept isolated on the heating plate over time and only taken for mass determination, microscopy, and electrochemical impedance spectroscopy according to the measurement protocol. Prior to mass determination on an analytical balance (Kern ADB 200-4; Kern & Sohn GmbH; Balingen; Germany), the samples were blown dry with a nitrogen jet and then further dried in the climate chamber for 30 min at 40 °C and 5% humidity. Immediately after the mass determination, electrodes were examined under a stereomicroscope (Stemi 508; Carl Zeiss Microscopy GmbH; Jena; Germany) and electrochemical impedance spectroscopy was performed. After measuring, the test container was rinsed first with isopropanol and then with deionized water before 15 mL of new PBS was filled in, and the sample was reinserted.

2.3.1. Testing—Assessing Long-Term Electrical Stability via Electrochemical Impedance Spectroscopy

Electrochemical impedance spectroscopy (EIS) was performed to analyze the quality performance shift of the electrodes during the aging process. A two-electrode

setup, electrically shielded in a Faraday cage, with a platinum wire (∅ 0.5 mm) as a counter electrode (CE = 50.42 $mm^2$) and the ring-shaped electrode as a working electrode ($WE_{inner}$ = 3.519 $mm^2$, $WE_{outer}$ = 4.351 $mm^2$) was placed in a 50 mL sample container filled with PBS (0.14 M NaCl, 2.7 mM KCl, 10 mM phosphate). A modified lid for the container ensured a distance of 35 mm between the counter electrode and the respective working electrode surfaces. Before measurement, the container was rinsed with isopropanol and distilled water. EIS was completed using a Solartron MaterialsLab XM (AMETEK Scientific Instruments; Berwyn; PA; USA) together with the XM-studios MTS Software (version 3.2). A sinusoidal voltage of 10 mV in a frequency range between 1 and 100 kHz, as recommended by Boehler et al. [37], was utilized as a stimulus with an offset voltage of 10 mV. Both electrode surfaces of the ring electrode were measured separately and analyzed using JMP® (Version 16.0.0.; SAS Institute Inc.; Cary; NC; USA; 1989–2023).

#### 2.3.2. Testing—In Vivo Experiment

The bipolar ring electrode was implanted in the *ciliary sulcus* of the right eyes of two 7-year-old male cynomolgus monkeys to serve as an animal model for the study of human accommodation. The in vivo testing was performed at Labcorp Early Development Services GmbH (Münster, Germany) in accordance with Directive 86/609/EEC on animal experimentation. The study protocol was approved by the Landesamt für Natur, Umwelt und Verbraucherschutz (LANUV) of North Rhine-Westphalia, Germany (registration number 81-02.04.2023.A032).

The electrodes were double-packed in self-sealing sterilization pouches and sterilized by overpressure ethylene oxide sterilization. Each electrode was implanted in the right eye, by rotating it into the *ciliary sulcus*, behind the iris, through a 3 mm corneal tunnel incision less than 1 mm posterior to the *limbus* at the superior temporal quadrant.

Monkey 1 was euthanatized at 101 days. The eye was enucleated and preserved in a solution of 2% buffered formaldehyde and 2.5% glutaraldehyde to prevent tissue shrinkage [44]. On the day of pathology, the eye was bisected from the superior hemisphere anteriorly to posteriorly toward the optic nerve and examined under the microscope (VHX 5000, Keyence, Osaka, Japan). For histological analysis, the sample was embedded in paraffin, cut (5 µm thickness) every 450 µm, stained utilizing a hematoxylin/eosin solution, and examined under the microscope to assess tissue responses.

The biopotentials shown here were measured on the animal's cage (monkey 2) and analyzed in JMP. A treat was presented to the animal and given after the corresponding change in focus. The top-level system architecture of the recording and transmission system and the associated specifications are explained separately [45]. In brief: the implant consists of a CR1025 lithium button cell battery (3V; 30 mAh), a flexible circuit board (2-layer) with an analog front end and a central control unit with a Bluetooth antenna, as well as the described bipolar ring electrode. Apart from the electrode, all components are coated with Parylene C (2 × 10 µm) using chemical vapor deposition (CVD) and partly covered in epoxy and silicone to increase mechanical stability while maintaining flexibility. Measurements are recorded with a sampling rate of 250 Hz, by a total signal-to-noise-and-distortion ratio (SNDR) of 56.7 dB, and an effective resolution of 3.64 µV. Details and additional data from these in vivo tests will be addressed in a subsequent publication.

## 3. Results and Discussion

The design of the intraocular electrode for recording electrical potentials of the ciliary muscle during accommodation was inspired by capsular tension rings used to stabilize the capsular bag in cases of zonular weakness during cataract surgery [29,46]. Commercially available capsular tension rings have a width of about 0.2 mm and are usually prestressed

and unfold to their full-size during implantation. Although typically implanted in the capsular bag, they can also be positioned in the *ciliary sulcus* [30]. In this location, implants, such as those designed to measure intraocular pressure [47] or to treat glaucoma [48], have also been reported. We utilized the centric lateral forces of the capsular tension ring [29] to minimize the distance and to achieve optimal contact with surrounding tissue of the ciliary muscle. The shape of the ring electrode represents a balance between important factors such as centering, tissue contact, and ease of implantation. This concentric ring design of the electrode, connected by 1 mm spokes, allows for increased electrode surface area and curvature, which improves signal-to-noise ratio (SNR) by reducing impedance [49,50]. The electrode's central placement within the *ciliary sulcus* minimizes the distance to the signal source and maximizes tissue contact, which is essential for capturing high-amplitude responses [51]. In addition, the design allows for temporary torsion during implantation, which facilitates surgical handling and ensures that the electrode, once in place, maintains optimal contact with the surrounding tissue. Unlike typical intraocular devices such as CTRs and intraocular lenses [29,46,52], which are often made of polymethylmethacrylate (PMMA) for its transparency and durability, polyethylenterephthalat (PET) was selected as the substrate for the electrode due to its superior chemical resistance to isopropanol used in manufacturing processes. PET, commercially available as Dacron® is established as biocompatible and has a long history of safe use in ocular implants for iridocapsular and iris-fixation lenses in humans [53].

### *3.1. Electrode Fabrication*

The masking approach used in the coating process enables selective coating of the entire circumferential surface of round objects, providing a simpler and more cost-effective alternative to conventional planar methods. The process eliminates the need for photoresists and solvents, relying only on the mild isopropanol for a brief rinse, which helps preserve the chemical and mechanical properties of PET. The scanning electron microscope (SEM) images show a melt transition zone that could be minimized with optimized laser parameters; for example, the use of a telecentric f-theta lens could further reduce edge angle errors. The design flexibility, miniaturization potential, and production adaptability offered by laser cutting make it a promising fabrication technique for capsular tension rings or ring-shaped eye electrodes. Future adjustments to the spoke design, such as rounded edges, are expected to better distribute torsional forces within the electrode during implantation. Figure 3a shows the dimensional accuracy of the laser-cut blank at the microscopic level. The edges on the spokes, wedge-shaped recesses, and drill holes were precisely shaped according to the CAD model. Scanning electron microscope images (Figure 3b,c) confirm this accuracy, showing a melting zone of less than 3 µm. Figure 3d shows the manual electrode contacting, validating the production method described in the methodology.

#### 3.1.1. Long-Term Stability During Accelerated Aging

Considering the reproducibility of the scale (0.0002 g), the weight of the tested electrodes along the testing time was constant. Except electrode #4, which steadily decreased in weight, leading to a breakage during preparation for weighting on the seventh measurement sequence (cf. Appendix A). Visual inspection of the electrode surfaces showed no delamination nor other abnormalities.

The results suggest that three of the four electrodes would likely maintain mechanical stability over a simulated implantation period of 391 days. The weight of three electrodes remained constant, supporting their stability, with initial weight variability attributed to the manual application of conductive adhesive. The weight loss observed in the fourth electrode appears to be due to a fracture in one of its spokes, which may have been

weakened during aging to the point of fracture. Alternatively, structural damage may have occurred during blow drying or handling. Some limitations of the test setup should be noted: Equation (1) is an approximation based on empirical data, considering only the temperature coefficient ($Q_{10}$) and omitting the material-specific activation energy of aging-related reactions [54]. In addition, the use of PBS generalizes body conditions and the setup does not account for micromovements and oxidative stress that occur in vivo [40]. Nevertheless, the test complies with the standards of ISO 10993-13 [38] and demonstrates an implantation duration of at least one year, which is confirmed by in vivo results over a period of 101 days in monkey 1.

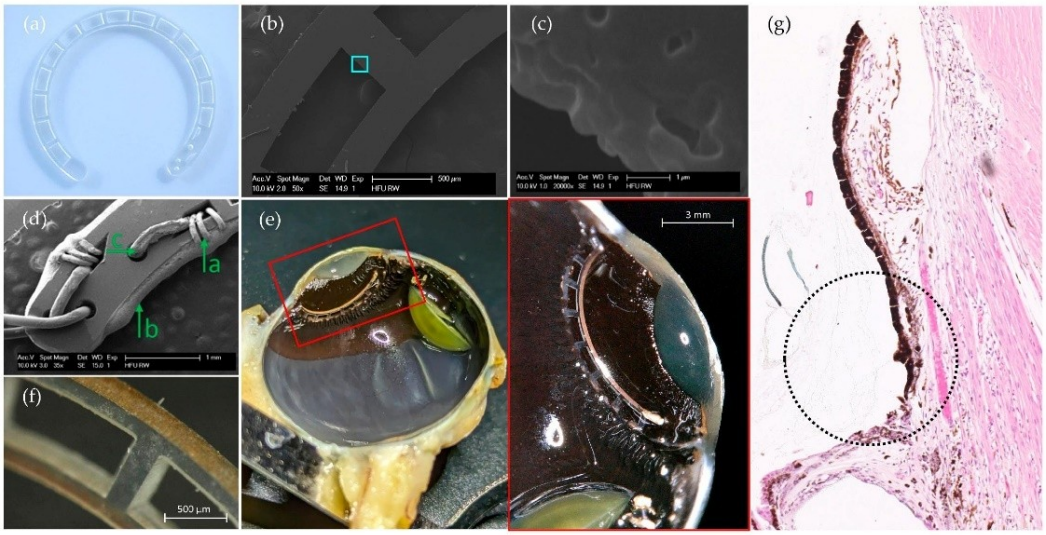


**Figure 3.** Microscope images. (**a**) The laser cut ring blank before connecting. (**b**,**c**) An edge at a spoke at different magnifications shows that there is a laser-induced melting zone of less than 3 µm. (Images (**b**–**d**) were taken with a SEM.) The light blue square shows the magnified area. (**d**) The wedge-shaped cut-out serves to temporarily fix the stripped gold wire (**d**-a) before it is bonded with an electrically conductive adhesive (**d**-b). The drill holes (**d**-c) serve as strain reliefs. (**e**) On the left-hand side, an overview of the left half of the enucleated eye (monkey 1) can be seen. The image on the right-hand side displays the magnification of the red box on the left-hand side and illustrates half of the electrode placed at the ciliary sulcus, anterior to the corona ciliaris, and posterior to the pupil. The yellow-greenish semi-circle is the lens, that slipped during cutting the eye. (**f**) An example of the outer, electrically conductive surface of the electrode #2 after the accelerated aging test. (**g**) Histological analysis of the ciliary sulcus (black dotted circle) in which the electrode was placed (cf. **e**). Above the circle is the posterior part of the iris and below, a base of the zonular fibers (ciliary process). The analysis, in the black dotted circle, shows a localized loss of ciliary body epithelium that may have occurred during surgery, although the ciliary body appears to be intact and unaffected.

Electrical impedance spectroscopy was conducted in a two-electrode setup to measure the total impedance of the test configuration, including the counter electrode, working electrode, and electrolyte. Using a static measurement arrangement, it is possible to infer time-dependent changes in the working electrode. As expected, the PBS medium produced characteristic curves, typical of a parallel capacitor-resistor circuit. At lower frequencies, the electrode/electrolyte interface capacitance dominated, showing the anticipated inverse relationship with frequency and decreasing in influence as frequency increased. Accordingly, impedance decreased, and phase shifted upward.

A comparison of the narrow confidence interval of the impedance with measurements from the first to the 55th day (day: 1; 15; 22; 48; 55) shows that the impedance differs only slightly during accelerated aging (Figure 4). In addition, comparing the 1 kHz impedance $|Z_{1kHz}|$, which can be taken as a benchmark parameter for electrode characterization [55] throughout simulated aging, the respective $|Z_{1kHz}|$ measurements on day 15 and day 55 are within the 95% confidence interval (cf. Figure 4—vertical line at 1 kHz) indicating a constant performance. The $|Z_{1kHz}|$ for the inner electrode surface is 483 ± 197 Ω (mean ± std.) and for the outer conductive surface, $|Z_{1kHz}|$ = 515 ± 227 Ω. Comparing the plots of the inner and outer electrode surface impedance and their phase shifts, a minimal difference is visible. The negative mean phase shift, which is the sum of the individual components in a parallel circuit, illustrates a predominant capacity behavior up to approximately 80 Hz for both surfaces which increases to −5.99° ± 1.9° (mean ± std.) for the inner electrode surface and to −5.98° ± 2.85° for the outer at 100 kHz, showing a diminishing capacity influence for high frequencies.

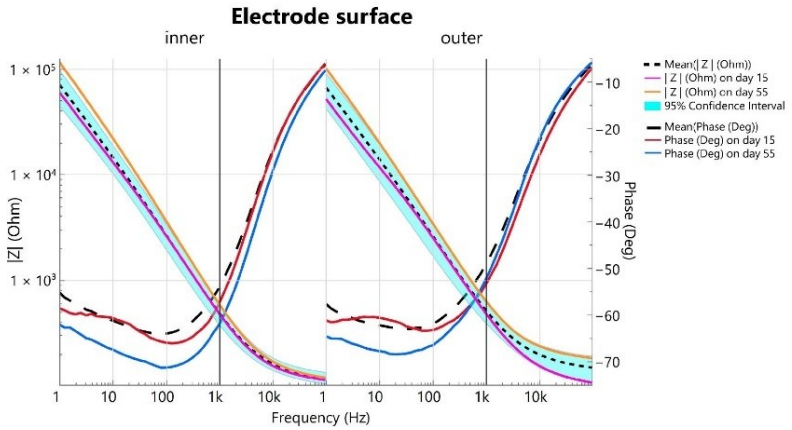


**Figure 4.** The electrochemical impedance spectroscopy. Bode plot of the inner (**left**) and the outer (**right**) electrode surface is shown up to day 55 equal to 391 days in vivo. Solid lines represent the mean, whereas the 95% confidence interval (cyan-colored area) is shaded. The dashed lines logarithmically represent the magnitude of impedance over the logarithmical scaled frequency range, whereas the long-dashed lines illustrate the phase shift over the frequency range.

As described by Oldroyd et al. [40], who also investigated the stability of electrodes during an accelerated aging period, we declared an electrode as functional as long as the $|Z_{1kHz}|$ remained below 1 MΩ. Measurements with $|Z_{100kHz}|$ above 250 Ω were excluded as they indicate incorrect spacing of the electrodes and excessive contact resistance, which is why a direct comparison between day 1 and day 55 is not performed. On day 1, the electrodes were not yet in the PBS before the EIS measurement, but they were stored accordingly for the rest of the aging period. Although the electrodes were dried before the respective EIS measurement, deposits were still to be expected, which hypothetically influence the impedance as well as the phase. To mimic in vivo conditions, no further cleaning was performed before each impedance measurement. This may explain why the mean impedance at frequencies below 100 Hz on day 55 falls slightly outside the confidence interval.

For a discrete electrode characterization, a 3-electrode EIS setup would be required. Our objective of observing electrode stability over an accelerated aging period was successfully achieved. After simulating a one-year in vivo period (391 days), the electrodes

maintained reliable functionality for detecting bioelectric potentials, with a mean $|Z_{1kHz}|$ of 583 Ω for the inner and 629 Ω for the outer electrode surface on day 55. The consistency of the $|Z_{1kHz}|$ values within the 95% confidence interval for days 15 and 55 highlights the stability of the electrode.

#### 3.1.2. Histology and In Vivo Recording

The bisected ring electrode can be seen in the anterior part of the sectioned eye of monkey 1 (Figure 3e). The electrode is intact after approximately three months (101 days) of implantation and is separated only at the site of the pathologic incision. There is no discoloration or opacification of the material nor any encapsulation. The inner electrode surface also shows no delamination, confirming the previously simulated results of accelerated aging (Figure 3f).

Histologic analysis of the eye of monkey 1, stained and examined microscopically (Figure 3g), revealed localized loss of ciliary body epithelium adjacent to the implanted ring electrode. This epithelial disruption is likely due to the mechanical action involved in positioning the electrode within the *ciliary sulcus* during implantation. While such minor epithelial changes are common with similar intraocular procedures and are generally not expected to interfere with device functionality, the literature notes that floating pigment particles resulting from chafing of an intraocular lens (IOL) in the *ciliary sulcus* have been associated with pigment dispersion syndrome, uveitis-glaucoma-hyphema (UGH) syndrome, iridocyclitis, and elevated intraocular pressure [56]. However, in this case, no significant adverse effects were observed, and the remaining ciliary structures and adjacent tissues appeared intact and unaffected, suggesting a low likelihood of complications from the epithelial disruption seen here.

The short-term measurement in monkey 2 (Figure 5) demonstrates the functionality and the detected raw biopotential during change in focus. Approximately three seconds into the trial, a treat was presented at a distance of 1 m and approached by about 40 cm. This increased the measured biopotential by more than 0.2 mV. The treat was held at this distance (approx. 60 cm; time: 5–8 s) to allow the animal time to focus on it. The treat was then brought closer to about 15 cm and held at this distance for an additional 3 s. During this time, the detected voltage increased from −0.26 to 0.48 mV and formed a plateau (time: 11.5–14 s). At the 14 s mark, the animal shifted its gaze into the distance (>2 m), causing a voltage drop (−0.47 mV; time: 20 s). The animal refocused on the treat, which had been moved back to 1 m, resulting the voltage to increase to −0.13 mV (time: 22 s). After the short-term measurement, the treat was given to ensure positive reinforcement.

The short-term measurement is in agreement with the previous literature that measured accommodation-dependent biopotentials with a contact lens electrode [6–9,11] and plunge needle electrode [7,9]. They also describe the formation of a plateau during accommodation. The detected voltage change (≈0.7 mV) of the intraocular electrode is higher than the signals recorded with contact lens electrodes (up to 0.3 mV, c.f. Schubert et al. [6]) and, interestingly, higher compared with the needle electrode (up to 0.15 mV, cf. Hagiwara and Ishikawa, [9]). Due to the proximity to the origin, we expected higher amplitudes compared to the contact lens electrodes but not necessarily compared to the needle electrodes. A possible explanation is that the insertion of the needle electrode does not ensure correct positioning on the ciliary muscle if this is not additionally monitored. We are aware that the short-term measurement at this point represents only a moment in time and does not allow any comprehensive statements to be made about long-term functionality. In order to obtain detailed and reliable results, further investigations under controlled conditions are therefore in progress. Nevertheless, the data collected show that the characteristic,

accommodation-dependent signal could be detected in vivo and the basic functionality of the developed electrode was successfully demonstrated.

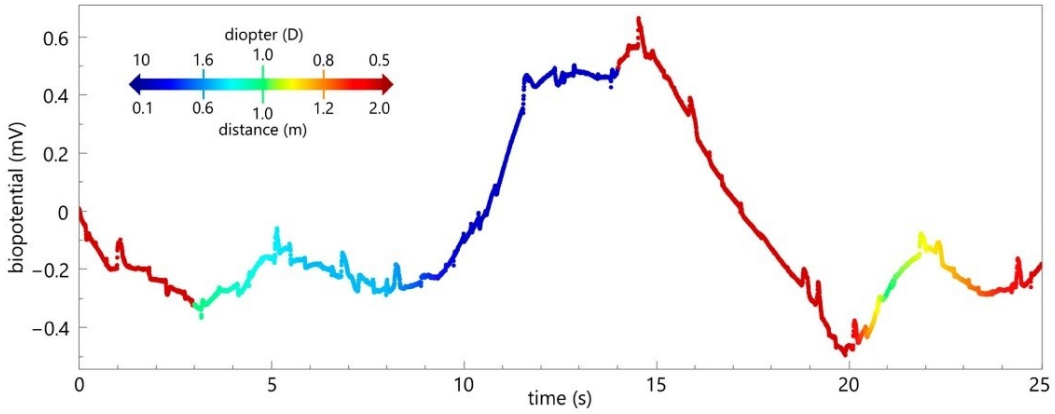


**Figure 5.** In vivo measurement. The raw measured biopotentials of the intraocular implant over a period of 25 s, with the approximate distance of the focus color-coded. The focus on the treat, which gradually moved towards the monkey, resulted in an increasing biopotential. A constant distance of about 15 cm (time: 11.5–14 s) caused a plateau-like shape while looking into the distance led to a voltage drop.

## 4. Conclusions

In addition to the existing needle and contact lens electrodes, we have developed a new type of electrode that can be utilized to measure the biopotentials of the ciliary muscle. All steps from the design to the manufacturing of the electrodes along with the long-term tests in a body-like environment and the behavior of the electrode in vivo are addressed in this work. The electrode's design is inspired by capsular tension, allowing it to be placed in the *ciliary sulcus* and combines mechanical flexibility with good electrical conductivity. Key design features include a concentric ring structure that increases surface area and curvature, thereby improving the signal-to-noise ratio, and a central placement within the *ciliary sulcus* for optimal tissue contact. Accelerated aging tests indicate that the electrode retains its functionality for a simulated implantation period exceeding one year. In vivo testing in a cynomolgus monkey model demonstrated the electrode's capability to record biopotentials during accommodation, with recorded amplitudes exceeding those from prior contact lens and needle electrode designs. This work marks a promising advance toward an implantable device that could enable biofeedback control of an artificial lens, offering potential restoration of accommodation in presbyopia.

## 5. Patents

Sven Schumayer, Torsten Strasser, and Volker Bucher have patent #10 2024 116 619.3 pending to, Eberhard Karls Universität Tübingen Medizinische Fakultät. If there are other authors, they declare that they have no known competing financial interests or personal relationships that could have appeared to influence the work reported in this paper.

**Author Contributions:** T.S. and S.S. were responsible for the design and configuration of the electrode. E.G.Z. and B.A. provided expertise on the laser cutting process and carried out the PET blank cutting. S.S. led the development of the manufacturing process, with V.B. and T.S. providing advice. V.B. and S.S. jointly designed the long-term testing protocol, including accelerated aging and impedance

measurement. S.S. set up and conducted the long-term tests and performed the data analysis in collaboration with V.B. and T.S. Both T.S. and S.S. actively contributed to the in vivo measurements. S.S. drafted this manuscript with the support and additional input of T.S. and all the other authors. All authors have read and agreed to the published version of the manuscript.

**Funding:** This project is funded by the Carl-Zeiss-Stiftung "Breakthroughs at Universities 2020: Intelligent Solutions for an Aging Society" (funding number P2019-01-001), the University of Tuebingen, the Faculty of Medicine of the University of Tuebingen, and the Center for Ophthalmology at the University of Tuebingen.

**Institutional Review Board Statement:** The animal study protocol was approved by the Landesamt für Natur, Umwelt und Verbraucherschutz (LANUV) of North Rhine-Westphalia, Germany (registration number 81-02.04.2023.A032) and conducted in accordance with Directive 86/609/EEC on animal experimentation.

**Data Availability Statement:** The original dataset for measuring electrical impedance during the period of accelerated ageing, presented in this study, is openly available in FigShare under the following: DOI: 10.6084/m9.figshare.28497302.

**Acknowledgments:** We thank Stefan Meyer, Eberhart Zrenner, and Albrecht Rothermel for the valuable discussions on the technical implementation and their expertise on this work. We thank Tobias Peters from the STZ Eyetrial Tübingen for his support in organizing this study. We also would like to acknowledge Karl Ulrich Bartz-Schmidt, Friederike Charlotte Kortuem, and Immanuel Philipp Seitz for their medical expertise and implantation. We thank Sylvia Bolz for preparing and staining the eye samples and Daniela Suesskind for her histological assessment. Furthermore, we thank Bishesh Sigdel and Sebastian Kaltenstadler for their highly valuable contribution and support with electronics, software, and in vivo measurements. The authors express their thanks to +GF+ Machining Solutions GmbH for their support. Furthermore, we would like to thank Labcorp Early Development Services GmbH for the support in surgery, training, and experimentation.

**Conflicts of Interest:** The authors declare no conflict of interest.

## Abbreviations

The following abbreviations are used in this manuscript:

| | |
|---|---|
| ECG | electrocardiogram |
| VEP | visually evoked potentials |
| ERG | electroretinogram |
| EOG | electrooculogram |
| EMG | electromyography |
| ECoG | electrocorticography |
| PET | polyethylenterephthalat |
| CTR | capsular tension ring |
| PFA | perfluoroalkoxy alkanes |
| IPA | isopropyl alcohol |
| Ti | titanium |
| Au | gold |
| Ar | argon |
| PVD | physical vapor deposition |
| PBS | phosphate-buffered saline |
| EIS | electrochemical impedance spectroscopy |
| CVD | chemical vapor deposition |
| SNDR | signal-to-noise-and-distortion ratio |
| SNR | signal-to-noise ratio |
| PMMA | polymethylmethacrylate |

| | |
|---|---|
| SEM | scanning electron microscope |
| CAD | computer-aided design |
| IOL | Intraocular lens |
| UGH | uveitis-glaucoma-hyphema |

## Appendix A

| | Day | | | | | | | |
|---|---|---|---|---|---|---|---|---|
| **Electrode** | **1** | **7** | **15** | **22** | **29** | **39** | **48** | **55** |
| #1 | 0.0150 g | 0.0149 g | 0.0149 g | 0.0134 × g | 0.0135 g | 0.0134 g | 0.0134 g | 0.0134 g |
| #2 | 0.0146 g | 0.0146 g | 0.0146 g | 0.0144 g | 0.0145 g | 0.0144 g | 0.0144 g | 0.0144 g |
| #3 | 0.0169 g | 0.0169 g | 0.0169 g | 0.0168 g | 0.0168 g | 0.0169 g | 0.0168 g | 0.0168 g |
| #4 | 0.0151 g | 0.0149 g | 0.0148 g | 0.0146 g | 0.0145 g | 0.0145 g | - | - |

The change in weight in grams during the accelerated aging of each electrode, illustrated in tabular form. (×) A small piece of the cable was torn off when electrode #1 was improperly removed from the EIS measurement setup (day 22). Electrode #4 broke on a spoke on day 48 of accelerated aging testing and was not further considered for analysis.

## References


1. AlGhatrif, M.; Lindsay, J. A Brief Review: History to Understand Fundamentals of Electrocardiography. *J. Community Hosp. Intern. Med. Perspect.* **2012**, 2, 14383. [CrossRef]
2. Creel, D.J. Visually Evoked Potentials. Available online: http://webvision.med.utah.edu/book/electrophysiology/visually-evoked-potentials/ (accessed on 1 September 2015).
3. Robson, A.G.; Nilsson, J.; Li, S.; Jalali, S.; Fulton, A.B.; Tormene, A.P.; Holder, G.E.; Brodie, S.E. ISCEV Guide to Visual Electrodiagnostic Procedures. *Doc. Ophthalmol.* **2018**, *136*, 1–26. [CrossRef]
4. Swegmark, G.; Olsson, T. Impedance Cyclography a New Method for Accommodation Recording. *Acta Ophthalmol.* **1968**, *46*, 946–968. [CrossRef] [PubMed]
5. Bornschein, H.; Schubert, G. Bestandpotential Und Akkommodationszustand Des Menschlichen Auges. *Albrecht Von Graefes Arch. Ophthalmol.* **1957**, *159*, 45–51. [CrossRef]
6. Schubert, G. Aktionspotentiale Des M. Ciliaris Beim Menschen. *Albrecht Von Graefes Arch. Ophthalmol. Ver. Arch. Augenheilkd.* **1955**, *157*, 116–121. [CrossRef]
7. Jacobson, J.H.; Romaine, H.H.; Halberg, G.P.; Stephens, G. The Electric Activity of the Eye During Accommodation. *Am. J. Ophthalmol.* **1958**, *46*, 231–238. [CrossRef] [PubMed]
8. Alpern, M.; Ellen, P.; Goldsmith, R. The Electrical Response of the Human Eye in Far-to-Near Accommodation. *AMA Arch. Ophthalmol.* **1958**, *60*, 592–602. [CrossRef]
9. Hagiwara, H.; Ishikawa, S. The Action Potential of the Ciliary Muscle. *Ophthalmologica* **1962**, *144*, 323–340. [CrossRef]
10. Bishop, S.; Nyboer, J. Electrical Impedance of the Anterior Eye Chamber. *Ann. N. Y. Acad. Sci.* **1970**, *170*, 793–800. [CrossRef]
11. Adel, N.L. Electromyographic and Entopic Studies Suggesting a Theory of Action of the Ciliary Muscle in Accommodation for Near and Its Influence on the Development of Myopia. *Optom. Vis. Sci.* **1966**, *43*, 27–38. [CrossRef]
12. Toates, F.M. Accommodation Function of the Human Eye. *Physiol. Rev.* **1972**, *52*, 828–863. [CrossRef] [PubMed]
13. Ahkami, B.; Ahmed, K.; Thesleff, A.; Hargrove, L.; Ortiz-Catalan, M. Electromyography-Based Control of Lower Limb Prostheses: A Systematic Review. *IEEE Trans. Med. Robot. Bionics* **2023**, *5*, 547–562. [CrossRef] [PubMed]
14. Asghar, A.; Jawaid Khan, S.; Azim, F.; Shakeel, C.S.; Hussain, A.; Niazi, I.K. Review on Electromyography Based Intention for Upper Limb Control Using Pattern Recognition for Human-Machine Interaction. *Proc. Inst. Mech. Eng. H* **2022**, *236*, 628–645. [CrossRef]
15. Chen, Z.; Min, H.; Wang, D.; Xia, Z.; Sun, F.; Fang, B. A Review of Myoelectric Control for Prosthetic Hand Manipulation. *Biomimetics* **2023**, *8*, 328. [CrossRef]
16. Vilela, M.; Hochberg, L.R. Applications of Brain-Computer Interfaces to the Control of Robotic and Prosthetic Arms. In *Handbook of Clinical Neurology*; Aminoff, M.J., Boller, F., Swaab, D.F., Eds.; Elsevier B.V.: Amsterdam, The Netherlands, 2020; pp. 87–99.
17. Kaphle, D.; Schmid, K.L.; Davies, L.N.; Suheimat, M.; Atchison, D.A. Ciliary Muscle Dimension Changes with Accommodation Vary in Myopia and Emmetropia. *Investig. Opthalmology Vis. Sci.* **2022**, *63*, 24. [CrossRef] [PubMed]
18. Wagner, S.; Zrenner, E.; Strasser, T. Emmetropes and Myopes Differ Little in Their Accommodation Dynamics but Strongly in Their Ciliary Muscle Morphology. *Vision Res.* **2019**, *163*, 42–51. [CrossRef]

19. Tabernero, J.; Chirre, E.; Hervella, L.; Prieto, P.; Artal, P. The Accommodative Ciliary Muscle Function Is Preserved in Older Humans. *Sci. Rep.* **2016**, *6*, 25551. [CrossRef]
20. Sheppard, A.L.; Davies, L.N. The Effect of Ageing on In Vivo Human Ciliary Muscle Morphology and Contractility. *Investig. Opthalmology Vis. Sci.* **2011**, *52*, 1809. [CrossRef]
21. Glasser, A.; Campbell, M.C.W. Presbyopia and the Optical Changes in the Human Crystalline Lens with Age. *Vision Res.* **1998**, *38*, 209–229. [CrossRef]
22. Koretz, J.F.; Cook, C.A.; Kaufman, P.L. Accommodation and Presbyopia in the Human Eye: Changes in the Anterior Segment and Crystalline Lens with Focus. *Investig. Ophthalmol. Vis. Sci.* **1997**, *38*, 569–578.
23. Duane, A. Normal Values of the Accommodation at All Ages. *J. Am. Med. Assoc.* **1912**, *59*, 1010–1013. [CrossRef]
24. Ma, X.; Ahadian, S.; Liu, S.; Zhang, J.; Liu, S.; Cao, T.; Lin, W.; Wu, D.; de Barros, N.R.; Zare, M.R.; et al. Smart Contact Lenses for Biosensing Applications. *Adv. Intell. Syst.* **2021**, *3*, 2000263. [CrossRef]
25. Han, F.; Ge, P.; Wang, F.; Yang, Y.; Chen, S.; Kang, J.; Ren, Y.; Liu, H.; Wei, Z.; He, Y.; et al. Smart Contact Lenses: From Rational Design Strategies to Wearable Health Monitoring. *Chem. Eng. J.* **2024**, *497*, 154823. [CrossRef]
26. Stingl, K.; Bartz-Schmidt, K.U.; Besch, D.; Braun, A.; Bruckmann, A.; Gekeler, F.; Greppmaier, U.; Hipp, S.; Hortdorfer, G.; Kernstock, C.; et al. Artificial Vision with Wirelessly Powered Subretinal Electronic Implant Alpha-IMS. *Proc. R. Soc. B Biol. Sci.* **2013**, *280*, 20130077. [CrossRef] [PubMed]
27. Zeng, F.G.; Rebscher, S.; Harrison, W.; Sun, X.; Feng, H. Cochlear Implants: System Design, Integration, and Evaluation. *IEEE Rev. Biomed. Eng.* **2008**, *1*, 115–142. [CrossRef] [PubMed]
28. Macherey, O.; Carlyon, R.P. Cochlear Implants. *Curr. Biol.* **2014**, *24*, R878–R884. [CrossRef]
29. Weber, C.H.; Cionni, R.J. All about Capsular Tension Rings. *Curr. Opin. Ophthalmol.* **2015**, *26*, 10–15. [CrossRef]
30. Chen, J.; Lan, L.; Tang, Y.; Lu, Y.; Jiang, Y. Placement of Dual Capsular Tension Rings for the Combined Management of Traumatic Cyclodialysis Cleft and Zonular Dialysis. *Eye Vis.* **2020**, *7*, 54. [CrossRef]
31. Glasser, A.; Kaufman, P.L. The Mechanism of Accommodation in Primates. *Ophthalmology* **1999**, *106*, 863–872. [CrossRef]
32. Törnqvist, G. Accommodation in Monkeys: Some Pharmacological and Physiological Aspects. *Acta Ophthalmol.* **1967**, *45*, 429–460. [CrossRef]
33. Mehdi, M.G.; Alireza, A.-S.; Pourazizi, P.M.; Ghoreishi, M.; Abdi-Shahshahani, M.; Peyman, Á.A.; Pourazizi, Á.M.; Pourazizi, M. A Model for Predicting Sulcus-to-Sulcus Diameter in Posterior Chamber Phakic Intraocular Lens Candidates: Correlation between Ocular Biometric Parameters. *Int. Ophthalmol.* **2019**, *39*, 661–666. [CrossRef]
34. Greenbaum, S.; Lee, P.Y.; Howard-Williams, J.; Podos, S.M. The Optically Determined Corneal and Anterior Chamber Volumes of the Cynomolgus Monkey. *Curr. Eye Res.* **1985**, *4*, 187–190. [CrossRef] [PubMed]
35. Crewther, S.; Brennan Johnson, N.; Vision, J.; Catherine Madigan, M. A Comparison of Ocular Development of the Cynomolgus Monkey and Man. *Clin. Vis. Sci.* **1987**, *1*, 269–280.
36. Simon, N.; Schmid, M.; Blendinger, F.; Bucher, V. Long Term Evaluation of the Barrier Properties of Polymer/Metal Oxide Hybrid Layers for Use in Medical Implants. *Curr. Dir. Biomed. Eng.* **2022**, *8*, 435–438. [CrossRef]
37. Boehler, C.; Carli, S.; Fadiga, L.; Stieglitz, T.; Asplund, M. Tutorial: Guidelines for Standardized Performance Tests for Electrodes Intended for Neural Interfaces and Bioelectronics. *Nat. Protoc.* **2020**, *15*, 3557–3578. [CrossRef]
38. *DIN EN ISO 10993-13*; Biological Evaluation of Medical Devices-Part 13: Identification and Quantification of Degradation Products from Polymeric Medical Devices. DIN Deutsches Institut für Normung: Berlin, Germany, 2010.
39. Hemmerich, K.J. General Aging Theory and Simplified Protocol for Accelerated Aging of Medical Devices. *Med. Plast. Biomater.* **1998**, *5*, 16–23.
40. Oldroyd, P.; Gurke, J.; Malliaras, G.G. Stability of Thin Film Neuromodulation Electrodes under Accelerated Aging Conditions. *Adv. Funct. Mater.* **2023**, *33*, 2208881. [CrossRef]
41. Rubehn, B.; Stieglitz, T. In Vitro Evaluation of the Long-Term Stability of Polyimide as a Material for Neural Implants. *Biomaterials* **2010**, *31*, 3449–3458. [CrossRef]
42. Podrazký, O.; Mrázek, J.; Jasim, A.A.; Proboštová, J.; Vytykáčová, S.; Kašík, I.; Pitrová, Š. Ex-Vivo Measurement of the Ph in Aqueous Humor Samples by a Tapered Fiber-Optic Sensor. *Sensors* **2021**, *21*, 5075. [CrossRef]
43. Shinoda, K.; Yagura, K.; Matsumoto, S.; Terauchi, G.; Mizota, A.; Miyake, Y. Intraocular Temperature at Different Sites in Eye Measured at the Beginning of Vitreous Surgery. *J. Clin. Med.* **2021**, *10*, 3412. [CrossRef]
44. Margo, C.E.; Lee, A. Fixation of Whole Eyes: The Role of Fixative Osmolarity in the Production of Tissue Artifact. *Graefe's Arch. Clin. Exp. Ophthalmol.* **1995**, *233*, 366–370. [CrossRef] [PubMed]
45. Kaltenstadler, S.; Sigdel, B.; Schumayer, S.; Steinhoff, R.; Straßer, T.; Rothermel, A. An Implantable Ciliary Muscle LFP Recording and Transmitting System. In Proceedings of the 46th Annual International Conference of the IEEE Engineering in Medicine and Biology Society (EMBC), Orlando, FL, USA, 15–19 July 2024; pp. 1–4. [CrossRef]
46. Menapace, R.; Findl, O.; Georgopoulos, M.; Rainer, G.; Vass, C.; Schmetterer, K. The Capsular Tension Ring: Designs, Applications, and Techniques. *J. Cataract Refract. Surg.* **2000**, *26*, 898–912. [CrossRef]

47. Koutsonas, A.; Walter, P.; Roessler, G.; Plange, N. Implantation of a Novel Telemetric Intraocular Pressure Sensor in Patients with Glaucoma (ARGOS Study): 1-Year Results. *Investig. Ophthalmol. Vis. Sci.* **2015**, *56*, 1063–1069. [CrossRef]
48. Bernardino, C.R.; Chang, E.L.; Hatton, M.P.; Rubin, P.A.D.; Dohlman, C.H. Glaucoma Drainage Devices: A Systematic Literature Review and Current Controversies. *Surv. Ophthalmol.* **2005**, *50*, 411. [CrossRef] [PubMed]
49. Neuman, M.R. Biopotential Electrodes. In *Medical Instrumentation: Application and Design*, 4th ed.; John Wiley & Sons Inc.: Hoboken, NJ, USA, 1998; pp. 189–240.
50. Lewis, C.M.; Boehler, C.; Liljemalm, R.; Fries, P.; Stieglitz, T.; Asplund, M. Recording Quality Is Systematically Related to Electrode Impedance. *Adv. Healthc. Mater.* **2024**, *13*, e2303401. [CrossRef] [PubMed]
51. Fuglevand, A.J.; Winter, D.A.; Patla, A.E.; Stashuk, D. Detection of Motor Unit Action Potentials with Surface Electrodes: Influence of Electrode Size and Spacing. *Biol. Cybern.* **1992**, *67*, 143–153. [CrossRef]
52. Mehta, R.; Aref, A.A. Intraocular Lens Implantation in the Ciliary Sulcus: Challenges and Risks. *Clin. Ophthalmol.* **2019**, *13*, 2317–2323. [CrossRef]
53. Jaffe, N.S. Polyethylene Terephthalate (Dacron®) in Intraocular Surgery. *Ophthalmology* **1981**, *88*, 955–958. [CrossRef]
54. Hukins, D.W.L.; Mahomed, A.; Kukureka, S.N. Accelerated Aging for Testing Polymeric Biomaterials and Medical Devices. *Med. Eng. Phys.* **2008**, *30*, 1270–1274. [CrossRef]
55. Schiavone, G.; Kang, X.; Fallegger, F.; Gandar, J.; Courtine, G.; Lacour, S.P. Guidelines to Study and Develop Soft Electrode Systems for Neural Stimulation. *Neuron* **2020**, *108*, 238–258. [CrossRef]
56. Chang, D.F.; Masket, S.; Miller, K.M.; Braga-Mele, R.; Little, B.C.; Mamalis, N.; Oetting, T.A.; Packer, M. Complications of Sulcus Placement of Single-Piece Acrylic Intraocular Lenses. Recommendations for Backup IOL Implantation Following Posterior Capsule Rupture. *J. Cataract Refract. Surg.* **2009**, *35*, 1445–1458. [CrossRef] [PubMed]

## 2.4 Unpublished Results

This chapter presents findings that have not yet been published, including preliminary results. It contains approaches that are of interest for future research on this topic.

### 2.4.1 Tunable Spectacles in Presbyopes

Schumayer, S., Sigdel, B., Nikolaidou, A., Wolfram, L., Wagner, S., Zrenner, E., Bucher, V., & Straßer, T. (2025). Preserved ciliary muscle biopotentials enable artificial lens control and near vision recovery in long-term presbyopia (Abstract P2-15). In Abstracts of the 62nd annual symposium of the International Society for Clinical Electrophysiology of Vision (ISCEV 2025), Utrecht, the Netherlands. Documenta Ophthalmologica, 150(Suppl 1), 5–51. doi:10.1007/s10633-025-10031-4

The abstract "*Design and In Vivo Evaluation of an Intraocular Electrode for Ciliary Muscle Biopotential Measurement in a Non-Human Primate Model of Human Accommodation*" (P2-15) was presented as a poster at the annual International Society for Clinical Electro-physiology of Vision (ISCEV) Congress 2025 and is published in Documenta Ophthalmologica (Schumayer, Sigdel, Nikolaidou, *et al.*, 2025). It is based on the preliminary results of a study investigating the applicability of electrical biopotentials of the ciliary muscle in presbyopes to adjust a spectacle-mounted tunable lens to the participants' required refraction. Figure 4 is intended to enhance comprehension. The study follows the tenets of the Declaration of Helsinki and was approved by the Ethics Committee of the Medical Faculty of the University of Tuebingen (394/2024BO1).

amplitude assessment in patients with cataract, it has demonstrated for the first time numerically the impact of cataract, depending on its' grade, can have on PERG P50 amplitude.

## P2-14

### Beyond acuity: psychophysical and photopic ERG changes after Anti-VEGF in patients with diabetic macular edema

**Amithavikram R Hathibelagal, Suchana SS Shirodker, Brijesh Takkar**

L V Prasad Eye Institute, Hyderabad, India

**Purpose** Visual acuity is often an insensitive marker for detecting functional changes following treatment in Diabetic Macular Edema (DME). This study aimed to evaluate more sensitive psychophysical and objective markers, including photopic ERG, to assess visual function in patients with DME.
**Methods** Patients with clinically diagnosed DME were recruited. Baseline assessments included visual acuity, color vision (using Color Assessment and Diagnosis test), cone flicker sensitivity (central and 5o eccentricity, and photopic flash and flicker ERG (RETeval, LKC; skin electrodes). Structural parameters were measured using Fundus photography, Optical coherence tomography and Optical coherence tomography angiography. Follow-up testing was conducted 4–6 weeks later. ERG data were available for seven patients across both time points.
**Results** A total of 9 patients (5 males; mean age 56.7 ± 9.0 years) participated in this study. Post-treatment, visual acuity improved in 22.2% (2/9) of patients. A ≥ 30% improvement in red-green color vision thresholds was observed in 55.5% (5/9), while yellow-blue thresholds improved only in 22.2% (2/9) of the individuals. Psychophysical photopic flicker thresholds improved in 55.5% (5/9) of the individuals. Photopic a-wave and flicker amplitudes improved by ≥ 20% from baseline in 71% (5/7) of cases. Although mean photopic flicker amplitudes increased at follow-up (15.04 ± 9.61 μV) compared to baseline (10.34 ± 5.04 μV), the change was not statistically significant ($p = 0.14$). In contrast, photopic flash a-wave amplitudes showed a significant improvement (baseline: 2.19 ± 1.65 μV; follow-up: 4.77 ± 2.13 μV; $p = 0.024$), whereas b-wave amplitudes did not (14.74 ± 8.59 μV vs. 11.36 ± 6.43 μV; $p = 0.38$). No significant correlation was observed between change in structural and functional parameters.
**Conclusion** Psychophysical measures and photopic ERG capture subtle visual function improvements that are not reflected in standard acuity assessments. These tools may serve as valuable adjuncts in monitoring functional outcomes following anti-VEGF treatment in DME.

## P2-15

### Preserved ciliary muscle biopotentials enable artificial lens control and near vision recovery in long-term presbyopia

**Sven Schumayer[1,2], Bishesh Sigdel[2], Anna Nikolaidou[2], Lasse Wolfram[3,2], Sandra Wagner[4,5], Eberhart Zrenner[2], Volker Bucher[1], Torsten Straßer[2,3]**

[1]Institute for Microsystems Technology (iMST), Furtwangen University, Furtwangen, Germany. [2]Institute for Ophthalmic Research, University of Tuebingen, Tuebingen, Germany. [3]University Eye Hospital Tuebingen, Tuebingen, Germany. [4]Herbert Wertheim School of Optometry & Vision Science, University of California, Berkeley, CA, USA. [5]Royal Institute of Technology / KTH—AlbaNova, Stockholm, Sweden

**Purpose** Presbyopia, an age-related impairment of near vision that affects more than 1.8 billion people (Frick et al. *Ophthalmology* 2015;122:1706–1710), is a major public health issue and a constriction of many daily life activities. Lens stiffening impairs near vision and thereby disrupts the accommodative feedback loop (Toates, *Physiol Rev* 1972;52:828–863). Conventional correction restores near vision but not dynamic accommodation. Evidence is at hand that even in long-term presbyopia, the ciliary muscle remains functional. We aim to utilize its neuro-muscular electrical potentials to control an artificial lens and restore the feedback loop of accommodation. Here we present preliminary results from two presbyopic participants demonstrating the ciliary muscle's remaining functionality in long-term presbyopia, showing that its biopotentials can be used to control an artificial lens, restoring dynamic accommodation and improving near visual acuity to levels comparable to those of young adults.
**Methods** Accommodative stimuli (four Sloan letters) were randomly presented to two presbyopic volunteers (female: 76, male: 79 years; BCVA ≥ 20/25) at either 500 cm or 33 cm using an optical setup developed by Wagner et al. *Exp Eye Res* 2019;186:107,741). Letter size was adjusted to determine the near and distance visual acuity thresholds using an interleaved adaptive staircase method (QUEST) in PsychoPy (2022.2.4), with a confidence interval width of 0.1 logMAR used as a stopping criterion. Ciliary muscle biopotentials, recorded noninvasively from the right eye with a scleral lens bipolar electrode (Schumayer et al. *Front Med Technol* 2022;4:1–10), were analyzed using a supervised machine learning method and decision support algorithm to control a tunable lens (EL-16–40-TC-VIS-5D, Optotune AG, Dietikon, Switzerland) in front of the left eye. Each participant completed the test twice: once with the tunable lens turned off (fixed at 0 D), and once with it turned on.
**Results** The scleral lens was well tolerated apart from transient mild conjunctival hyperemia in both participants, which resolved quickly. Biopotential waveforms resembled characteristics previously observed in young adults. With the artificial lens activated both participants achieved a substantial improvement in their near vision: Near visual acuity improved by 0.24 logMAR in the male participant and by 0.41 logMAR in the female participant. Distance visual acuity remained stable, with

Doc Ophthalmol (2025) 150 (Suppl 1):S5–S51 

a difference of − 0.05 logMAR for the male and 0.08 logMAR for the female participant.

**Conclusion** Our results provide clear evidence that ciliary muscle function is preserved despite long-term presbyopia and that its neuromuscular biopotentials can be used to control an artificial lens, thereby recovering accommodation for near vision. Presbyopes can use—even unconsciously—the natural accommodation reflex to control a feedback loop, in which an addressable artificial lens restores disrupted function caused by lens stiffening. While currently limited to a fixed near distance, further training of the machine learning algorithm will enable dynamic accommodation at varying distances, paving the way for a new generation of vision aids improving the quality-of-life presbyopes.

## P2-16

### VEP in preoperative assessment of strabismus: insights from a 20,000-patient cohort

**Songmu Huang Yanzi Wang, Meihua Pan**

Xiamen Eye Center and Eye Institute of Xiamen University, Xiamen, China

**Purpose** To investigate the clinical utility of preoperative VEP in detecting occult neurogenic pathology and guiding the identification of the dominant eye in patients with strabismus.

**Methods** This retrospective study analyzed preoperative VEP data from 20,000 patients with strabismus (2014–2024). Method 1: Patients with corrected visual acuity ≥ 20/20 but severe VEP abnormalities (defined as peak latency delay > 140 ms and amplitude reduction > 50%) underwent neuroimaging (MRI/CT). Method 2: Inter eye VEP differences were evaluated in patients with stereoscopic deficits.

**Results** Among the 20,000 patients, 5 (0.025%) with normal corrected visual acuity exhibited severe VEP abnormalities (peak latency delay and amplitude reduction beyond thresholds). Neuroimaging confirmed compressive optic neuropathy or intracranial mass lesions in these patients. In paralytic strabismus, a subset of cases was linked to undiagnosed intracranial pathology, with VEP abnormalities preceding clinically detectable symptoms. Additionally, in patients with stereoscopic impairment, the non-dominant eye showed consistent inter eye VEP differences compared to the dominant eye: a 3–5% delay in peak latency and a 2–3% reduction in amplitude. These differences provided objective support for dominant eye determination.

**Conclusion** Preoperative VEP is a sensitive tool for identifying occult neurogenic pathology in patients with strabismus, even when standard visual acuity metrics remain normal, particularly in patients with paralytic strabismus or acute comitant esotropia. Quantitative inter eye VEP differences may aid in objectively assessing the dominant eye.

## P2-17

### Ocular effects of various deep sedation protocols in dogs undergoing electroretinography before cataract surgery

**Lucia Ambrosio[1], Fabiana Micieli[1], Dario Basso[2], Cristina Di Palma[1], Ciro Costagliola[1], Barbara Lamagna[1]**

[1]University of Naples Federico II, Naples, Italy. [2]Veterinary Clinic Lucrino, Pozzuoli, Italy

**Purpose** The aim of this study was to evaluate the efficacy of two different deep sedation protocols (DEX-BUT-KET and MID-BUT-KET) and their ophthalmological effects in dogs undergoing electroretinographic examination before cataract surgery.

**Methods** The included animals, belonging to different breeds and differing in age and weight, underwent an electroretinographic examination after 20 min of dark-adaptation, using the ERG (RETevet, LKC Technologies, Gaithersburg, MD, USA) ECVO 5-step short protocol. Topical administration of tropicamide and phenylephrine was performed to obtain a full mydriasis before ERG testing. Contact lens electrodes (ERG-jet) were used as corneal electrodes, while subcutaneous platinum needle electrodes were used as reference and ground electrodes. Sedation was induced in all healthy animals by intravenous administration of 1 µg/kg dexmedetomidine, 0.2 mg/kg butorphanol, and 1 mg/kg ketamine (DEX-BUT-KET protocol). In patients with coexistent diseases, 0.3 mg/kg midazolam, 0.2 mg/kg butorphanol, and 1 mg/kg ketamine were administered (MID-BUT-KET protocol). If deep sedation was not sufficient for the ERG procedure, propofol was administered intravenously as emergency sedation.

**Results** In all 14 examined dogs, both deep sedation protocols enabled successful ERG recording. In all analyzed ERG records, signal-to-noise-ratio was greater than 10. Eleven dogs had DEX-BUT-KET protocol, in absence of coexistent morbidities (i.e., diabetes); three dogs had MID-BUT-KET. Two of the three dogs underwent MID-BUT-KET had diabetes; thus, ERG dark-adapted responses were normal, but light adapted ERG (Photopic 3.0 and Flicker 30 Hz responses) was reduced. The DEX-BUT-KET protocol caused no significant changes in heart rate, temperature, pupil size and intraocular pressure, but resulted in a statistically significant reduction in tear secretion and respiratory rate between T0 (pre-anesthesia) and T1 (post-anesthesia) compared to baseline values.

**Conclusion** The combination of dexmedetomidine, butorphanol and ketamine (DEX-BUT-KET protocol) can be considered a good protocol for deep sedation during ERG before cataract surgery. Further evaluation of the MID-BUT-KET protocol requires its use in a larger number of animals.

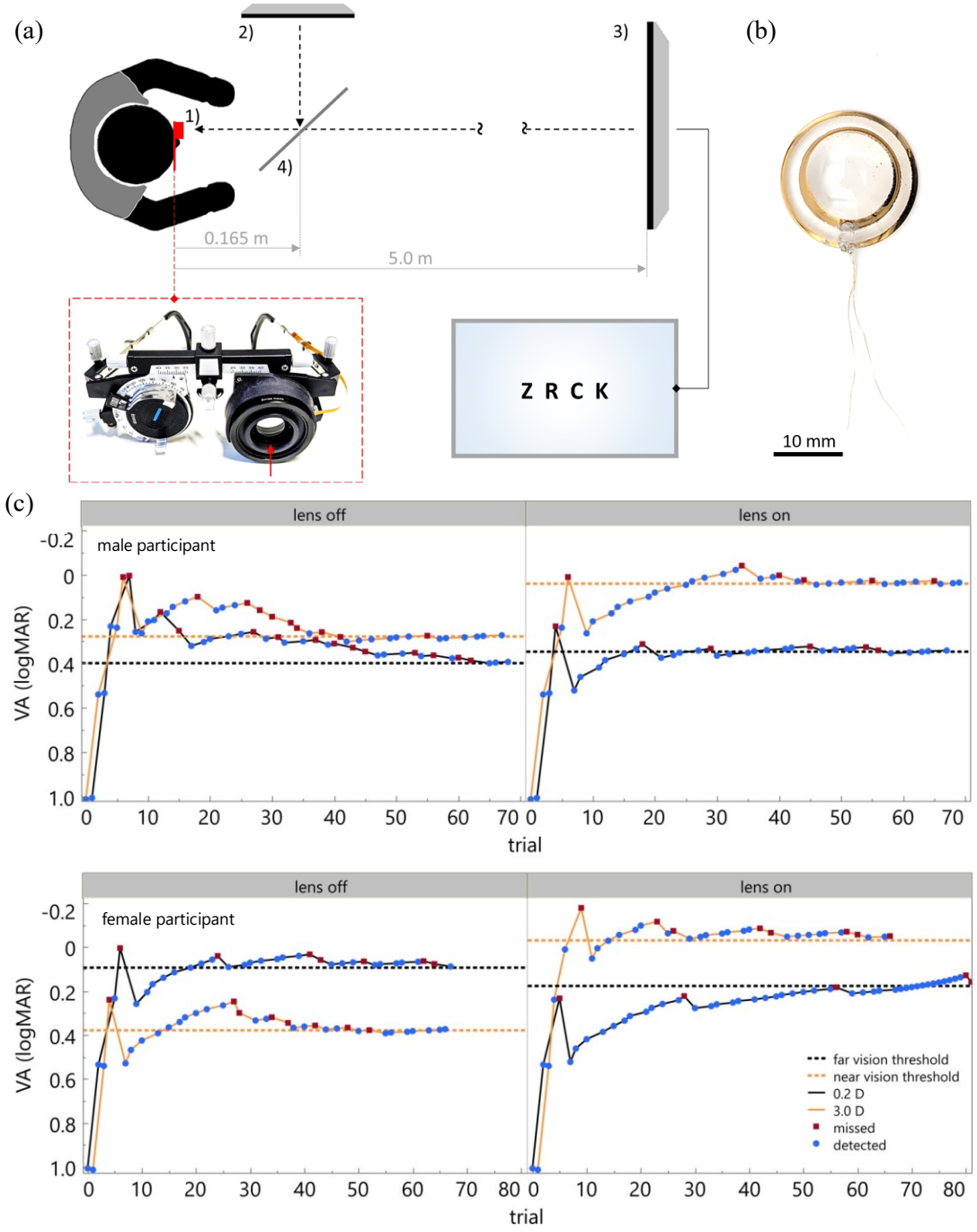


Figure 4 - Measurement setup and results for presbyopes: (a) Schematic of the experimental setup: (a1) Tunable lens (red arrow) mounted in a modified universal trial frame; (a2) near target (3.0 D) and (a3) far target (5 m) with a sample illustration of a four-letter word stimulus; (a4) semi-transparent mirror assuring a stable visual axis during the change of the targets. (b) The custom-made contact lens electrode. (c) Measurement results of the visual acuity (VA): The near (orange) and far (black) VA according to the presented letter sizes of the male and the female (lower charts) participant are shown according to the letter size presented, with the tunable lens turned off (0 D) and on (right). Red squares indicate incorrect (≥ 1 letter misread), and blue dots indicate correct responses. The dashed lines represent the maximum attainable VA for near and far accommodation.

### 2.4.2 Towards a novel closed-loop accommodating contact lens

Another approach towards a biomimetic visual aid is a contact lens electrode combined with a tunable lens. Since the size of the electronics currently poses a major limitation, a hybrid design, where the electronics are separated from the scleral lens itself, represents a first step towards this concept.

For this purpose, a (3.2 x 3.2 mm) pocket was milled into a custom-made polymethyl methacrylate (PMMA) scleral lens, 20 mm in diameter. Two 140 µm gold wires coated with PFA were used to electrically connect the scleral lens by a electrical conductive adhesive (EPO-TEK® MED H20S; Epoxy Technology Inc.; Billerica; MA; USA). The variable lens (TLens® Silver Premium; poLight ASA; Tønsberg; Norway) was fixed to the scleral lens (Figure 5a) using epoxy (MED-OG198-55; Epoxy Technology Inc.; Billerica; MA; USA). Due to the complex three-dimensional surface of the scleral lens, pad printing (pad hardness: 3–4 Shore) was used to apply the conductive traces between the peripheral gold wires and the tunable lens in the center (cf. Figure 5b). Therefore, an electrically conductive ink (CRSN2419; SunChemical; Parsippany-Troy Hills; NJ; USA), which was diluted with 40% thinner by weight (HM additive A; SunChemical; Parsippany-Troy Hills; NJ; USA), was utilized. The pad print cliché used for this process was produced via SLA 3D printing.

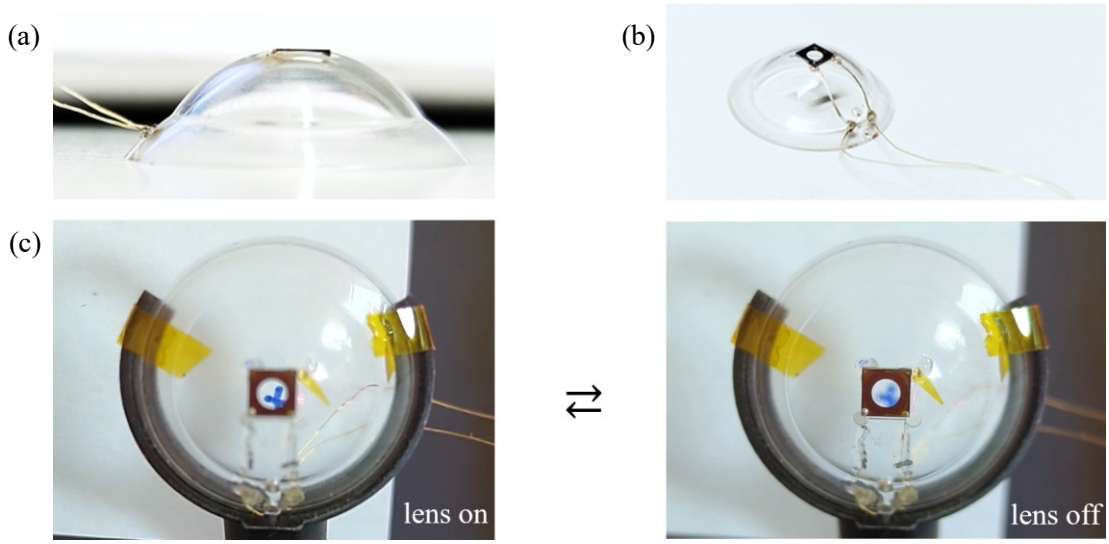


Figure 5 - Tunable contact lens: (a) Side view of the scleral lens profile with the pocket and the inserted tunable lens. (b) The tunable lens and the pad-printed conductor paths. (c) Conducted via gold wires, the tunable lens can be switched on (left) and off, changing the refractive power (cf. blue plus sign in 5 cm distance) in correlation to the applied voltage.

Connected to the evaluation kit (TLens® Eval Kit Ver3; polight ASA; Tønsberg; Norway), the lens can be tuned according to the applied voltage, allowing the refractive power to be adjusted accordingly (cf. Figure 5c).

Although the integration of individual electronic components remains a limitation for a fully functional smart contact lens electrode, the feasibility of integrating a tunable lens into a scleral contact lens has been demonstrated.

### 2.4.3 Implant

Due to its complexity, the implant was developed in cooperation. The electronics (Kaltenstadler *et al.*, 2024) and the software (Sigdel, unpublished data, 2025) are described elsewhere. As part of this work, the ring electrode, in *2.3 Publication – Ring Electrode* and the partial encapsulation of the implant were developed (see Figure 6a). Furthermore, accelerated aging to evaluate the implants' encapsulation in simulated conditions, as well as recording the energy demand at elevated temperature, was investigated.

The implant is powered by a CR1025 battery (Renata SA; Itingen; Swiss). The battery is spot-welded (UB25; AMADA Weld Tech GmbH; Puchheim; Germany) with two PFA-coated gold wires (A-M Systems, Inc.; Carlsborg; WA; USA). The exploratively developed welding program first fixates the respective gold wire to the corresponding pole of the battery (10 ms, 0.12 V) before it is then firmly welded (38 ms, 1.1 V). Three welding points are placed on the stripped ends of each wire and, after cleaning with an isopropanol (IPA)-soaked Q-tip, these are then additionally bonded with silver conductive adhesive (EPO-TEK MED-H20S; Epoxy Technology Inc; Billerica; MA; USA) to obtain a double redundancy. While the conductive glue needs heat to be crosslinked, the adhesive was cured at 65°C for at least five hours in a climate chamber (MKF115 E1.3; Binder GmbH; Tuttlingen; Germany).

The PCB is cleaned mechanically with a fine brush for at least two minutes using IPA. This is followed by low-temperature soldering (solder wire: F-SW32, 1.0 mm, L-Sb60Pb) at 290°C, attaching the battery ends and the reference electrode to the PCB. The solder joints are then cleaned with a Q-tip soaked in IPA before the battery-PCB construct is ultrasonically cleaned for two minutes at 35°C in IPA. This is followed by soldering the ring electrode connections to the PCB, which are afterwards also cleaned with a Q-tip

soaked in IPA. The smartphone app (nRF Connect for Mobile version 4.29.1; Nordic Semiconductor; Trondheim; Norway) is then used to verify whether a Bluetooth connection to the implant can be established before the implant is placed on a holder in the parylene machine (Labcoater 300; Plasma Parylene Systems GmbH; Rosenheim; Germany) together with a 100 silicon wafer for layer thickness measurement. The ring electrode itself is covered with two silicone pads. According to the coating protocol (Figure 6b), the coating process is preceded by an argon plasma cleaning (300 W, 5 min) at a base pressure of 2.5 Pa before silane (3-Methacryloxypropyltrimethoxysilane, CAS 2530-85-0; abcr GmbH; Karlsruhe; German) is added to the coating chamber as an adhesion promoter. Polymerization starts at a set pressure of 3.5 Pa and ends self-limiting when the pressure difference to the set pressure is 1.5 Pa. For repositioning and layer thickness measurement using a spectrometer (NanoCalc-XR; Ocean Optics Deutschland GmbH; Ostfildern; Germany), the vacuum is broken before the second Parylene C coating. The battery is then dip-coated with epoxy (Epo-Tek MED-302-3M; Epoxy Technology Inc; Billerica; MA; USA), placed on a silicone mat and cured for three hours at 60°C in the climate chamber. This process is repeated before the reference electrode is stripped from the Parylene C layer by heat. This is followed by covering the legs of the H-shaped implant, both on the back and the front, using a UV-curing epoxy (Med-OG198-66-UV; Epoxy Technology Inc; Billerica; MA; USA), shown schematically in Figure 6a. The surfaces are cleaned using a Q-tip soaked in IPA before the implant is checked for function using Bluetooth and fixed on a magnetic fixture in order to switch it off using a reed contact. The holder with the implant is double sterile packed (sterilization bag 57 x 130 mm, 90 x 170 mm, Medi Pack GmbH; Mönchengladbach; Germany).

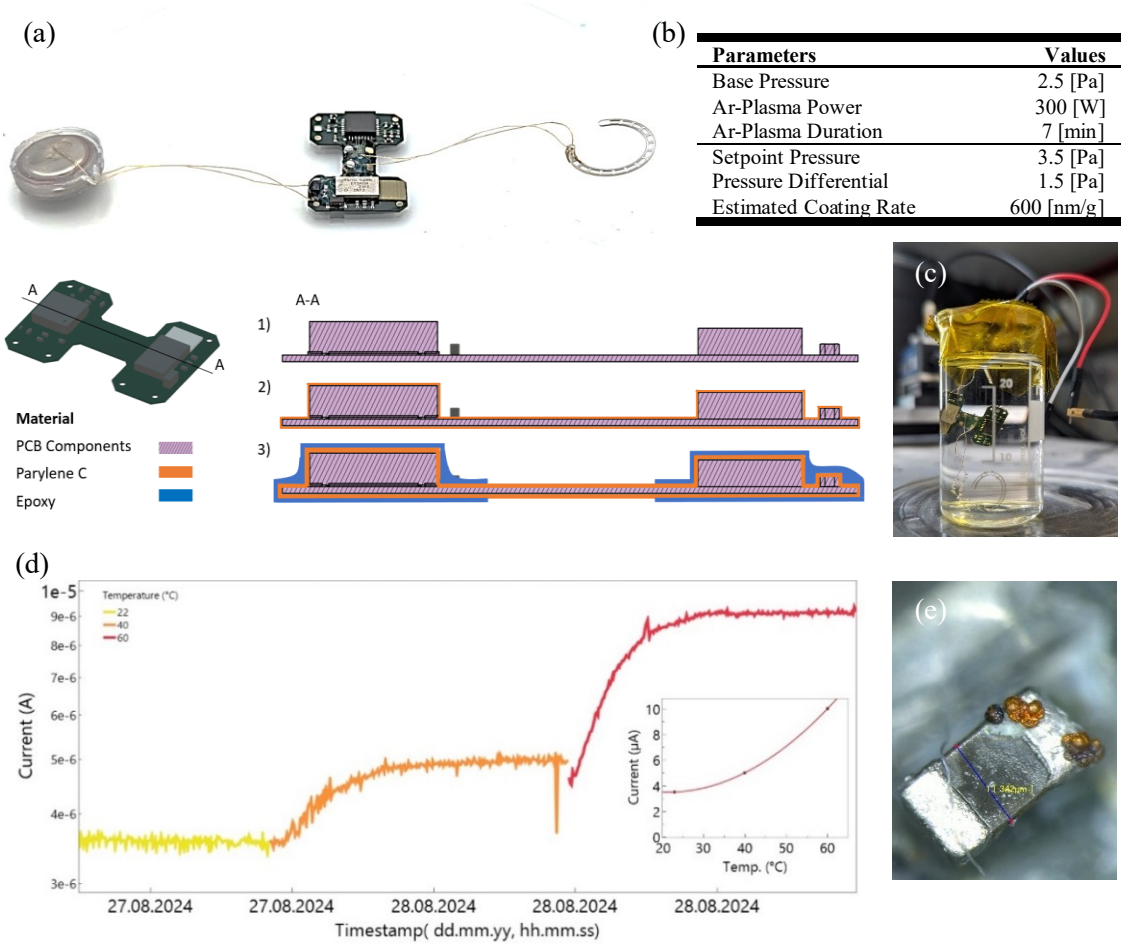


| Parameters | Values |
|---|---|
| Base Pressure | 2.5 [Pa] |
| Ar-Plasma Power | 300 [W] |
| Ar-Plasma Duration | 7 [min] |
| Setpoint Pressure | 3.5 [Pa] |
| Pressure Differential | 1.5 [Pa] |
| Estimated Coating Rate | 600 [nm/g] |

Figure 6 - The intraocular implant: (a) Left-hand side the epoxy-parylene encapsulated lithium battery (diameter 10 mm) connected by a parylene-teflon coated gold wire with a total diameter of 150 µm. In the center, the flexible printed circuit board (PCB) is connected to the ring electrode (right-hand side). The PCB is also shown as a schematic to illustrate the partial coatings. (b) The parameter used for the Parylene C coating, before the encapsulated PCB with the ring electrode is placed in a beaker filled with PBS (c), to simulate a body-like environment, connected to a LabVIEW-controlled constant voltage source. (d) The long-term measurement, where every 30 s the current (A) was measured while the voltage was kept constant at 3.0 V. The color coding implies that a rising temperature let to a rising consumption, which is expressed by the function represented in the plot-in-plot. (e) After the long-term measurement, simulated 698 days in vivo, the encapsulation failed. Using galvanic treatment, the leakage could be found under the microscope in the form of copper depositions at a resistance.

To evaluate the long-term stability of implant, an accelerated aging test was conducted in a biosimilar environment following ISO 10993-13:2010-11 guidelines and is described in detail in (Schumayer, Zahrani, *et al.*, 2025). Testing conditions, including phosphate-buffered saline, where the PCB with ring electrode was placed (Figure 6c), and elevated temperatures, were selected to simulate an accelerated physiological exposure during the

implantation period. For this, the working current of the implant was detected via an electrometer (6517B; Keithley Instruments; Solon; OH; USA) under a constant DC voltage of 3.0 V using a program written in LabVIEW (version: 13.0f2; National Instruments; Austin; TY; USA) (cf. Figure 6d). The measurement was considered finished once the self-defined breakdown current (10 x $I_{rated}$) of 5.0 e-5 A was exceeded. A temperature-current dependence in ultra-low-energy mode could be determined with the following function:

$$\text{Current } (\mu A) = -1{,}857 + 0{,}171*x + 0{,}004*(x - 41)^2, \text{ for x in } °C \quad (1)$$

After exceeding the breakdown current (simulated 698 days in vivo), the implant, as cathode, was coated by electroplating in a copper solution (Cu(II) acetate monohydrate; Carl Roth GmbH + Co. KG; Karlsruhe; Germany) to visually highlight the breakdown point of the coating (cf. Figure 6e). For this purpose, a DC voltage source (6080; PeakTech Prüf- und Messtechnik GmbH; Ahrensburg; Germany) was connected in series to a multimeter (VC150-1; Voltcraft - Conrad Electronics SE; Hirschau; Germany) and a voltage of 2.0 V was set at a current of 200 mA. After 15 min coating time, the PCB was rinsed with IPA and inspected under a microscope (VHX-700F; Keyence; Osaka; Japan).

All required manufacturing steps and test protocols for the assembly, coating, and electrical characterization of the implant were successfully implemented and documented. The key functionality was reviewed at each step of the process and verified.

# 3. Discussion

Due to the scope of this interdisciplinary doctoral thesis, the discussion is initially organized into subchapters addressing the individual topics, followed at the end by an integrative discussion and the resulting conclusions.

## 3.1 Motorized Push-up Test

In the presented work *2.1 Publication – Motorized Push-Up Ruler*, the reliability of a new motorized push-up method for determining the amplitude of accommodation (AoA) was compared with conventional subjective measurement methods (Schumayer, Laukhuf and Straßer, 2025).

While society is rapidly aging, many countries face an economic necessity to keep older workers in the workforce for social and sustainable terms (World Health Organization, 2015). In this context of a population where older individuals are remaining in the workforce, presbyopia is increasingly coming into focus. Therefore, the progression of presbyopia can be determined with subjective and objective methods. While subjective methods evaluate the patient's functional experience, objective methods provide clinical data to optimize optical performance and adjust treatment (Wolffsohn, Berkow, *et al.*, 2024). Although objective methods measure refraction more precisely, these methods require trained personnel, expensive equipment, and a considerable amount of time to perform the measurement. The described novel motorized accommodation ruler (MAR) is intended to reduce known limitations of common subjective methods, such as a varying focus target speed and examiner-related latencies (Burns *et al.*, 2020; Salvador-Roger *et al.*, 2025), which was proven in the study. The measurements carried out there have shown that MAR is more consistent and reliable compared to the other methods investigated. Furthermore, participants rated the novel subjective method as significantly easier to use and showed significantly more confidence in the reliability of the measurement.

Nevertheless, the MAR, as well as the methodology of measuring the AoA with push-up techniques, still has room for improvement. While no speed at which the focus target is moved towards the participant has yet been defined as a standard, the suggested 2 cm/s could be a point of reference. This linear speed is based on the self-defined criteria, taking the reaction time of the participants into consideration. Simultaneously, as the target

moves towards the participants' near point, the target size could be linearly decreased to prevent the claimed overestimation of the push-up method (Atchison, Capper and McCabe, 1994). Because the MAR is operated solely by the participants, it was occasionally observed during studies and preliminary investigations that the participants were inclined to bring the target closer again after near adaptation. Therefore, the next MAR generation should lock the trigger button after the first release and ignore further activation to capture the first distance at which blur was perceived.

While the focus of the mentioned study was on the reliability of the new motorized version compared to conventional ones, emmetropes were considered as the study population. It will certainly be interesting for future research to see how presbyopes cope with the MAR and how the device proves itself in everyday clinical practice. Beyond the obvious use case to determine the residual AoA in presbyopes, the MAR could be utilized in children in the future, as the AoA parameter is also used for determine binocular accommodation insufficiency (Hussaindeen and Murali, 2020; Franco *et al.*, 2022).

### 3.2 Non-invasive biopotentials of the ciliary muscle

Despite known approaches to detect the accommodation-dependent biopotentials from previous work (Schubert, 1955; Alpern, Ellen and Goldsmith, 1958; Jacobson *et al.*, 1958; Hagiwara and Ishikawa, 1962; Clouse M.M, 2017), interest in this field has declined over the years. Perhaps this was because the measuring electrodes were not very comfortable, as bulky contact lens electrodes made of oxygen-impermeable materials and invasive needle electrodes were used (Alpern, Ellen and Goldsmith, 1958; Jacobson *et al.*, 1958; Hagiwara and Ishikawa, 1962). Another reason may have been that there was no obvious use for these neuromuscular signals. However, it was not until the work "*Recording and Processing of Tissue-Specific Ocular Electrical Biosignals for Applications in Biomedical Devices"* in the research group of Prof. Zrenner at the Institute of Ophthalmic Research at the University of Tübingen that these electrical signals of the ciliary muscle were addressed again (Clouse M.M, 2017). Based on this work, scleral contact lens electrodes were developed for a comparatively high wearing comfort (Schumayer *et al.*, 2022). To achieve such a comfort, gold wires with a diameter of 140 µm are bonded into the contact lens so no rigid geometries extend from the lens surface.

In the study *2.2 Publication – Contact Lens Electrode*, these new contact lens electrodes were used to record biopotentials of the ciliary muscle in 12 emmetropes along with their actual refractive changes (Schumayer, Sigdel, Jarboui, *et al.*, 2025). This revealed that all near targets showed significant differences in both biopotentials and refractive changes compared to the far target when the participants shifted their gaze towards the near targets. Although the signals were highly variable between participants, the accommodation-related signals were compared to confounding biopotentials triggered by eye movement, blinking, or pupil constriction and showed a unique sigmoidal-like signal characteristic. Similar to the measurement findings of Clouse M.M (2017), and contrary to the measurement results on two emmetropes of Alpern et al. (1958), the measurement results indicated that the amplitude heights with the focal target show a saturation with increased accommodation effort. Temporary paralysis of the ciliary muscle, known as cycloplegia and caused by drugs like atropine and cyclopentolate (Mutti *et al.*, 1994), still allowed the detection of accommodation-related signals during shifts in focus (Hagiwara and Ishikawa, 1962; Clouse M.M, 2017). These findings were also observed in the contact lens electrode study, where the characteristic biopotential remained measurable in three out of five participants despite the administration of cyclopentolate. Taken together, these findings suggest that at least a portion of the measured signals are of neurological origin. Further support for this assumption comes from the observed saturation of the biopotentials despite increasing stimulus intensity. Action potentials of neurons have a constant amplitude, which, based on the “all-or-none” principle, encode information through frequency and temporal patterns (Kandel *et al.*, 2000). In contrast, the amplitude of synaptic potentials on the postsynaptic muscular side varies with the amount, duration, and activation of the neurotransmitter (Kandel *et al.*, 2000). Any future development of a visual aid that utilizes these neuromuscular biopotentials of accommodation should take these points into account when determining a control variable. The aforementioned intrasubject variability and the observed saturation of the amplitude level despite increasing stimulus indicate that the signal curve and its derivation alone are insufficient as a control variable. Furthermore, blink-related signal curves tend to interfere most with accommodation signals and should therefore be carefully considered. Any system using these ocular biopotentials to steer a tunable lens would benefit from applying a bandpass filter, such as a

Butterworth filter, to suppress known confounding signals. Preliminary (q.v. *2.4.1 Tunable Spectacles in Presbyopes*) results of such a system relying on accommodation-related signals while filtering confounding signals are promising. The system, based on a combined supervised machine learning and decision algorithm, relies on the assumption that the neurological feedback loop can be closed via a tunable lens. Accordingly, the brain controls the ciliary muscle, and thereby accommodation-related biopotentials are emitted until the refractive power of the tunable lens compensates for the detected defocus. Initial evaluations in presbyopes demonstrated an improvement in near visual acuity approximating that of young adults in their early twenties. However, at this point, it must be noted that the final results and analysis of the study are still pending. Nonetheless, while the principle is working, the setbacks and limitations must also be acknowledged. For instance, before the study started, adhesion problems of the electrode material at the contact lens electrodes, manufactured utilizing PVD, occurred. By micro-roughening the concave electrode surface before the actual deposition process, this issue could be solved (Vafaiee *et al.*, 2019). Another issue of the scleral lens is its large diameter of 20 mm and the rigid structure. While a large diameter allows a self-centering in the eye and a greater spacing between the two electrodes, resulting in higher biopotential amplitudes (Schumayer *et al.*, 2022), it also makes insertion into the eye more difficult. The wearing of the rigid contact lens electrode was not a problem for any of the participants, while the insertion and removal process was tolerated to varying degrees. Another compromise was the lens geometry with a base curve of 8.1 mm. Because the corneo-scleral junction and anterior sclera profile varies between individuals (Van Der Worp, 2015), the concave side of the scleral contact lens, mainly defined by the base curve, could be personalized to optimize electrical conduction between the electrode surface and the eye and thus improve signal quality.

With the future in mind, one concept to correct presbyopia would be via a smart contact lens electrode that measures the accommodation-related biosignals to adjust a tunable lens integrated into the contact lens (c.f. Figure 5) according to the wearer's desired refraction. However, to place all the electrical components, the available construction area on the lens is limited, and of the shelf electronic parts are an additional compromise in size. Beyond that, the construction area is further constrained, as the cornea relies on avascular oxygen diffusion to remain transparent (Beebe, 2008). Therefore, certain areas of the oxygen-permeable lens surface must remain free of components and coatings. To

still accommodate all the necessary electronic components, a hybrid version seems to be a first step towards a fully functional smart contact lens electrode. Such a hybrid version could provide a certain proportion of the components to be fixed to the temple outside the eye using a patch. For a fully integrated system, an energy carrier would have to be used that fulfills both the form factor and the possibility of recharging. Furthermore, it would have to provide sufficient power to ensure that the contact lens does not have to be constantly removed, recharged, and reinserted. In order to minimize the number of electrical components required on the circular construction surface, an application-specific integrated circuit (ASIC) in the form of a chip needs to be developed. When using hard lenses, the necessary components, such as the ASIC, could be accommodated in pockets that are cut into the convex side of the lens using a five-axis milling machine or a laser to save space. This manufacturing step would need a lot of attention, as the oxygen-permable polymer is brittle during manufacture. However, the lens materials for such smart applications, commonly described in research like PMMA (Tremblay *et al.*, 2013; Khaldi *et al.*, 2020; Bailey *et al.*, 2022; Pielot *et al.*, 2025) or PET (Lingley *et al.*, 2011), are not oxygen permeable and thus no alternatives. The pocket placed components could be electrically conducted via Ink-jet printing. This process allows to apply conductive ink directly into the geometric body, but requires expensive equipment. Pad printing, on the other hand, is an indirect printing process, in which a soft silicone mold transfers the ink from a printing plate to a component, transferring two-dimensional patterns onto three-dimensional bodies (c.f. Figure 5b). The hermetic encapsulation of partial areas by a 5 µm Parylene layer on the convex side of the lens would guarantee electrical safety while maintaining oxygen permeability. Concluding, the hybrid approach described here with pockets for the individual electronic components seems to be feasible and could pave the way towards a fully closed system like a smart contact lens.

### 3.3 Intraocular Implant

The philosophy of the implant is that it can be implanted in presbyopes who would have received an intraocular lens (IOL) after a cataract surgery. Usually, before undergoing surgery, where the crystalline lens is removed, the patient can choose between a monofocal or a multifocal IOL. However, the latter often leads to a higher risk in contrast sensi-

tivity, glare or halo effects (Khandelwal *et al.*, 2019; Schallhorn *et al.*, 2021). This circumstance is caused by the simultaneous projection of multiple focal planes onto the retina, which can reduce the amount of light available for each image and lead to overlapping visual impressions. This is why they tend to be a niche product (Bellucci, 2013), whereas monofocal IOLs are the most common (Boyd and Lipsky, 2019). Due to their fixed focal distance, monofocal IOLs have the drawback that they can only cover the entire visual range in combination with spectacles. In addition, there are also accommodating IOLs that utilize different approaches such as shifting lenses or gel-based designs to actively vary dioptric power, but these still face challenges as none have yet been able to achieve three diopters or more (Varssano, 2024). According to Schor, at least five diopters are required to correct presbyopia (Schor, 2012). This shortcoming shall be closed in the long term with the approach presented here. By continuously detecting the accommodation-dependent biopotentials and the resulting control of a tunable lens, the neurological feedback loop of accommodation could be closed. It was shown that the neuromuscular signals from the ciliary muscle in vivo can be recorded using needle electrodes (Jacobson *et al.*, 1958). While the previous contact lens study (Schumayer, Sigdel, Jarboui, *et al.*, 2025) indicated accommodation-related biopotential signal characteristics, the question remains regarding the influence of blinks, for instance, on intraocular electrical conduction. In comparison with needle electrodes, a more practical approach for recording the ciliary muscles' biopotentials is presented in *2.3 Publication – Ring Electrode* and can be implanted additionally during IOL surgery. By positioning the ring electrode directly in the sulcus, anterior to the ciliary body and posterior to the iris, it is possible to record accommodation-dependent biopotentials. While the in vivo signal characteristics will be described elsewhere (Sigdel, unpublished data, 2025), this approach demonstrated that artifacts caused by blinkers are not present in a non-human primate. Due to the complexity of implanting the ring electrode into the sulcus via a 2 mm incision at the limbus, the geometry of the ring electrode was revised to better withstand torsion and bending stresses. In the future, it will be interesting to investigate whether a modified circular segment (e.g., 120°) is also sufficient as the electrode geometry to measure the ciliary muscles' signals reliably. These segments are usually used as a supplement to conventional capsular tension rings (Weber and Cionni, 2015) and would simplify implantation.

While currently the inner and outer surface of the ring electrode serve as electrode surfaces, it also raises the question of whether one electrode surface is sufficient. Utilizing only one electrode surface would simplify the manufacturing process of the ring electrode, as a ring made of solid metallic material, such as gold, could be used instead of a coated polymer. Another advantage of this suggestion would be that the contacting, which is currently carried out precisely by hand, could be replaced by spot welding. Another approach to simplify the surgery procedure would be to use shape memory materials like alloys (Kim *et al.*, 2023) or polymers (Xia *et al.*, 2021). Thereby, a self-positioning of the electrode along the ciliary sulcus would theoretically be possible. Since thermal shape memory materials, for instance, require high temperatures for form-imprint, the so-called transition temperature, they show a flexible behavior at room temperature, which subsequently changes back to the imprinted form after reaching a certain temperature (e.g., body temperature). While these improvements in geometry and materials of the electrode could simplify the surgery procedure, another approach would be to use a capsular tension ring applicator, as these are commonly utilized. The applicator has a cannula-like tip, similar to a syringe, leading only to a minimal incision. The capsular tension ring is advanced through the applicators' cannula and unfolds at the intended location like the capsular bag or the ciliary sulcus.

Due to the arrangement of the implant's three main components (battery, PCB, electrode) on and in the eye, a partial and flexible encapsulation of the electronics is required. The transmission of the measured values via Bluetooth makes metallic encapsulation unsuitable due to electromagnetic shielding. Ceramic, being brittle, is also unsuitable for an implant that is implanted in a curved state. An appropriate material was found by using Parylene C, a flexible and biocompatible polymer with a low moisture vapor transmission, withstanding harsh conditions of the body and common sterilization procedures such as the ethylene oxide sterilization process. Previous tests in the field of accelerated aging at 60°C preceded the use of the double Parylene layer. Here, it could be verified that the encapsulation will not fail within a simulated lifetime of two years. Therefore, the implant was coated two times (2 x 10 µm) to ensure redundancy, preventing imperfections such as pinholes that can cause implant failure. Furthermore, critical geometries of the implant and the entire battery were primarily coated with silicone. However, the first surgery in a non-human primate showed that the metallic surgical instruments punctured the

Parylene C coating, which led to an implant failure. Retrospective examination showed a pitting corrosion at the battery that might have been triggered during the surgery by pushing the battery behind the bulbus. Therefore, the whole battery and PCB, except the PCB's flexible bridge, as shown in Figure 6a, were covered with epoxy from then on. To further reduce the risk of failure due to a punctured encapsulation, an instruction for the physicians was written to raise awareness where and how the implant is to be handled.

Already, the preliminary laboratory tests indicated that the power consumption of the implant shows a temperature-specific dependency. This circumstance must be taken into account for further estimations on the energy requirements of the implant. The initially used stacked (2x 1.55 V) silver oxide batteries (V319; Varta AG; Ellwangen; Germany) proved to be unreliable under high power loads resulting from, among others, Bluetooth events. As recommended for biomedical purposes (Takeuchi *et al.*, 2009; Newaskar and Patil, 2021), the primary non-rechargeable lithium battery (CR1025; Renata AG; Itingen; Swiss) was selected due to its high energy density, the predictable discharge curve, and the ability to provide high energy rapidly (Root, 2013). While rechargeable batteries have not yet been considered due to their additional need for charging electronics and increased operational complexity, this is something that needs to be addressed in the future in order to be able to operate the implant ideally for decades. Additionally, such a power supply would be beneficial as it could be charged inductively, similar to the subretinal alpha-IMS implant (Alpha IMS; Retina Implant AG; Reutlingen; Germany) (Stingl *et al.*, 2013), or that of a cochlear implant (Zeng *et al.*, 2008; Macherey and Carlyon, 2014). While these systems rely on an implanted inductive charging system behind the ear, another approach would be to place the inductive coil outside on the bulb, like the Argus® II retinal Prosthesis (Second Sight Medical Products, Inc.; Sylmar; CA; USA) (Luo and da Cruz, 2016).

In the future, in addition to the energy supply, the encapsulation and implementation of a tunable lens should be addressed. One approach to improve encapsulation is multi-layer organic-inorganic systems. By combining the excellent properties of ceramics in terms of hermeticity and the mechanical flexibility of polymers, both the brittle behavior of ceramics and the relative water vapor permeability of polymers could be compensated for. A favorable ceramics nanolaminates combination is $Al_2O_3/TiO_2$, as it has already proven

its long-term stability in a simulated body-like environment (Passlack *et al.*, 2023). Additionally, by adding a polymer for flexibility, a multilayer system including Parylene C and $Al_2O_3/TiO_2$ is favorable (Kirsten *et al.*, 2013; Nanbakhsh *et al.*, 2025). The literature describes that $Al_2O_3$/Parylene C has a 4.6 to 10 times longer lifetime compared to a Parylene C coating due to the excellent moisture barrier of aluminum oxide (Minnikanti *et al.*, 2014; Xie *et al.*, 2015). Unfortunately, $Al_2O_3$ does not resist biodegradation in a body-like environment, which could be compensated by the use of $TiO_2$ and its good chemical stability (Mario and Morales, 2015). The resulting multilayer system consisting of Parylene C, $TiO_2$, and $Al_2O_3$ could ensure a flexible and long-term encapsulation. In addition, a partial outer epoxy layer provides proven protection against the effects of mechanical forces.

### 3.4 Integrative Discussion & Conclusion

In light of the economic (Frick *et al.*, 2015; Berdahl *et al.*, 2020; Ma *et al.*, 2022) and individual (Berdahl *et al.*, 2020; Markoulli *et al.*, 2024) impact of uncorrected presbyopia, various approaches are being developed to restore vision and improve patients' quality of life. However, all these vision treatments have their merits and limitations, influence normal vision, and do not restore the natural accommodation. For this reason, this interdisciplinary work explores advancements in accommodating visual aids by integrating innovations in measurement tools and different approaches to bioelectric potential detection. The long-term goal is to develop a closed-loop, biomimetic visual aid like a smart contact lens or an intraocular implant. While a contact lens may be more suitable in the early stages of presbyopia, insertion becomes increasingly difficult as motor skills decline with age (Seidler *et al.*, 2010). This suggests that an implant may be a more appropriate solution in advanced age or could serve as a replacement for the crystalline lens in cataract treatment. Therefore, the progression of presbyopia as well as the efficiency of the presbyopic correction has to be determined. One approach is to determine the presbyope's near point of clear vision, also known as Amplitude of Accommodation (AoA) via the subjective push-up method. While clinically common, this method has some sources of errors caused by the operation, examiner, and displacement, for example (Burns *et al.*, 2020). Therefore, a motorized push-up version with a constant travel speed of the visual

target and operated by the participant themselves was developed. By measuring 26 emmetropes, it was shown that the known limitation of the examiner (Burns *et al.*, 2020) can be reduced while simultaneously improving the subject's credibility of the measurement device. For this reason, the motorized accommodation ruler was also utilized in the contact lens electrode study to determine the AoA of the 24 emmetropes. This study aimed to non-invasively investigate the accommodation-related, electrical signals associated with ciliary muscle and confounding signals, in relation to the actual refractive changes measured using an eccentric infrared Photorefractor. Parallel to the non-invasive approach, an in vivo measurement was conducted to verify whether the biopotentials could be measured via an implant. While the flexible printed circuit board (Kaltenstadler *et al.*, 2024) and the software (Sigdel, unpublished data, 2025) were developed in separate research efforts, the design of the ring electrode and the encapsulation of the implant were developed within the scope of this project. Inspired by conventional capsular tension rings, the geometry of the ring electrode was modified to meet the specific requirements of biopotential recordings. Meanwhile, the ring electrode manufacturing process combined microsystem technologies such as laser application and thin film coating. The urge for the PCB's flexibility to fixate it directly on the bulbus with the simultaneous mechanical stability to withstand the surgery procedure and sterilization process challenged the encapsulation development. Therefore, the encapsulated implant but also the ring electrode were tested via accelerated aging to confirm that they could withstand the body's harsh environment for at least half a year. Thereafter, the implant was tested in a non-human primate and showed the expected biopotential signal curve known from the contact lens electrode study. Summarizing, the accommodation-related neuromuscular signals are non-invasively but also invasively measurable. The next step includes utilizing these biopotentials to steer a tunable lens into the needed refraction, thus closing the dynamic feedback-loop of accommodation. Although dynamic closed-loop accommodation represents the ideal treatment for presbyopia, no current treatments are based on this principle (Chang *et al.*, 2021). As a first step towards such an approach, a spectacle-mounted tunable lens was steered according to the non-invasively measured biopotentials of the ciliary muscle in presbyopes (q.v. *2.4.1 Tunable Spectacles in Presbyopes*). Although these are only preliminary results, they confirm the effect of the natural feedback loop

(Toates, 1972) in which the ciliary muscle is activated according to the perceived blurring. These were the first experiments to record ciliary muscle signals via contact lens electrodes to control tunable lenses and restore accommodation in presbyopes.

To conclude, the biopotentials of the ciliary muscle could be measured non-invasively in 12 emmetropes using a scleral contact lens electrode and invasively in cynomolgus monkeys via an intraocular implant and a novel ring electrode. The contact lens electrode study showed that the accommodation-related biopotentials of the ciliary muscle are differentiable compared to expected confounding signals. Furthermore, the study revealed that the electrical signal of the ciliary muscle has at least some neurological component, as the characteristic signals could still be measured in three out of five participants despite temporarily paralyzing the intraocular muscles. In the premeasurements of the contact lens electrode study, the newly developed motorized accommodation ruler was used due to its superiority over conventional push-up rulers for determining the amplitude of accommodation. Additionally, the motorized ruler is used in the study involving presbyopic individuals to determine their residual accommodation ability. This study, *Tunable Spectacles in Presbyopes*, though still ongoing, shows promising results, suggesting that it is possible to restore the natural accommodation reflex by using biopotentials from the ciliary muscle as a control input for a tunable lens.

# 4. Summary

The focus shift from far to near, called accommodation, is controlled by a contraction of the ciliary muscle, leading to a change in the curvature of the crystalline lens. This contraction leads to changes in electrical potentials, which are recorded as neuromuscular biosignals. While the ciliary muscle stays functional throughout life, the crystalline lens gets stiffer, leading to a decline in the ability to change its shape and to focus on near objects. This condition, called "Presbyopia", starts during the mid-forties and progresses with age. Current vision treatments, like progressive lenses, contact lenses, and intraocular lenses, as well as pharmaceutical treatments, have their merits and limitations, but none of them restore natural accommodation. To this day, the subjective amplitude of accommodation (AoA) is used not only to monitor the progress of presbyopia and help opticians assess subjective visual perception, but also in ongoing research investigating the related accommodative-biopotentials. Even though the limitations of subjective measurement methods to determine the AoA are known, they are still applied in daily clinical practice because of their ease and speed of the procedure. Within the scope of the work "*Comparing a Novel Motorized Push-Up Ruler with Conventional Subjective Methods for Measuring the Amplitude of Accommodation*", an improved, motorized push-up ruler was developed and compared against the clinical standards push-up and push-down methods. Additionally, the volunteers were asked about their satisfaction with the ease of use, and their confidence in the measurement reliability. The findings showed that the motorized version was superior in reliability without compromising precision, reducing known examiner limitations of the standard subjective procedures. Besides that, the subjective impression showed that the participants were more convinced by the motorized push-up ruler. Therefore, the motorized ruler was utilized in the contact lens electrode study "*Non-invasive measuring of biopotentials of the ciliary muscle during accommodation in emmetropes*" in 12 participants, in which the biopotentials of the ciliary muscle during accommodation were characterized. Even though accommodation-related biopotentials and artifacts characteristics are essential for the adaptive control of an artificial lens in the future, previous studies have only demonstrated their presence without providing a detailed characterization of these signals and artifacts. By comparing these biopotentials with refractive measurements using eccentric infrared photorefraction during a controlled change in focus, it was possible to characterize accommodation-related biopotentials and

related artifacts such as blinking or eye movements. An intraocular measurement of the signals, taken directly at the origin, is expected to be less influenced by artifacts. For this reason, a novel approach to detecting ciliary muscle biopotentials is to use a ring electrode implant. In the manuscript "*Design and In Vivo Evaluation of an Intraocular Electrode for Ciliary Muscle Biopotential Measurement in a Non-Human Primate Model of Human Accommodation*" the consecutive steps from the conception phase towards testing, first in a simulated, and subsequently in an *in vivo* model are presented. The manufacturing included femto-laser cutting and physical vapor coating. The long-term stability was assessed via accelerated aging at 60°C in phosphate-buffered saline solution together with an electrical impedance measurement to detect possible electrical shifts over time. This is the first work measuring biopotentials of the ciliary muscle via a wireless intraocular implant.

The ring electrode implant and the contact lens electrode pave the way towards new presbyopia treatments. They enable the control of tunable lenses and thereby restore natural accommodation through neuromuscular signals of the ciliary muscle, as indicated by the preliminary results of the study "*Preserved Ciliary Muscle Biopotentials Enable Artificial Lens Control and Near Vision Recovery in Long-Term Presbyopia"*. In parallel, the motorized AoA measurement helps to improve the study and clinical quality of subjective measurement methods. Overall, this work enhances our understanding of accommodation by focusing on the electrical biopotentials of the ciliary muscle, which have been poorly investigated to date. The findings hold promising potential for the development of new visual aids that enable more natural focusing.

# 5. Zusammenfassung der Dissertation

Der Fokuswechsel von fern zu nah, genannt Akkommodation, wird durch eine Kontraktion des Ziliarmuskels gesteuert, was zu einer Anpassung der Krümmung der Augenlinse führt. Die beschriebene Kontraktion führt zu Veränderungen des elektrischen Potenzials, die als neuromuskuläre Biosignale aufgezeichnet werden. Während der Ziliarmuskel über das ganze Leben funktionsfähig bleibt, wird die Linse steifer, was zu einer nachlassenden Nahsehschärfe führt. Dieser als „Presbyopie“ oder „Alterssichtigkeit“ bezeichnete Zustand beginnt mit Mitte vierzig und schreitet mit der Zeit voran. Aktuelle Sehhilfen wie Gleitsicht- und Kontaktlinsen oder Intraokularlinsen, aber auch pharmazeutische Behandlungen haben alle ihre Vor- und Nachteile, aber keine kann die natürliche Akkommodation wiederherstellen. Bis heute wird die subjektive Akkommodationsbreite nicht nur zur Verlaufsbeobachtung der Presbyopie und zur Unterstützung von Optiker und Optikerinnen bei der Beurteilung der subjektiven visuellen Wahrnehmung verwendet, sondern auch in der laufenden Forschung zur Untersuchung der damit verbundenen akkommodativen Biopotenziale. Obwohl die Limitationen der subjektiven Messmethoden zur Bestimmung der Akkommodationsbreite bekannt sind, werden sie aufgrund ihrer Einfachheit und Schnelligkeit in der täglichen klinischen Praxis immer noch angewendet. Im Rahmen der Arbeit „*Comparing a Novel Motorized Push-Up Ruler with Conventional Subjective Methods for Measuring the Amplitude of Accommodation*“ wurde ein verbesserter, motorisierter Push-Up Stab entwickelt und mit den klinischen Standards Push-Up und Push-Down Methoden verglichen. Dazu wurde die Akkommodationsbreite von 26 normalsichtige Probanden mit den drei Messmethoden in randomisierter Reihenfolge gemessen. Zusätzlich wurden die Freiwilligen zu ihrer Zufriedenheit hinsichtlich der Benutzerfreundlichkeit und dem Vertrauen in die Zuverlässigkeit der jeweiligen Messmethode befragt. Die Ergebnisse zeigen, dass die motorisierte Version in Bezug auf die Zuverlässigkeit überlegen ist, ohne die Präzision zu beeinträchtigen, wodurch die bekannten Limitationen der subjektiven Standardverfahren verringert wurden. Zusätzlich zeigte der subjektive Eindruck der Teilnehmenden, dass sie von der motorisierten Version stärker überzeugt waren. Daher wurde der motorisierte Akkommodationsmessstab auch in der Kontaktlinsen-Elektrodenstudie „*Non-invasive measuring of biopotentials of the ciliary muscle during accommodation in emmetropes*“ mit 12 Teilnehmern eingesetzt. Obwohl die akkommodationsbedingten Biopotenziale und die Eigenschaften der Artefakte für die

adaptive Steuerung einer variablen Linse in Zukunft essentiell sind, haben frühere Studien ihr Vorhandensein nur nachgewiesen, ohne eine detaillierte Charakterisierung dieser Signale zu liefern. Durch den Vergleich dieser Biopotenziale mit Refraktionsmessungen mittels exzentrischer Infrarot-Photorefraktion während eines kontrollierten Fokuswechsels war es möglich, akkommodationsbedingte Biopotenziale und damit verbundene Artefakte wie Blinzeln oder Augenbewegungen zu beschreiben. Die intraokulare Messung der Signale direkt am Ursprung, dem Ziliarmuskel, sollte weniger durch Artefakte beeinflusst sein. Aus diesem Grund wurde ein weiterer neuartiger Ansatz zur Erfassung der Ziliarmuskelbiopotenziale über ein Ringelektrodenimplantat entwickelt. In dem Manuskript „*Design and In Vivo Evaluation of an Intraocular Electrode for Ciliary Muscle Biopotential Measurement in a Non-Human Primate Model of Human Accommodation*“ werden die einzelnen Schritte von der Konzeptionsphase bis zur Erprobung in einem simulierten, und später in einem präklinischen in vivo Modell beschrieben. Während die Herstellung das Schneiden mittels Femtosekundenlaser und physikalisches Aufdampfen umfasste, wurde die Langzeitstabilität für ein Jahr durch beschleunigte Alterung bei 60°C in phosphatgepufferter Kochsalzlösung bewertet. Gleichzeitig erfolgte eine elektrische Impedanzmessung, um mögliche elektrische Veränderungen im Laufe der Zeit zu erfassen. Dies ist die erste Arbeit, bei der Biopotenziale des Ziliarmuskels über ein drahtloses intraokulares Implantat gemessen wurden.

Das Ringelektrodenimplantat und die Kontaktlinsenelektrode ebnen den Weg für neue Behandlungsmethoden der Presbyopie. Sie ermöglichen die Verwendung neuroelektrischer Signale des Ziliarmuskels zur Steuerung von adaptiven Linsen und damit die Wiederherstellung der natürlichen Akkommodation, wie die vorläufigen Ergebnisse der Studie „*Preserved Ciliary Muscle Biopotentials Enable Artificial Lens Control and Near Vision Recovery in Long-Term Presbyopia*” belegen. Begleitend dazu trägt die motorisierte AoA-Messung dazu bei, die Forschungs- und klinische Qualität subjektiver Messmethoden zu verbessern. Insgesamt verhilft diese Arbeit zu einem besseren Verständnis der Akkommodation, wobei der Schwerpunkt auf den bisher kaum untersuchten elektrischen Biopotenzialen des Ziliarmuskels während der Akkommodation liegt. Sie eröffnet vielversprechende Aussichten für neue Sehhilfen, die eine natürlichere Fokussierung ermöglichen.

# 6. List of References

Adel, N.L. (1966) 'Electromyographic and Entopic Studies suggesting a Theory of Action of the Ciliary Muscle in Accommodation for Near and its Influence on the Development of Myopia*', *Optometry and Vision Science*, 43(1). Available at: https://journals.lww.com/optvissci/fulltext/1966/01000/electromyographic_and_entoptic_studies_sug_gesting.4.aspx.

Adler, P., Scally, A.J. and Barrett, B.T. (2013) 'Test-retest reproducibility of accommodation measurements gathered in an unselected sample of UK primary school children', *British Journal of Ophthalmology*, 97(5), pp. 592–597. Available at: https://doi.org/10.1136/bjophthalmol-2012-302348.

Agarwala, R. *et al.* (2022) 'Evaluation of a liquid membrane-based tunable lens and a solid-state LIDAR camera feedback system for presbyopia', *Biomedical Optics Express*, 13(11), p. 5849. Available at: https://doi.org/10.1364/boe.471190.

Ahn, S.H., Jeong, J. and Kim, S.J. (2019) 'Emerging encapsulation technologies for long-term reliability of microfabricated implantable devices', *Micromachines*. MDPI AG. Available at: https://doi.org/10.3390/mi10080508.

Alpern, M., Ellen, P. and Goldsmith, R. (1958) 'The Electrical Response of the Human Eye in Far-to-Near Accommodation', *A.M.A. Archives of Ophthalmology*, 60(4), pp. 592–602. Available at: https://doi.org/10.1001/archopht.1958.00940080612007.

AlRyalat, S.A. *et al.* (2022) 'The Effect of Wearing Eyeglasses on the Perception of Attractiveness, Confidence, and Intelligence', *Cureus*. Available at: https://doi.org/10.7759/cureus.23542.

Ashish Daniel *et al.* (2024) 'Advancement in biomedical implant materials—a mini review', *Frontiers in Bioengineering and Biotechnology*. Frontiers Media SA. Available at: https://doi.org/10.3389/fbioe.2024.1400918.

Ashwini and Raju (2023) 'Autonomic Nervous System and Control of Visual Function', *Annals of Neurosciences*. SAGE Publications Inc., pp. 151–153. Available at: https://doi.org/10.1177/09727531231176119.

Atchison, D. (2023) *Optics of the human eye*. CRC Press. Available at: https://doi.org/10.1201/9781003128601.

Atchison, D.A. (1995) 'Accommodation and presbyopia', *Ophthalmic and Physiological Optics*, 15(4), pp. 255–272. Available at: https://doi.org/10.1046/j.1475-1313.1995.9500020e.x.

Atchison, D.A., Capper, E.J. and McCabe, K.L. (1994) 'Critical Subjective Measurement of Amplitude of Accommodation', *Optometry and Vision Science*, 71(11). Available at: https://journals.lww.com/optvissci/Fulltext/1994/11000/Critical_Subjective_Measurement_of_Amplitude_of.5.aspx.

Augusteyn, R.C. (2007) *Growth of the human eye lens*, *Molecular Vision*.

Bababekova, Y. *et al.* (2011) 'Font Size and Viewing Distance of Handheld Smart Phones', *Optometry and Vision Science*, 88(7). Available at: https://doi.org/10.1097/OPX.0b013e3182198792.

Bailey, J. *et al.* (2022) 'Infrared triggered smart contact lens for the treatment of presbyopia', *Journal of Physics D: Applied Physics*, 55(21). Available at: https://doi.org/10.1088/1361-6463/ac52cc.

Bassnett, S. (2021) 'Zinn's zonule', *Progress in Retinal and Eye Research*. Elsevier Ltd. Available at: https://doi.org/10.1016/j.preteyeres.2020.100902.

Bastawrous, A. and and Suni, A.-V. (2020) 'Thirty Year Projected Magnitude (to 2050) of Near and Distance Vision Impairment and the Economic Impact if Existing Solutions are Implemented Globally', *Ophthalmic Epidemiology*, 27(2), pp. 115–120. Available at: https://doi.org/10.1080/09286586.2019.1700532.

Beebe, D.C. (2008) 'Maintaining transparency: A review of the developmental physiology and pathophysiology of two avascular tissues', *Seminars in Cell and Developmental Biology*. Elsevier Ltd, pp. 125–133. Available at: https://doi.org/10.1016/j.semcdb.2007.08.014.

Beiko, G.H.H. (2013) 'Comparison of visual results with accommodating intraocular lenses versus mini-monovision with a monofocal intraocular lens', *Journal of Cataract and Refractive Surgery*, 39(1), pp. 48–55. Available at: https://doi.org/10.1016/j.jcrs.2012.08.059.

Bellucci, R. (2013) 'An introduction to intraocular lenses: Material, optics, haptics, design and aberration', in *Cataract*. S. Karger AG, pp. 38–55. Available at: https://doi.org/10.1159/000350902.

Berdahl, J. *et al.* (2020) 'Patient and Economic Burden of Presbyopia: A Systematic Literature Review', *Clinical Ophthalmology*, Volume 14, pp. 3439–3450. Available at: https://doi.org/10.2147/opth.s269597.

Bornschein, H. and Schubert, G. (1957) 'Bestandpotential und Akkommodationszustand des menschlichen Auges', *Albrecht von Graefes Archiv für Ophthalmologie*, 159, pp. 45–51. Available at: https://doi.org/10.1007/BF00683597.

Bourne, R.R.A. *et al.* (2021) 'Causes of blindness and vision impairment in 2020 and trends over 30 years, and prevalence of avoidable blindness in relation to VISION 2020: The Right to Sight: An analysis for the Global Burden of Disease Study', *The Lancet Global Health*, 9(2), pp. e144–e160. Available at: https://doi.org/10.1016/S2214-109X(20)30489-7.

Breitweiser, G., Varadarajan, B.N. and Wafer, J. (1970) 'Influence of Film Condensation and Source Radiation on Substrate Temperature', *Journal of Vacuum Science and Technology*, 7(1), pp. 274–277. Available at: https://doi.org/10.1116/1.1315817.

Burns, D. *et al.* (2014) 'Clinical measurement of amplitude of accommodation: a review', *Optometry in Practice*, 15, pp. 75–86.

Burns, D.H. *et al.* (2020) 'Sources of error in clinical measurement of the amplitude of accommodation', *Journal of Optometry*, 13(1), pp. 3–14. Available at: https://doi.org/10.1016/J.OPTOM.2019.05.002.

Callou, T.P. *et al.* (2016) 'Advances in femtosecond laser technology', *Clinical Ophthalmology*. Dove Medical Press Ltd, pp. 697–703. Available at: https://doi.org/10.2147/OPTH.S99741.

Campbell, F.W. and Westheimer, G. (1960) 'Dynamics of accommodation responses of the human eye', *The Journal of physiology*, 151(2), p. 285. Available at: https://doi.org/10.1113/jphysiol.1960.sp006438.

Canals, M. *et al.* (1996) 'Scanning electron microscopy of the human zonule of the lens (Zonula ciliaris)', *Cells Tissues Organs*, 157(4), pp. 309–314. Available at: https://doi.org/10.1159/000147893.

Chang, D.H. *et al.* (2021) 'Presbyopia treatments by mechanism of action: A new classification system based on a review of the literature', *Clinical Ophthalmology*. Dove Medical Press Ltd, pp. 3733–3745. Available at: https://doi.org/10.2147/OPTH.S318065.

Charman, W.N. (2008) 'The eye in focus: Accommodation and presbyopia', *Clinical and Experimental Optometry*, 91(3), pp. 207–225. Available at: https://doi.org/10.1111/j.1444-0938.2008.00256.x.

Charman, W.N. (2014a) 'Developments in the correction of presbyopia I: Spectacle and contact lenses', *Ophthalmic and Physiological Optics*, pp. 8–29. Available at: https://doi.org/10.1111/opo.12091.

Charman, W.N. (2014b) 'Developments in the correction of presbyopia II: Surgical approaches', *Ophthalmic and Physiological Optics*, 34(4), pp. 397–426. Available at: https://doi.org/10.1111/opo.12129.

Charman, W.N. (2017) 'Virtual Issue Editorial: Presbyopia – grappling with an age-old problem', *Ophthalmic and Physiological Optics*. Blackwell Publishing Ltd, pp. 655–660. Available at: https://doi.org/10.1111/opo.12416.

Chen, J. *et al.* (2020) 'Placement of dual capsular tension rings for the combined management of traumatic cyclodialysis cleft and zonular dialysis', *Eye and Vision*, 7(1). Available at: https://doi.org/10.1186/s40662-020-00219-x.

Chen, W., Tan, X. and Chen, X. (2016) 'Anatomy and physiology of the crystalline lens', in *Pediatric Lens Diseases*. Springer Singapore, pp. 21–28. Available at: https://doi.org/10.1007/978-981-10-2627-0_3.

Cholewiak, S.A., Love, G.D. and Banks, M.S. (2018) 'Creating correct blur and its effect on accommodation', *Journal of Vision*, 18(9), pp. 1–29. Available at: https://doi.org/10.1167/18.9.1.

Ciuffreda (2006) 'Accommodation, the pupil, and presbyopia', *Borish's clinical refraction*, pp. 93–144. Available at: https://doi.org/10.1016/B978-0-7506-7524-6.50009-0.

Clouse M.M (2017) *Recording and Processing of Tissue-Specific Ocular Electrical Biosignals for Applications in Biomedical Devices*. Dissertation. Available at: https://doi.org/10.15496/publikation-19708.

Cogan (1937) 'ACCOMMODATION AND THE AUTONOMIC NERVOUS SYSTEM', *Archives of Ophthalmology*, 18(5), pp. 739–766. Available at: https://doi.org/10.1001/archopht.1937.00850110055004.

Coleman, D.J. (1970) 'Unified model for accommodative mechanism', *American journal of ophthalmology*, 69(6), pp. 1063–1079. Available at: https://doi.org/10.1016/0002-9394(70)91057-3.

Croft, M.A. *et al.* (2013) 'Accommodative movements of the vitreous membrane, choroid, and sclera in young and presbyopic human and nonhuman primate eyes', *Investigative Ophthalmology and Visual Science*, 54(7), pp. 5049–5058. Available at: https://doi.org/10.1167/iovs.12-10847.

Croft, M.A., Glasser, A. and Kaufman, P.L. (2001) 'Accommodation and Presbyopia', *International Ophthalmology Clinics*, 41(2). Available at: https://journals.lww.com/internat-ophthalmology/fulltext/2001/04000/accommodation_and_presbyopia.5.aspx.

Deflorian, F. (2020) 'Special issue: "advanced hybrid coatings and thin films for surface functionalization"', *Coatings*. MDPI AG, pp. 1–3. Available at: https://doi.org/10.3390/coatings10111020.

Delamere, N.A. (2005) 'Ciliary Body and Ciliary Epithelium', *Advances in Organ Biology*, pp. 127–148. Available at: https://doi.org/10.1016/S1569-2590(05)10005-6.

Deutsches Institut für Normung e.V. (2016) 'EN 62047-1:2016 - Semiconductor devices – Microelectromechanical devices – Part 1: Terminology (IEC 62047-1:2016); German version', *CENELEC*. Berlin: DIN; Brussels: CENELEC.

Duane, A. (1912) 'Normal values of the accommodation at all ages', *Journal of the American Medical Association*, 59(12), pp. 1010–1013. Available at: https://doi.org/10.1001/jama.1912.04270090254042.

Duane, A. (1922) 'Studies in monocular and binocular accommodation, with their clinical application', *Transactions of the American Ophthalmological Society*, 20, p. 132.

Esmail, H. and Arblaster, G. (2017) 'A comparison of conventional and modified push-up methods of measuring the near point of accommodation', *British and Irish Orthoptic Journal*, 13. Available at: https://doi.org/10.22599/bioj.100.

Fincham, E.F. (1937) *The Mechanism of Accommodation*. G. Pulman & sons, Limited (British journal of ophthalmology. Monograph supplement). Available at: https://books.google.de/books?id=ujDPGAAACAAJ (Accessed: 23 June 2025).

Fincham, E.F. (1951) 'The accommodation reflex and its stimulus', *The British journal of ophthalmology*, 35(7), p. 381. Available at: https://doi.org/10.1136/bjo.35.7.381.

Fincham, E.F. (1953) 'Defects of the colour-sense mechanism as indicated by the accommodation reflex', *The Journal of physiology*, 121(3), pp. 570–580. Available at: https://doi.org/10.1113/jphysiol.1953.sp004965.

Flügel-Koch, C.M. *et al.* (2016) 'Anteriorly located zonular fibres as a tool for fine regulation in accommodation', *Ophthalmic and Physiological Optics*, 36(1), pp. 13–20. Available at: https://doi.org/10.1111/opo.12257.

Franco, S. *et al.* (2022) 'Accommodative and binocular vision dysfunctions in a Portuguese clinical population', *Journal of Optometry*, 15(4), pp. 271–277. Available at: https://doi.org/10.1016/j.optom.2021.10.002.

Frick, K.D. *et al.* (2015) 'The Global Burden of Potential Productivity Loss from Uncorrected Presbyopia', *Ophthalmology*, 122(8), pp. 1706–1710. Available at: https://doi.org/10.1016/j.ophtha.2015.04.014.

Fricke, T.R. *et al.* (2018) 'Global Prevalence of Presbyopia and Vision Impairment from Uncorrected Presbyopia: Systematic Review, Meta-analysis, and Modelling', *Ophthalmology*, 125(10), pp. 1492–1499. Available at: https://doi.org/10.1016/j.ophtha.2018.04.013.

Gawron (1983) 'Ocular Accommodation, Personality, and Autonomic Balance', *Optometry and Vision Science*, 60(7), pp. 630–639.

George, S.M. (2010) 'Atomic layer deposition: An overview', *Chemical Reviews*, 110(1), pp. 111–131. Available at: https://doi.org/10.1021/cr900056b.

Gilmartin, B. (1986) *A REVIEW OF THE ROLE OF SYMPATHETIC INNERVATION OF THE CILIARY MUSCLE IN OCULAR ACCOMMODATION*, *Ophlhal. Physiol. Opt*. Available at: https://doi.org/10.1111/j.1475-1313.1986.tb00697.x.

Gilmartin, B., Mallen, E.A.H. and Wolffsohn, J.S. (2002) 'Sympathetic control of accommodation: Evidence for inter-subject variation', *Ophthalmic and Physiological Optics*, 22(5), pp. 366–371. Available at: https://doi.org/10.1046/j.1475-1313.2002.00054.x.

Glasser, A. (2006) 'Accommodation: mechanism and measurement', *Ophthalmol Clin North Am*, 19(1), pp. 1–12. Available at: https://doi.org/10.1016/j.ohc.2005.09.004.

Glasser, A. and Kaufman, P.L. (1999) 'The Mechanism of Accommodation in Primates', *Ophthalmology*, 106, pp. 863–872. Available at: https://doi.org/10.1016/S0161-6420(99)00502-3.

Golda-Cepa, M. *et al.* (2020) 'Recent progress on parylene C polymer for biomedical applications: A review', *Progress in Organic Coatings*. Elsevier B.V. Available at: https://doi.org/10.1016/j.porgcoat.2019.105493.

Griesser, H.J. (2016) *Thin film coatings for biomaterials and biomedical applications*. Edited by Griesser J Hans. Woodhead Publishing. Available at: https://doi.org/10.1016/C2014-0-01872-2.

Grzybowski, A., Kapitanovaite, L. and Zemaitiene, R. (2024) 'An Updated Systematic Review of Pharmacological Treatments for Presbyopia', *Advances in Ophthalmology Practice and Research.* Available at: https://doi.org/10.1016/j.aopr.2024.09.001.

Grzybowski, A., Markeviciute, A. and Zemaitiene, R. (2020) 'A review of pharmacological presbyopia treatment', *Asia-Pacific Journal of Ophthalmology*. Lippincott Williams and Wilkins, pp. 226–233. Available at: https://doi.org/10.1097/APO.0000000000000297.

Grzybowski, A. and Ruamviboonsuk, V. (2022) 'Pharmacological Treatment in Presbyopia', *Journal of Clinical Medicine*. MDPI. Available at: https://doi.org/10.3390/jcm11051385.

Gualdi, L. *et al.* (2017) 'Ciliary muscle electrostimulation to restore accommodation in patients with early presbyopia: Preliminary results', *Journal of Refractive Surgery*, 33(9), pp. 578–583. Available at: https://doi.org/10.3928/1081597X-20170621-05.

Hagiwara, H. and Ishikawa, S. (1962) 'The Action Potential of the Ciliary Muscle', *Ophthalmologica*, 144(5), pp. 323–340. Available at: https://doi.org/10.1159/000304372.

Hasart, J.K. and Hutchinson, K.L. (1993) 'The effects of eyeglasses on perceptions of interpersonal attraction', *Journal of Social Behavior and Personality*, 8(3), p. 521.

Hassler, C., Boretius, T. and Stieglitz, T. (2011) 'Polymers for neural implants', *Journal of Polymer Science, Part B: Polymer Physics*, pp. 18–33. Available at: https://doi.org/10.1002/polb.22169.

He, R. *et al.* (2018) 'New Insights Into Interactions of Presynaptic Calcium Channel Subtypes and SNARE Proteins in Neurotransmitter Release', *Frontiers in Molecular Neuroscience*, 11. Available at: https://doi.org/10.3389/fnmol.2018.00213.

Heath, G.G. (1956) 'COMPONENTS OF ACCOMMODATION*', *Optometry and Vision Science*, 33(11). Available at: https://journals.lww.com/optvissci/fulltext/1956/11000/components_of_accommodation_.1.aspx.

Helmholtz, H. von (1855) 'Ueber die accommodation des auges', *Archiv für Ophthalmologie*, 1(2), pp. 1–74. Available at: https://doi.org/10.1007/BF02720789.

Heron, G., Charman, W.N. and Schor, C. (2001) *Dynamics of the accommodation response to abrupt changes in target vergence as a function of age*, *Vision Research*. Available at: https://doi.org/10.1016/S0042-6989(00)00282-0.

Holden, B.A. *et al.* (2008) *Global Vision Impairment Due to Uncorrected Presbyopia*, *Arch Ophthalmol*. Available at: https://doi.org/10.1001/archopht.126.12.1731.

Hosp, B.W. *et al.* (2024) 'Simulation of various tuning methods in autofocals using a virtual reality headset', *Optics Continuum*, 3(8), pp. 1273–1290. Available at: https://doi.org/10.1364/OPTCON.520728.

Hussaindeen, J.R. and Murali, A. (2020) 'Accommodative insufficiency: Prevalence, impact and treatment options', *Clinical Optometry*. Dove Medical Press Ltd., pp. 135–149. Available at: https://doi.org/10.2147/OPTO.S224216.

International Organization for Standardization (2010) 'ISO 10993-13:2010-11- Biological evaluation of medical devices – Part 13: Identification and quantification of degradation products from polymeric medical devices', *International Organization for Standardization*. Geneva, Switzerland. Available at: www.din.de.

International Organization for Standardization (2024a) 'ISO 10993-1:2024-07 - Biological evaluation of medical devices – Part 1: Evaluation and testing within a risk management process.', *International Organization for Standardization*. Geneva, Switzerland: International Organization for Standardization. Available at: https://doi.org/10.31030/3551000.

International Organization for Standardization (2024b) 'ISO 10993-6:2024-06 - Biological evaluation of medical devices —Part 6: Tests for local effects after implantation', *International Organization for Standardization*. Geneva, Switzerland: International Organization for Standardization. Available at: www.din.de.

International Organization for Standardization (2024c) 'ISO 11139:2018 + Amd 1:2024 - Vocabulary of terms used in sterilization and related equipment and process standards', *International Organization for Standardization*. Geneva, Switzerland: International Organization for Standardization.

Ittelson, W.H. and Ames, A. (1950) 'Accommodation, Convergence, and Their Relation to Apparent Distance', *The Journal of Psychology*, 30(1), pp. 43–62. Available at: https://doi.org/10.1080/00223980.1950.9916050.

Jacobson, J.H. *et al.* (1958) 'The Electric Activity of the Eye During Accommodation', *American Journal of Ophthalmology*, 46(5, Part 2), pp. 231–238. Available at: https://doi.org/https://doi.org/10.1016/0002-9394(58)90802-X.

Jilani, A., Abdel-wahab, M.S. and Hammad, A.H. (2017) 'Advance Deposition Techniques for Thin Film and Coating', in *Modern Technologies for Creating the Thin-film Systems and Coatings*. InTech. Available at: https://doi.org/10.5772/65702.

Jones, C.E., Atchison, D.A. and Pope, J.M. (2007) 'Changes in Lens Dimensions and Refractive Index with Age and Accommodation', *Optometry and Vision Science*, 84(10). Available at: https://doi.org/10.1097/OPX.0b013e318157c6b5.

Kaltenstadler, S. *et al.* (2024) 'An Implantable Ciliary Muscle LFP Recording and Transmitting System', in *IEEE Engineering in Medicine and Biology Conference (EMBC)*. IEEE. Available at: https://doi.org/10.1109/EMBC53108.2024.10781543.

Kandel, E.R. *et al.* (2000) *Principles of neural science*. McGraw-Hill New York.

Kaplan, S.L. and Rose, P.W. (1991) 'Plasma surface treatment of plastics to enhance adhesion', *International Journal of Adhesion and Adhesives*, 11(2). Available at: https://doi.org/10.1016/0143-7496(91)90035-G.

Karkhanis, M.U. *et al.* (2022) 'Correcting Presbyopia with Autofocusing Liquid-Lens Eyeglasses', *IEEE Transactions on Biomedical Engineering*, 69(1), pp. 390–400. Available at: https://doi.org/10.1109/TBME.2021.3094964.

Kasthurirangan, S. *et al.* (2011) 'MRI study of the changes in crystalline lens shape with accommodation and aging in humans', *Journal of Vision*, 11(3), pp. 19–19. Available at: https://doi.org/10.1167/11.3.19.

Khaldi, A. *et al.* (2020) 'A laser emitting contact lens for eye tracking', *Scientific Reports 2020 10:1*, 10(1), pp. 1–8. Available at: https://doi.org/10.1038/s41598-020-71233-1.

Khandelwal, S.S. *et al.* (2019) 'Effectiveness of multifocal and monofocal intraocular lenses for cataract surgery and lens replacement: a systematic review and meta-analysis', *Graefe's Archive for Clinical and Experimental Ophthalmology*. Springer Verlag, pp. 863–875. Available at: https://doi.org/10.1007/s00417-018-04218-6.

Kim, M.S. *et al.* (2023) 'Shape Memory Alloy (SMA) Actuators: The Role of Material, Form, and Scaling Effects', *Advanced Materials*. John Wiley and Sons Inc. Available at: https://doi.org/10.1002/adma.202208517.

Kirsten, S. *et al.* (2013) 'Barrier properties of polymer encapsulation materials for implantable microsystems', in *2013 IEEE XXXIII International Scientific Conference Electronics and Nanotechnology (ELNANO)*, pp. 269–272. Available at: https://doi.org/10.1109/ELNANO.2013.6552075.

Knaus, K.R., Hipsley, A.M. and Blemker, S.S. (2021) 'The action of ciliary muscle contraction on accommodation of the lens explored with a 3D model', *Biomechanics and Modeling in Mechanobiology*, 20(3), pp. 879–894. Available at: https://doi.org/10.1007/s10237-021-01417-9.

Kolb, H. *et al.* (2020) 'The architecture of the human fovea [Updated 2020 May 20]', *Webvision: The Organization of the Retina and Visual System [Internet]*. Available at: https://www.ncbi.nlm.nih.gov/books/NBK554706/ (Accessed: 28 February 2025).

Koretz, J.F. *et al.* (1989) 'Accommodation and presbyopia in the human eye—aging of the anterior segment', *Vision Research*, 29(12), pp. 1685–1692. Available at: https://doi.org/https://doi.org/10.1016/0042-6989(89)90150-8.

Labhishetty, V. *et al.* (2021) 'Lags and leads of accommodation in humans: Fact or fiction?', *Journal of Vision*, 21(3), p. 21. Available at: https://doi.org/10.1167/jov.21.3.21.

Levin, L.A. *et al.* (2011) *Adler's Physiology of the Eye*. 11th edn. St. Louis, MO: Saunders, Elsevier.

Lin, C.-Y. *et al.* (2020) 'Bio-Compatibility and Bio-insulation of implantable electrode prosthesis ameliorated by A-174 Silane Primed Parylene-C deposited embedment', *Micromachines*, 11(12), p. 1064. Available at: https://doi.org/https://doi.org/10.3390/mi11121064.

Lin, K.H. *et al.* (2021) 'Age-related changes in the rhesus macaque eye', *Experimental eye research*, 212, p. 108754. Available at: https://doi.org/10.1016/j.exer.2021.108754.

Lingley, A.R. *et al.* (2011) 'A single-pixel wireless contact lens display', *Journal of Micromechanics and Microengineering*, 21(12), p. 125014. Available at: https://doi.org/10.1088/0960-1317/21/12/125014.

Liu, Y.C. *et al.* (2017) 'Cataracts', *The Lancet*. Lancet Publishing Group, pp. 600–612. Available at: https://doi.org/10.1016/S0140-6736(17)30544-5.

Luo, B.P. *et al.* (2008) 'The Quality of Life Associated with Presbyopia', *American Journal of Ophthalmology*, 145(4). Available at: https://doi.org/10.1016/j.ajo.2007.12.011.

Luo, Y.H.-L. and da Cruz, L. (2016) 'The Argus® II Retinal Prosthesis System', *Progress in Retinal and Eye Research*, 50, pp. 89–107. Available at: https://doi.org/10.1016/j.preteyeres.2015.09.003.

Ma, Q. *et al.* (2022) 'Potential productivity loss from uncorrected and under-corrected presbyopia in low-and middle-income countries: A life table modeling study', *Frontiers in Public Health*, 10. Available at: https://doi.org/10.3389/fpubh.2022.983423.

Macherey, O. and Carlyon, R.P. (2014) 'Cochlear implants', *Current Biology*, 24(18), pp. R878–R884. Available at: https://doi.org/10.1016/j.cub.2014.06.053.

Mallen, E.A.H., Gilmartin, B. and Wolffsohn, J.S. (2005) 'Sympathetic innervation of ciliary muscle and oculomotor function in emmetropic and myopic young adults', *Vision Research*, 45(13), pp. 1641–1651. Available at: https://doi.org/10.1016/j.visres.2004.11.022.

Manion, G. and Stokkermans, T. (2024) 'The effect of pupil size on visual resolution', *StatPearls*. Available at: https://www.ncbi.nlm.nih.gov/books/NBK603732/ (Accessed: 1 July 2025).

De Maria, A. *et al.* (2017) 'Proteomic analysis of the bovine and human ciliary zonule', *Investigative Ophthalmology and Visual Science*, 58(1), pp. 573–585. Available at: https://doi.org/10.1167/iovs.16-20866.

Mariello, M. *et al.* (2022) 'Recent advances in encapsulation of flexible bioelectronic implants: materials, technologies and characterization methods', *Advanced Materials*, p. 2201129. Available at: https://doi.org/10.1002/adma.202201129.

Mario, J. and Morales, H. (2015) *Evaluating bicompatible barrier films as encpasulants of medical micro devices*.

Markoulli, M. *et al.* (2024) 'BCLA CLEAR Presbyopia: Epidemiology and impact', *Contact Lens and Anterior Eye*, 47(4). Available at: https://doi.org/10.1016/j.clae.2024.102157.

Mattox, D.M. (2002) 'Physical vapor deposition (PVD) processes', *Metal Finishing*, 100, pp. 394–408. Available at: https://doi.org/10.1016/S0026-0576(02)82043-8.

McBrien, N.A. and Millodot, M. (1987) 'The relationship between tonic accommodation and refractive error', *Investigative ophthalmology & visual science*, 28(6), pp. 997–1004.

McDougal, D.H. and Gamlin, P.D. (2015) 'Autonomic control of the eye', *Comprehensive Physiology*, 5(1), pp. 439–473. Available at: https://doi.org/10.1002/cphy.c140014.

Mehta, R. and Aref, A.A. (2019) 'Intraocular lens implantation in the ciliary sulcus: Challenges and risks', *Clinical Ophthalmology*. Dove Medical Press Ltd, pp. 2317–2323. Available at: https://doi.org/10.2147/OPTH.S205148.

Mendes, G.C.C., Brandão, T.R.S. and Silva, C.L.M. (2007) 'Ethylene oxide sterilization of medical devices: A review', *American Journal of Infection Control*. Mosby Inc., pp. 574–581. Available at: https://doi.org/10.1016/j.ajic.2006.10.014.

Menko, S.A. (2002) 'Lens epithelial cell differentiation', *Experimental Eye Research*. Academic Press, pp. 485–490. Available at: https://doi.org/10.1006/exer.2002.2057.

von Metzen, R. and Stieglitz, T. (2013) 'Impact of Sterilization Procedures on the Stability of Parylene Based Flexible Multilayer Structures', *Biomedical Engineering / Biomedizinische Technik*, 58(SI-1-Track-C). Available at: https://doi.org/doi:10.1515/bmt-2013-4089.

Minnikanti, S. *et al.* (2014) 'Lifetime assessment of atomic-layer-deposited Al2O 3-Parylene C bilayer coating for neural interfaces using accelerated age testing and electrochemical characterization', *Acta Biomaterialia*, 10(2), pp. 960–967. Available at: https://doi.org/10.1016/j.actbio.2013.10.031.

Mitchelson, F. (2012) 'Muscarinic Receptor Agonists and Antagonists: Effects on Ocular Function', in A.D. Fryer, A. Christopoulos, and N.M. Nathanson (eds) *Muscarinic Receptors*. Berlin, Heidelberg: Springer Berlin Heidelberg, pp. 263–298. Available at: https://doi.org/10.1007/978-3-642-23274-9_12.

Miwa, T. (1992) 'Instrument myopia and the resting state of accommodation', *Optometry and vision science*, 69(1), pp. 55–59.

Moarefi, M.A., Bafna, S. and Wiley, W. (2017) 'A Review of Presbyopia Treatment with Corneal Inlays', *Ophthalmology and Therapy*. Springer Healthcare, pp. 55–65. Available at: https://doi.org/10.1007/s40123-017-0085-7.

Moffat, B.A., Atchison, D.A. and Pope, J.M. (2002) 'Explanation of the Lens Paradox', *Optometry and Vision Science*, 79(3). Available at: https://journals.lww.com/optvissci/fulltext/2002/03000/explanation_of_the_lens_paradox.8.aspx.

Momeni-Moghaddam, H., Kundart, J. and Askarizadeh, F. (2014) 'Comparing measurement techniques of accommodative amplitudes', *Indian journal of ophthalmology*, 62(6), pp. 683–687. Available at: https://doi.org/10.4103/0301-4738.126990.

Morgan (1944) 'Accommodation and its relationship to convergence', *Optometry and Vision Science*, 21(5), pp. 183–195.

Morgan, M.W. (1968) 'Accommodation and vergence', *Optometry and Vision Science*, 45(7). Available at: https://journals.lww.com/optvissci/Fulltext/1968/07000/ACCOMMODATION_AND_VERGENCE_.1.aspx.

Muranov, K.O. and Ostrovsky, M.A. (2022) 'Biochemistry of Eye Lens in the Norm and in Cataractogenesis', *Biochemistry (Moscow)*. Pleiades journals, pp. 106–120. Available at: https://doi.org/10.1134/S0006297922020031.

Mutti, D.O. *et al.* (1994) 'The effect of cycloplegia on measurement of the ocular components', *Investigative ophthalmology & visual science*, 35(2), pp. 515–527.

Myers, G.A. and Stark, L. (1990) 'Topology of the near response triad', *Ophthalmic and Physiological Optics*, 10(2), pp. 175–181. Available at: https://doi.org/10.1111/j.1475-1313.1990.tb00972.x.

Nanbakhsh, K. *et al.* (2025) 'An In Vivo Biostability Evaluation of ALD and Parylene-ALD Multilayers as Micro-Packaging Solutions for Small Single-Chip Implants', *Small*. Available at: https://doi.org/10.1002/smll.202410141.

Nesterov, A.P. and Khadikova, E. V (1997) 'Effect of ciliary muscle electrical stimulation on ocular hydrodynamics and visual function in patients with glaucoma', *Vestnik Oftalmologii*, 113(4), pp. 12–14.

Newaskar, D. and Patil, B.P. (2021) 'Batteries For Active Implantable Medical Devices', in *2021 International Conference on Intelligent Technologies (CONIT)*. IEEE, pp. 1–7. Available at: https://doi.org/10.1109/CONIT51480.2021.9498319.

Onyszkiewicz, M. *et al.* (2024) 'Effects of Miosis on the Visual Acuity Space under Varying Conditions of Contrast and Ambient Luminance in Presbyopia', *Journal of Clinical Medicine*, 13(5). Available at: https://doi.org/10.3390/jcm13051209.

Orman, B. and Benozzi, G. (2021) 'Overview of pharmacological treatments for presbyopia', *Medical Hypothesis, Discovery & Innovation in Optometry*, 1(2), pp. 67–77. Available at: https://doi.org/10.51329/mehdioptometry110.

Padmanaban, N., Konrad, R. and Wetzstein, G. (2019) *Autofocals: Evaluating gaze-contingent eyeglasses for presbyopes*, *Sci. Adv*. Available at: https://doi.org/10.1126/sciadv.aav6187.

Papadopoulos, P.A. and Papadopoulos, A.P. (2014) 'Current management of presbyopia', *Middle East African Journal of Ophthalmology*, 21(1), pp. 10–17. Available at: https://doi.org/10.4103/0974-9233.124080.

Passlack, U. *et al.* (2023) 'Flexible Ultrathin Chip-Film Patch for Electronic Component Integration and Encapsulation using Atomic Layer-Deposited Al2O3-TiO2 Nanolaminates', *ACS Applied Materials and Interfaces*, 15(12), pp. 16221–16231. Available at: https://doi.org/10.1021/acsami.2c22513.

Pepose, J.S., Burke, J. and Qazi, M.A. (2017) 'Benefits and barriers of accommodating intraocular lenses', *Current Opinion in Ophthalmology*. Lippincott Williams and Wilkins, pp. 3–8. Available at: https://doi.org/10.1097/ICU.0000000000000323.

Pesudovs, K. *et al.* (2024) 'Global estimates on the number of people blind or visually impaired by cataract: a meta-analysis from 2000 to 2020', *Eye*, 38(11), pp. 2156–2172. Available at: https://doi.org/10.1038/s41433-024-02961-1.

Petasch, W. *et al.* (1995) *Improvement of the adhesion of low-energy polymers by a short-time plasma treatment*, *Surface and Coatings Technology*. Available at: https://doi.org/10.1016/0257-8972(94)08209-X.

Pielot, A. *et al.* (2025) 'Design of a smart contact lens for controlled retinal lighting in red light therapy', *Biomedical Optics Express*, 16(6), p. 2400. Available at: https://doi.org/10.1364/BOE.559469.

Plainis, S., Charman, W.N. and Pallikaris, I.G. (2014) 'The physiologic mechanism of accommodation', *Cataract & Refractive Surgery Today Europe*, 4, pp. 23–29.

Poyer, J.F., B'Ann, T.G. and Kaufman, P.L. (1994) 'The effect of muscarinic agonists and selective receptor subtype antagonists on the contractile response of the isolated rhesus monkey ciliary muscle', *Experimental eye research*, 59(6), pp. 729–736. Available at: https://doi.org/10.1006/exer.1994.1159.

Pu, Y. *et al.* (2025) 'Age-Related Changes in Lens Elasticity Contribute More to Accommodative Decline Than Shape Change', *Investigative Ophthalmology and Visual Science*, 66(1). Available at: https://doi.org/10.1167/iovs.66.1.16.

Qiao-Grider, Y. *et al.* (2007) 'Normal ocular development in young rhesus monkeys (Macaca mulatta)', *Vision research*, 47(11), pp. 1424–1444. Available at: https://doi.org/10.1016/j.visres.2007.01.025.

Rahmati, M. *et al.* (2018) 'Biomaterials for regenerative medicine: Historical perspectives and current trends', in *Advances in Experimental Medicine and Biology*. Springer New York LLC, pp. 1–19. Available at: https://doi.org/10.1007/5584_2018_278.

Read, J.C.A. *et al.* (2022) 'Seeing the future: Predictive control in neural models of ocular accommodation', *Journal of Vision*, 22(9), pp. 4–5. Available at: https://doi.org/10.25405/data.ncl.14945550.

'Regulation (EU) 2017/745' (2017) *Official Journal*, pp. 1–175.

Rio, D., Woog, K. and Legras, R. (2016) 'Effect of age, decentration, aberrations and pupil size on subjective image quality with concentric bifocal optics', *Ophthalmic and Physiological Optics*, 36(4), pp. 411–420. Available at: https://doi.org/10.1111/opo.12300.

Root, M.J. (2013) 'Medical Device Batteries', in R.J. Brodd (ed.) *Batteries for Sustainability: Selected Entries from the Encyclopedia of Sustainability Science and Technology*. New York, NY: Springer New York, pp. 359–392. Available at: https://doi.org/10.1007/978-1-4614-5791-6_11.

Rosenfield, M. *et al.* (1993) 'Tonic accommodation: a review I. Basic aspects', *Ophthalmic and Physiological Optics*, 13(3), pp. 266–283. Available at: https://doi.org/10.1111/j.1475-1313.1993.tb00469.x.

Rosenfield, M. and Gilmartin, B. (1989) 'Temporal aspects of accommodative adaptation', *Optometry and Vision Science*, 66(4), pp. 229–234.

Ruskell, G.L. (1990) 'Accommodation and the nerve pathway to the ciliary muscle: a review', *Ophthalmic and Physiological Optics*, 10(3), pp. 239–242. Available at: https://doi.org/10.1111/j.1475-1313.1990.tb00858.x.

Rutstein, R.P., Fuhr, P.D. and Swiatocha, J. (1993) 'Comparing the amplitude of accommodation determined objectively and subjectively.', *Optometry and vision science: official publication of the American Academy of Optometry*, 70(6), pp. 496–500.

Salvador-Roger, R. *et al.* (2025) 'Subjective and objective measurements of the amplitude of accommodation: Revisiting the existing methods and clinical evaluation of newer techniques', *Ophthalmic and Physiological Optics*. Available at: https://doi.org/10.1111/opo.13482.

Schachar, R.A. *et al.* (1996) 'In vivo increase of the human lens equatorial diameter during accommodation', *American Journal of Physiology-Regulatory, Integrative and Comparative Physiology*, 271(3), pp. R670–R676. Available at: https://doi.org/10.1152/ajpregu.1996.271.3.R670.

Schachar, R.A. *et al.* (2024) 'Model of zonular forces on the lens capsule during accommodation', *Scientific Reports*, 14(1), p. 5896. Available at: https://doi.org/10.1038/s41598-024-56563-8.

Schallhorn, J.M. *et al.* (2021) 'Multifocal and Accommodating Intraocular Lenses for the Treatment of Presbyopia: A Report by the American Academy of Ophthalmology', *Ophthalmology*, 128(10), pp. 1469–1482. Available at: https://doi.org/10.1016/j.ophtha.2021.03.013.

Schober, H.A.W., Dehler, H. and Kassel, R. (1970) 'Accommodation During Observations with Optical Instruments', *Journal of the Optical Society of America*, 60(1), pp. 103–106. Available at: https://doi.org/10.1364/JOSA.60.000103.

Schor, C.M. (2012) 'Accommodating intraocular lenses', *Presbyopia: Origins, Effects and Treatment*, pp. 167–173.

Schor, C.M., Johnson, C.A. and Post, R.B. (1984) 'Adaptation of tonic accommodation', *Ophthalmic and Physiological Optics*, 4(2), pp. 133–137. Available at: https://doi.org/10.1111/j.1475-1313.1984.tb00346.x.

Schubert, G. (1955) 'Aktionspotentiale des M. ciliaris beim Menschen', *Albrecht von Graefes Archiv für Ophthalmologie Vereinigt mit Archiv für Augenheilkunde*, 157(2), pp. 116–121. Available at: https://doi.org/10.1007/BF00682518.

Schumayer, S. *et al.* (2022) 'Novel Three-Dimensional and Biocompatible Lift-Off Method for Selective Metallization of a Scleral Contact Lens Electrode for Biopotential Detection', *Frontiers in Medical Technology | www.frontiersin.org*, 1, p. 920384. Available at: https://doi.org/10.3389/fmedt.2022.920384.

Schumayer, S., Zahrani, E.G., *et al.* (2025) 'Design and In Vivo Evaluation of an Intraocular Electrode for Ciliary Muscle Biopotential Measurement in a Non-Human Primate Model of Human Accommodation', *Biosensors*, 15(4), p. 247. Available at: https://doi.org/10.3390/bios15040247.

Schumayer, S., Sigdel, B., Jarboui, M.A., *et al.* (2025) 'Non-invasive measuring of biopotentials of the ciliary muscle during accommodation in emmetropes', *Scientific Reports*, 15(1), p. 19389. Available at: https://doi.org/10.1038/s41598-025-04165-3.

Schumayer, S., Sigdel, B., Nikolaidou, A., *et al.* (2025) 'Preserved ciliary muscle biopotentials enable artificial lens control and near vision recovery in long-term presbyopia (Abstract P2-15). In Abstracts of the 62nd annual symposium of the International Society for Clinical Electrophysiology of Vision (ISCEV 2025), Utrecht, the Netherlands.', *Documenta Ophthalmologica*, 150(Suppl 1), pp. 5–51. Available at: https://doi.org/10.1007/s10633-025-10031-4.

Schumayer, S., Laukhuf, J. and Straßer, T. (2025) 'Comparing a Novel Motorized Push-Up Ruler with Conventional Subjective Methods for Measuring the Amplitude of Accommodation', *Current Eye Research*, pp. 1–9. Available at: https://doi.org/10.1080/02713683.2025.2531524.

Sehrin, F. *et al.* (2024) 'The effect on income of providing near vision correction to workers in Bangladesh: The THRIVE (Tradespeople and Hand-workers Rural Initiative for a Vision-enhanced Economy) randomized controlled trial', *PLoS ONE*, 19(4 April). Available at: https://doi.org/10.1371/journal.pone.0296115.

Seidemann, A. and Schaeffel, F. (2002) 'Effects of longitudinal chromatic aberration on accommodation and emmetropization', *Vision research*, 42(21), pp. 2409–2417. Available at: https://doi.org/10.1016/S0042-6989(02)00262-6.

Seidler, R.D. *et al.* (2010) 'Motor control and aging: Links to age-related brain structural, functional, and biochemical effects', *Neuroscience and Biobehavioral Reviews*, pp. 721–733. Available at: https://doi.org/10.1016/j.neubiorev.2009.10.005.

Shekhawat, D. *et al.* (2021) 'A Short Review on Polymer, Metal and Ceramic Based Implant Materials', in *IOP Conference Series: Materials Science and Engineering*. IOP Publishing Ltd. Available at: https://doi.org/10.1088/1757-899X/1017/1/012038.

Sheppard, A.L. and Davies, L.N. (2011) 'The Effect of Ageing on In Vivo Human Ciliary Muscle Morphology and Contractility', *Investigative Opthalmology & Visual Science*, 52(3), p. 1809. Available at: https://doi.org/10.1167/iovs.10-6447.

Shintani, H. (2017) 'Ethylene oxide gas sterilization of medical devices', *Biocontrol science*, 22(1), pp. 1–16. Available at: https://doi.org/10.4265/bio.22.1.

Stark, L.R. *et al.* (2002) 'Accommodation to simulations of defocus and chromatic aberration in the presence of chromatic misalignment', *Vision Research*, 42(12), pp. 1485–1498. Available at: https://doi.org/10.1016/S0042-6989(02)00074-3.

Stingl, K. *et al.* (2013) 'Artificial vision with wirelessly powered subretinal electronic implant alpha-IMS', *Proceedings of the Royal Society B: Biological Sciences*, 280(1757). Available at: https://doi.org/10.1098/rspb.2013.0077.

Stokes, J. *et al.* (2022) 'Exploring the Experience of Living with and Managing Presbyopia', *Optometry and Vision Science*, 99(8). Available at: https://doi.org/10.1097/OPX.0000000000001913.

Streeten, B.W. (1977) 'The zonular insertion: a scanning electron microscopic study.', *Investigative ophthalmology & visual science*, 16(4), pp. 364–375.

Sun, L. *et al.* (2021) 'Chemical vapour deposition', *Nature Reviews Methods Primers*. Springer Nature. Available at: https://doi.org/10.1038/s43586-020-00005-y.

Sundaram Muthuraman, M. (2015) *Systematic Review on Sterilization Methods of Implants and Medical Devices*, *Article in International Journal of ChemTech Research*. Available at: https://www.researchgate.net/publication/278242593.

Tabernero, J. *et al.* (2016) 'The accommodative ciliary muscle function is preserved in older humans.', *Scientific reports*, 6(May), p. 25551. Available at: https://doi.org/10.1038/srep25551.

Takeuchi, E.S. *et al.* (2009) 'Lithium batteries for medical applications', in *Lithium Batteries*. Springer, pp. 686–700. Available at: https://doi.org/10.1007/978-0-387-92675-9_22.

Tamm, E.R. and Lütjen-Drecoll, E. (1996) 'Ciliary body', *Microscopy research and technique*, 33(5), pp. 390–439. Available at: https://doi.org/10.1002/(SICI)1097-0029(19960401)33:5<390::AID-JEMT2>3.0.CO;2-S.

Terry, R.L. (1990) 'Social and personality effects of vision correctives', *Journal of Social Behavior and Personality*, 5(6), p. 683.

Toates, F.M. (1972) 'Accommodation function of the human eye', *Physiological reviews*, 52(4), pp. 828–863. Available at: https://doi.org/10.1152/physrev.1972.52.4.828.

Törnqvist, G. (1967) 'Accommodation in monkeys: some pharmacological and physiological aspects', *Acta Ophthalmologica*, 45(3), pp. 429–460. Available at: https://doi.org/10.1111/j.1755-3768.1967.tb06508.x.

Tremblay, Eric.J. *et al.* (2013) 'Switchable telescopic contact lens', *Optics Express*, 21(13), p. 15980. Available at: https://doi.org/10.1364/oe.21.015980.

Vafaiee, M. *et al.* (2019) 'Gold-Plated Electrode with High Scratch Strength for Electrophysiological Recordings', *Scientific Reports*, 9(1). Available at: https://doi.org/10.1038/s41598-019-39138-w.

Vargas, V. *et al.* (2019) 'Methods for the study of near, intermediate vision, and accommodation: an overview of subjective and objective approaches', *Survey of Ophthalmology*. Elsevier USA, pp. 90–100. Available at: https://doi.org/10.1016/j.survophthal.2018.08.003.

Varssano, D. (2024) 'Accommodating Intraocular Lenses', in Rami Zalish and Dana Shoham-Hazon (eds) *Surgical Correction of Presbyopia*. CRC Press, pp. 95–102. Available at: https://doi.org/https://doi.org/10.1201/9781003526667.

VSI Parylene (2025) *Complete Guide to Parylene Coatings*, *VSI Parylene*. Available at: https://www.vsiparylene.com (Accessed: 30 April 2025).

Wagner, S. *et al.* (2023) 'Monocular transcorneal electrical stimulation induces ciliary muscle thickening in contralateral eye', *Experimental Eye Research*, 231. Available at: https://doi.org/10.1016/j.exer.2023.109475.

Wakabayashi, T. *et al.* (2023) 'Google Search Trends to assess public interest in and concern about Vuity for treating presbyopia', *PLoS ONE*, 18(10 October). Available at: https://doi.org/10.1371/journal.pone.0293066.

Warwick, R. (1954) 'The ocular parasympathetic nerve supply and its mesencephalic sources', *Journal of anatomy*, 88(Pt 1), p. 71.

Weber, C.H. and Cionni, R.J. (2015) 'All about capsular tension rings', *Current Opinion in Ophthalmology*. Lippincott Williams and Wilkins, pp. 10–15. Available at: https://doi.org/10.1097/ICU.0000000000000118.

Wolffsohn, J.S., Naroo, S.A., *et al.* (2024) 'BCLA CLEAR Presbyopia: Definitions', *Contact Lens and Anterior Eye*, 47(4), p. 102155. Available at: https://doi.org/10.1016/j.clae.2024.102155.

Wolffsohn, J.S., Berkow, D., *et al.* (2024) 'BCLA CLEAR Presbyopia: Evaluation and diagnosis', *Contact Lens and Anterior Eye*, 47(4). Available at: https://doi.org/10.1016/j.clae.2024.102156.

World Health Organization (2015) *World report on ageing and health*. World Health Organization.

Van Der Worp, E. *et al.* (2014) 'Modern scleral contact lenses: A review', *Contact Lens and Anterior Eye*, 37, pp. 240–250. Available at: https://doi.org/10.1016/j.clae.2014.02.002.

Van Der Worp, E. (2015) *A Guide to Scleral Lens Fitting, Version 2.0 [monograph online]*. Available at: http://commons.pacificu.edu/monohttp://commons.pacificu.edu/mono/10/.

Xia, Y. *et al.* (2021) 'A Review of Shape Memory Polymers and Composites: Mechanisms, Materials, and Applications', *Advanced Materials*. Wiley-VCH Verlag. Available at: https://doi.org/10.1002/adma.202000713.

Xie, X. *et al.* (2015) 'Effect of bias voltage and temperature on lifetime of wireless neural interfaces with Al2O3 and parylene bilayer encapsulation', *Biomedical Microdevices*, 17(1). Available at: https://doi.org/10.1007/s10544-014-9904-y.

Xu, H. *et al.* (2021) 'Atomic layer deposition – state-of-the-art approach to nanoscale hetero-interfacial engineering of chemical sensors electrodes: A review', *Sensors and Actuators, B: Chemical*. Elsevier B.V. Available at: https://doi.org/10.1016/j.snb.2020.129403.

Young, T. (1801) 'II. The Bakerian Lecture. On the mechanism of the eye', *Philosophical Transactions of the Royal Society of London*, (91), pp. 23–88. Available at: https://doi.org/10.1098/rstl.1801.0004.

Yu, B. *et al.* (2024) 'Influences of deposition conditions on atomic layer deposition films for enhanced performance in perovskite solar cells', *Energy Materials*. Available at: https://doi.org/10.20517/energymater.2023.150.

Zeng, F.G. *et al.* (2008) 'Cochlear Implants: System Design, Integration, and Evaluation', *IEEE Reviews in Biomedical Engineering*, 1, pp. 115–142. Available at: https://doi.org/10.1109/RBME.2008.2008250.

Zrenner, E. *et al.* (2017) 'The subretinal implant ALPHA: implantation and functional results', *Artificial vision: a clinical guide*, pp. 65–83. Available at: https://doi.org/10.1007/978-3-319-41876-6_6.

# 7. Declaration of Contribution to the Dissertation

The work was carried out at the Institute for Ophthalmic Research at the University of Tübingen under the supervision of Dr. T. Straßer. In addition, the infrastructure of the Institute for Microsystems Technology (iMST) at Furtwangen University, under the supervision of Prof. Dr. V. Bucher was used.

For spelling and grammar verification, the program Grammarly (v1.2.168.1686) as well as ChatGPT–3.5 was used. I ensure that I have carefully checked and adjusted the output of the AI tools (Grammarly, ChatGPT) before implementing the enhancements in the manuscript.

The explanation of the respective work of this cumulative dissertation can be found below.

I declare that I have written the manuscript independently and have not used any sources other than those I have indicated.

Tübingen, the

_____

## 7.1 Declaration of Contribution: Motorized Push-up Ruler

Schumayer, S., Laukhuf, J., & Straßer, T. (2025). Comparing a Novel Motorized Push-Up Ruler with Conventional Subjective Methods for Measuring the Amplitude of Accommodation. Current Eye Research, 1–9.

### Authors contributions

T.S. and S.S. conceptualized the research and developed the study protocol. S.S. and J.L. were responsible for participant recruitment. Data acquisition was primarily conducted by J.L., with support from S.S. All authors contributed to data analysis, while S.S. and T.S. interpreted the results. The manuscript was written by S.S., with input from T.S. and J.L. All authors have read and approved the final version of the manuscript.

### 7.2 Declaration of Contribution: Contact Lens Electrode

Schumayer, S., Sigdel, B., Jarboui, M. A., Zrenner, E., Bucher, V., Straßer, T., & Wagner, S. (2025). Non-invasive measuring of biopotentials of the ciliary muscle during accommodation in emmetropes. Scientific Reports, 15(1), 19389.

**Authors contributions**

The initial study idea originated from E.Z. The study protocol was designed by S.W. and S.S., while the setup was developed by S.W. and T.S. The technical aspects of the contact lens electrodes and their subsequent use in the trial design were developed by E.Z, V.B and S.S. While the measurements were carried out by S.S. and B.S., the data analysis was performed by S.S., T.S. and M.J. S.S wrote the manuscript with input from S.W. and T.S. Results and the final version of the manuscript were discussed by all authors.

### 7.3 Declaration of Contribution: Intraocular Implant

Schumayer, S., Zahrani, E. G., Azarhoushang, B., Bucher, V., & Straßer, T. (2025). Design and In Vivo Evaluation of an Intraocular Electrode for Ciliary Muscle Biopotential Measurement in a Non-Human Primate Model of Human Accommodation. Biosensors, 15(4), 247.

**Authors contributions**

T.S. and S.S. were responsible for the design and configuration of the electrode. E.G.Z. and B.A. provided expertise on the laser cutting process and carried out the PET blank cutting. S.S. led the development of the manufacturing process, with V.B. and T.S. providing advice. V.B. and S.S. jointly designed the long-term testing protocol, including accelerated aging and impedance measurement. S.S. set up and conducted the long-term tests and performed the data analysis in collaboration with V.B. and T.S. Both T.S. and S.S. actively contributed to the in vivo measurements. S.S. drafted this manuscript with the support and additional input of T.S. and all the other authors. All authors have read and agreed to the published version of the manuscript.

### 7.4 Declaration of Contribution: Tunable Spectacles in Presbyopes

Schumayer, S., Sigdel, B., Nikolaidou, A., Wolfram, L., Wagner, S., Zrenner, E., Bucher, V., & Straßer, T. (2025). Preserved ciliary muscle biopotentials enable artificial lens control and near vision recovery in long-term presbyopia (Abstract P2-15). In Abstracts of the 62nd annual symposium of the International Society for Clinical Electrophysiology of Vision (ISCEV 2025), Utrecht, the Netherlands. Documenta Ophthalmologica, 150(Suppl 1)

**Authors contributions**

Together with S.W., E.Z., and V.B., S.S. and T.S. were responsible for the research concept, including both the scope of the research and its technical aspects. S.S., S.W., and T.S. selected the study methods, which included pre- and post-examinations as well as the actual measurements. Patient recruitment was carried out by A.N., E.Z., and T.S., while S.S. handled additional inquiries and provided participants with the necessary information. Data collection involved a medical examination performed by A.N. and L.W., while experimental data acquisition was conducted by B.S. and S.S. Data analysis was performed by T.S. and S.S., with support from B.S. and A.N., and the interpretation of results was carried out by T.S. and S.S. The final abstract was written by S.S., with input and support from E.Z., S.W., and T.S. All authors have read and approved the published version of the manuscript.

# 8. Dedication

I would like to express my deepest gratitude to Dr. Straßer, whose guidance and support throughout the entirety of my PhD have been truly invaluable. Your insightful feedback, patience, and steady encouragement have not only shaped this project but have also played a significant role in my academic and personal growth.

Furthermore, my sincere thanks also go to Prof. Dr. Bucher, whose technical expertise and clear, solution-oriented input were essential to the success of this work. His precise feedback and practical approach greatly enriched the technical implementation and overall quality of the project.

As an interdisciplinary project, this work benefited greatly from the contributions of many dedicated colleagues who shared their knowledge and expertise. I would like to express my gratitude to Professor Zrenner for his profound insights, forward-thinking perspective, and continuous support. I am also especially thankful to Bishesh Sigdel from the Institute for Ophthalmic Research and to Sebastian Kaltenstadler. Working with you both has been a pleasure, and your collaboration made a lasting impact on this project.

Above all, my deepest thanks go to my family, without whom I would not be the person I am today. To my wonderful parents, Karl-Otto and Heike, thank you for being such inspiring role models and for always standing by me with wisdom, encouragement, and unwavering belief in me. I am also deeply grateful to my brother Robin, not only for his support but for being such a true friend throughout the years.

- To know where you're going, remember where you're from -

Last but not least, I would like to express my deepest gratitude to Lea for never letting me down, for being by my side with unwavering support, infinite patience, and a comforting presence that carried me through every high and low of this journey. Your strength, kindness, and quiet encouragement meant more than I can put into words.